Aus dem Paul Langerhans Institut des Helmholtz Zentrum München am Universitätsklinikum Carl Gustav Carus der Technischen Universität Dresden

Direktor: Herr Prof. Dr. Michele Solimena

Aldh1b1-mediated metabolism regulates pancreas progenitor differentiation and β-cell maturation

DISSERTATIONSSCHRIFT

zur Erlangung des akademischen Grades

Doctor of Philosophy (Ph.D.)

vorgelegt

der Medizinischen Fakultät Carl Gustav Carus

der Technischen Universität Dresden

von

M.Sc. Mandy Rödiger

aus Nordhausen, Deutschland

Dresden 2023

1. Gutachter:

2. Gutachter:

Tag der mündlichen Prüfung:

gez.:_____

Vorsitzender der Promotionskommission

Summary

Pancreatic β-cells have a central function in the regulation of glucose homeostasis by releasing the blood sugar-lowering hormone insulin. Disruption of this process results in diabetes, which has a tremendous impact on the quality of life and requires lifelong treatment. Elucidating the mechanisms of pancreatic progenitor cell differentiation into fully functional β-cells will contribute to identifying the underlying reasons for β-cell dysfunction and to finding a cure for diabetes.

Aldh1b1 was identified by our research group as a regulator of pancreas development and β-cell functionality. Aldh1b1 is a mitochondrial enzyme, expressed in all embryonic pancreas progenitors. Its expression is switched off during the process of differentiation and is undetectable in differentiated cells. Functional inactivation of *Aldh1b1* in the mouse leads to premature differentiation of progenitor cells in the embryo and dysfunctional β-cells in the adult. However, the enzymatic function of Aldh1b1 in pancreas progenitors and how it ultimately affects β-cell functionality remained to be elucidated.

In this study, I analyzed the role of Aldh1b1 in the metabolism of embryonic pancreas progenitor cells and its impact on chromatin structure and gene expression in both, progenitors and postnatal β-cells. Flow cytometry analysis of freshly isolated *Aldh1b1* null embryonic pancreas progenitors showed a significant increase in ROS levels as well as a significant decrease in mitochondrial mass, whereas the mitochondrial membrane potential was not affected. To elucidate the impact of Aldh1b1 on cellular metabolism, I conducted metabolic flux experiments and untargeted metabolomics studies using FACS-isolated embryonic pancreas progenitors expanded in a 3D spheroid culture. Analyses following metabolic labeling with either $^{13}C_6$-Glucose or $^{13}C_2$-Glutamine showed that the absence of Aldh1b1 lead to an increase of the reductive glutamine metabolism towards citrate, a reaction that channels carbon units into the acetyl-CoA biosynthesis. However, the ACLy-dependent flux towards acetyl-coA synthesis was reduced and this was consistent with reduced expression of *ACLy* as well as the citrate transporter *SLC25a1*. A decrease in cellular acetyl-CoA would reduce histone acetylation. Untargeted metabolomics showed an increase in the concentration of S-adenosyl-methionine, suggesting increased DNA and histone methylation. Consistent with these findings, ATAC-Seq analyses on freshly isolated pancreatic progenitors showed reduced chromatin accessibility at genes implicated in chromatin organization, protein acetylation and histone modification. Transcription motif analysis showed that the affected genomic sites were mainly associated with the binding of Klf/Sp and Nrf1 transcription factors. Transcriptome analyses displayed that the expression of genes implicated in progenitor differentiation, ECM organization and transcriptional regulation was affected. Furthermore, transcriptome analyses

of early postnatal β-cells uncovered early signs of oxidative stress and increased proliferation, thus providing the basis to explain the β-cell phenotype in *Aldh1b1* null mice.

I then used organotypic cultures of embryonic pancreata to investigate the connection between high ROS levels and aberrant differentiation in the *Aldh1b1* null pancreata. Reducing ROS levels using NAC enabled the reversal of the aberrant transcription factor expression and increased viability of *Aldh1b1* null explants, thus identifying high ROS levels as a driving force in this process. To investigate how persisting Aldh1b1 expression would affect progenitor differentiation, I generated *ROSA26*^{*LSLAldh1b1*}, an inducible constitutive Aldh1b1 expression line. Progenitors with continuous *Aldh1b1* expression avoided the endocrine cell fate, underscoring the importance of timely *Aldh1b1* downregulation in the course of β-cell differentiation.

Altogether, my work provides strong evidence for the role of Aldh1b1 as a metabolic regulator in the process of progenitor cell differentiation and identifies a link between metabolism and gene regulation through chromatin accessibility during development. Aldh1b1 inactivity causes defects in embryonic progenitor cells as well as postnatal β-cells and could therefore contribute, as genetic risk factor, to the development of hyperglycemia and diabetes later in life. Comprehending the mechanisms underlying the process of pancreas progenitor differentiation as well as the origins of β cell dysfunction should assist in the design of novel therapeutic interventions for diabetes.

Zusammenfassung

β-Zellen des Pankreas besitzen, durch Freisetzung des blutzuckersenkenden Hormons Insulin eine zentrale Funktion in der Regulation der Glukosehomöostase. Eine Störung dieses Prozesses resultiert somit in der Entstehung von Diabetes mellitus. Für Betroffene bedeutet dies eine schwerwiegende Beeinträchtigung der Lebensqualität und oft lebenslange Behandlung. In diesem Verständnis können durch Erforschung der zugrundeliegenden molekularen Mechanismen der ß-Zell-Dysfunktion neue Therapien und vielleicht sogar Möglichkeiten zur Heilung von Diabetes mellitus erschlossen werden. Ein Verständnis des Differenzierungs-Vorganges von Progenitorzellen hin zu funktionalen ß-Zellen ist weiterhin Grundlage zur Entwicklung möglicher regenerativer Therapien.Aldh1b1 wurde von unserer Forschungsgruppe als ein Regulator der Pankreasentwicklung und β-Zellfunktionalität identifiziert. Aldh1b1 ist ein mitochondriales Enzym, das in allen embryonalen Pankreasprogenitoren exprimiert ist. Im Differenzierungs-Prozess wird die Enzym-Expression jedoch abgeschaltet. So ist das Enzym in ausdifferenzierten Zellen nicht mehr nachweisbar. Eine funktionelle Abschaltung von *Aldh1b1* in der Maus verursacht eine vorzeitige Differenzierung der Progenitoren in Embryonen und führt so zu dysfunktionalen β-Zellen in ausgewachsenen Mäusen. Die enzymatische Funktion von Aldh1b1 in Pankreas Progenitorzellen und wie es letztendlich die β-Zellfunktionalität beeinträchtigt verbleibt jedoch zu klären.

In dieser Studie analysiere ich die Rolle des Enzyms Aldh1b1 sowohl im Metabolismus von embryonalen Pankreas Progenitorzellen, als auch dessen Einfluss auf die Chromatinstruktur und Genexpression in Progenitoren und postnatalen β-Zellen. Durchflusszytometrische Analysen von frisch isolierten embryonalen Pankreas Progenitorzellen, in denen *Aldh1b1* Expression abgeschaltet wurde, zeigte eine signifikante Zunahme reaktiver Sauerstoffspezies (ROS). Zudem zeigten die Zellen eine signifikante Reduktion der mitochondrialen Masse, wohingegen das Membranpotential des Mitochondriums keine Veränderung zeigte.

Um den Einfluss von Aldh1b1 auf den zellulären Metabolismus zu beleuchten, führte ich metabolische Fluss Experimente und ungerichtete Metabolom-Studien durch. Dabei nutzte ich FACS-isolierte embryonale Pankreas Progenitoren, die in einer 3D Sphäroidenkultur vervielfacht wurden. Analysen, die nach einer metabolischen Markierung mit entweder $^{13}C_6$-Glukose oder $^{13}C_2$-Glutamin durchgeführt wurden, zeigten, dass die Abwesenheit von Aldh1b1 zur Verschiebung des reduktiven Glutamin-Stoffwechsels in Richtung Citrat führte. Diese Reaktion schleust Kohlenstoffeinheiten in die Acetyl-CoA Synthese. Dieser ACLy-abhängige Stoffwechselweg, der die Acetyl-CoA Synthese realisiert, zeigte jedoch eine verminderte Flussrate. Diese war auch konsistent mit der detektierten reduzierten Expression von *ACLy* und dem Citrattransporter *SLC25a1*. Verminderte zelluläre Acetyl-CoA Konzentrationen

könnten eine Reduktion von Histon-Acetylierungen verursachen. Ungerichtete Metabolom-Analysen zeigten einen Anstieg in der zellulären S-Adenosylmethionin Konzentration, was eine Zunahme von DNA- und Histonmethylierungen implizieren würde.

In Übereinstimmung mit den zuvor genannten Sachverhalten, konnten ATAC-Sequenzierungsanalysen, durchgeführt mit frisch isolierten *Aldh1b1* null Pankreasprogenitoren, eine verminderte Chromatin-Zugänglichkeit von Genen, die in Prozesse wie Chromatinorganisation, Protein-Acetylierung und Histonmodifikation involviert sind, nachweisen. Eine Untersuchung der DNA-Bindungsmotive zeigte, dass die betroffenen genomische Bereiche hauptsächlich mit der Bindung der Transkriptionsfaktoren Klf/Sp und Nrf1 assoziiert sind. Transkriptomanalysen enthüllten eine Beeinträchtigung von Genen, die mit Vorgängen wie Progenitorzellen Differenzierung, Organisation der extrazellulären Matrix und transkriptioneller Regulierung in Zusammenhang gebracht werden. Transkriptomanalysen von postnatalen β-Zellen zeigten außerdem frühe Anzeichen von oxidativem Stress und eine Zunahme der Zellproliferation. Diese Beobachtungen liefern eine Grundlage zur Erklärung des β-Zell Phänotyps in *Aldh1b1* null Mäusen.

Anschließend benutzte ich eine organotypische Zellkulturmethode mit embryonalen Pankreaten, um den Zusammenhang von erhöhter ROS Produktion mit den abweichenden Differenzierungsvorgängen in *Aldh1b1* null Pankreaten, zu untersuchen. Eine Reduktion des ROS-Levels durch den Gebrauch von NAC ermöglichte eine Reversion des abweichenden Expressionsprofils von *Aldh1b1* null Pankreaten und identifizierte damit ROS als treibende Kraft in diesem Prozess. Um den Einfluss von anhaltender *Aldh1b1* Exprimierung auf den Vorgang der Progenitoren Differenzierung zu untersuchen, erschuf ich eine Mauslinie mit induzierbarer, konstitutiver Aldh1b1 Expression (ROSA26^{LSLAldh1b1}). Progenitoren mit kontinuierlicher Aldh1b1 Expression, vermieden die Differenzierung zum β-Zelltyp, was die Notwendigkeit der zeitlichen Abschaltung der Aldh1b1 Expression verdeutlicht.

Zusammenfassend liefert meine Arbeit aussagekräftige Belege für die Rolle von Aldh1b1 als metabolischer Regulator im Prozess der Progenitordifferenzierung und präsentiert einen Zusammenhang zwischen dem zellulären Stoffwechsel und der durch Chromatin-Zugänglichkeit vermittelten Regulation der Gentranskription. Dadurch, dass eine Aldh1b1 Inaktivität Defekte in sowohl embryonalen Progenitoren, als auch postnatalen β-Zellen verursacht, könnte das Enzym ein genetischer Risikofaktor für die Entstehung von Hyperglykämie und Diabetes mellitus darstellen. Das Verständnis der Mechanismen, die dem Prozess der Progenitordifferenzierung und der Entstehung von β-Zell Dysfunktionen zugrunde liegen, könnten somit zur Findung von neuartigen Therapien in der Behandlung von Diabetes mellitus beitragen.

Table of contents

List of Figures

List of Tables

List of Abbreviations

ATP citrate lyase	**ACLy**	Isocitrate dehydrogenase	**IDH**
Adenosine diphosphate	**ADP**	Kilodalton	**kDa**
α-ketoglutarate	**αKG**	Minute	**min**
Aldehyde dehydrogenase	**Aldh**	Mitochondrial membrane potential	**MMP**
Adenosine triphosphate	**ATP**	Multipotent progenitor cells	**MPC**
Assay for transposase accessible chromatin	**ATAC**	Maturity onset diabetes of the young	**MODY**
Bovine serum albumin	**BSA**	Mitochondrial DNA	**mtDNA**
Cytokeratin 19	**CK19**	N-acetylcysteine	**NAC**
Citrate synthase	**CS**	Nicotinamide adenine dinucleotide phosphate	**NAD**
4',6-5 diamidino-2-Phenylindole	**DAPI**		
		Nicotinamide adenine dinucleotide	**NADP**
Dolichos biflorus agglutinin	**DBA**	Neurogenin3	**Ngn3**
Dihydroxyacetone phosphate	**DHAP**	NK6 homeobox 1/2	**Nkx6.1/6.2**
Deoxyribonucleic acid	**DNA**	Oxaloacetate	**OAA**
DNA methyltransferase	**Dnmt**	Passage 3/5	**P3/5**
Embryonic day 14.5	**E14.5**	Postnatal day 10	**P10**
Extracellular matrix	**ECM**	Phosphate buffered saline	**PBS**
Ethylenediaminetetraacetic acid	**EDTA**	Pyruvate dehydrogenase	**PDH**
Epidermal growth factor	**EGF**	Pancreatic and duodenal homeobox	**Pdx1**
Electron microscopy	**EM**	Phosphohistone H3	**PH3**
Endoplasmic reticulum	**ER**	Pancreas transcription factor 1 subunit alpha	**Ptf1a**
Electron transport chain	**ETC**		
Fluorescence activated cell Sorting	**FACS**	Retinoic acid	**RA**
		Ribonucleic acid	**RNA**
Fructose-6-phosphate	**F6P**	Reactive oxygen species	**ROS**
Fetal calf serum	**FCS**	Real-time polymerase chain reaction	**RT-PCR\qPCR**
False Discovery Rate	**FDR**		
Fibroblast growth factor	**FGF**	S-adenosylhomocysteine	**SAH**
Glucose-1-phosphate	**G1P**	S-adenosylmethionine	**SAM**
Glycerol-3-phosphate	**G3P**	Solute carrier	**SLC**
Glucose-6-phosphate	**G6P**	SRY-box transcription factor 9	**Sox9**

Glyceraldehyde-3-phosphate	**GA3P**	Type 1 diabetes mellitus	**T1DM**
Green fluorescent protein	**GFP**	Type 2 diabetes mellitus	**T2DM**
Gene ontology	**GO**	TdT-mediated dUTP-biotin nick end labeling	**TUNEL**
Gene set enrichment analysis	**GSEA**	Tricarboxylic acid	**TCA**
Hour	**h**	Ultraviolet	**UV**
4-(2-hydroxyethyl)-1-piperazineethanesulfonic acid	**HEPES**	Wild type	**WT**
Human embryonic stem cells	**hESC**		

1. Introduction

1.1 Structure and function of the murine pancreas

The pancreas is a glandular organ that exhibits a dual, exocrine and endocrine, function, providing digestive enzymes, as well as hormones regulating blood sugar levels. With its actions in food conversion and glucose homeostasis, the pancreas affects the whole body and a disorder in a single compartment of the organ can cause serious diseases (Karpińska and Czauderna, 2022). The pancreas has been extensively studied, especially due to the metabolic disease diabetes which is of great clinical importance. Diabetes is caused by an insufficient production of the hormone insulin by pancreatic β-cells or by a cellular inability to react to it (DeFronzo et al., 2015; Katsarou et al., 2017). To gain a better understanding of the physiological and pathological processes of the disease, mice were widely used as a model organism due to major similarities of the murine pancreas to the human organ (Dolenšek et al., 2015).

The murine pancreas is anatomically positioned caudal to the stomach and encircled by the spleen, duodenum and proximal jejunum. It is spread throughout the mesentery and displays a soft and macroscopically diffuse composition (Dolenšek et al., 2015; Longnecker, 2021). Nonetheless, three different anatomical parts can be distinguished, namely the duodenal, gastric and splenic lobes, which are loosely separated by connective, lymphatic or adipose tissue (Levetan and Pierce, 2013; Longnecker, 2021; Figure 1.1).
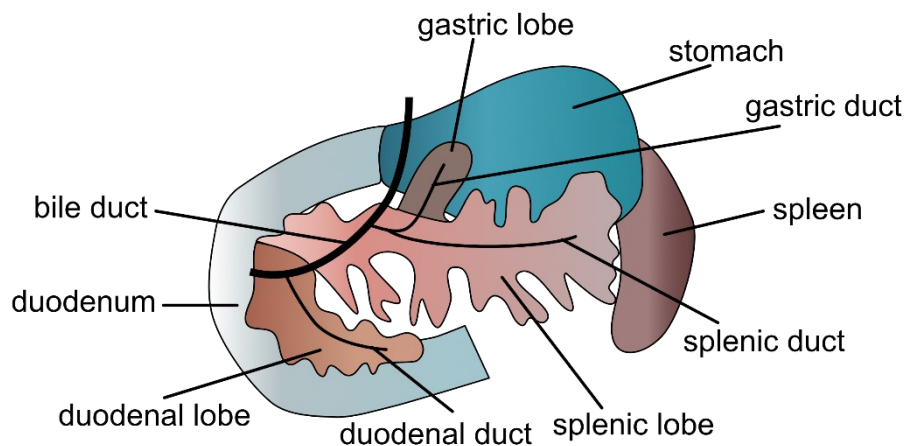
Figure 1.1: Anatomic structure and position of the murine pancreas. The pancreas is surrounded by the stomach, spleen, duodenum and jejunum and disperses throughout the mesentery. Macroscopically, three parts separated by connective, lymphatic or adipose tissue can be distinguished: the duodenal, gastric and splenic lobes. Digestive enzymes are collected by intercalated ducts that extent to the duodenal, gastric and splenic duct and eventually fuse with the bile duct that drains into the duodenum.

The histological composition of the different lobes remains very similar and displays only minor differences in the appearance of certain cell types. Within the lobes, the exocrine

part of the pancreatic epithelium is located, which is composed from small glandular lobules containing one major duct, arteries and structures called acini (Longnecker, 2021). An acinus consists of a layer of pyramidal acinar cells, arranged in a circular structure with apical-basal cellular polarity. The cytoplasm on the broad basal site of the acinar cell is enriched in RNA and an abundance of rough endoplasmic reticulum (ER) which serves the rapid production of digestive enzymes (Liggitt and Dintzis, 2018 Longnecker, 2021; Figure 1.2). These enzymes are stored in zymogen granules and transported to the small apical site of the acinar cell and released, in a tightly controlled manner, into the intra-acinar portion of the ductal system composed of centroacinar cells (Williams, 2006).

Centroacinar cells are simple squamous epithelial cells that form the connection between the intra-acinar cell compartment and the extra-acinar located intercalated ducts. The latter extend to the splenic, gastric or duodenal intra-lobular duct, which eventually merge and fuse with the common bile duct that drains into the duodenum (In't Veld and Marichal, 2010; Longnecker, 2021; Figure 1.1). The secretion of secretory granules from the acinar cells into the duct system is primarily controlled by stimulation of the vagal nerve and the release of gastrointestinal hormones which leads to a Ca^{2+}-driven exocytosis of the secretory granules (Husain and Thrower, 2009; Williams, 2006). Ducts and acinar cells form the exocrine part of the pancreas and account together for app. 98 % of the pancreas epithelium (Dolenšek et al., 2015).
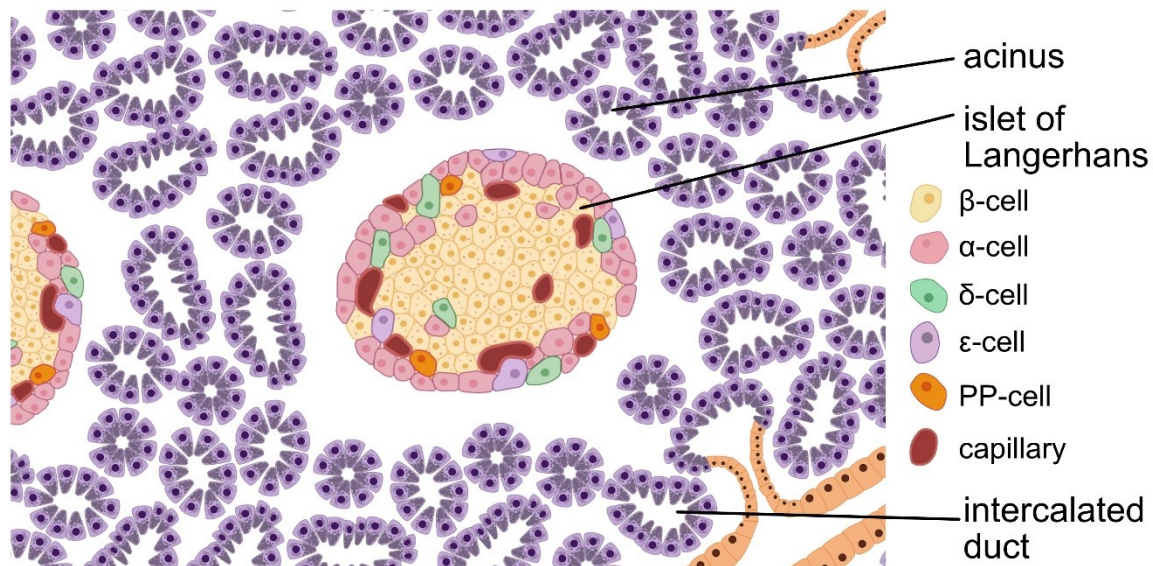
Figure 1.2: Microscopical structure of the murine pancreas. Exocrine cells form round structures called acini which are connected to the ductal system that transports the secreted digestive enzymes into the intestine. The islets of Langerhans sit in between the exocrine structures and harbor hormone producing cells that contribute to the blood glucose homeostasis. In the murine islet, β-cells form a mostly homogenic core whereas the other endocrine cells align in the periphery.

Interspersed among the exocrine lobules and ducts, surrounded by interstitial tissue, sit small organs of endocrine cells, the islets of Langerhans. They harbor hormone producing

cells, which make up 1-2 % of the pancreatic epithelium (In't Veld and Marichal, 2010). The core of the islet and approximately 65-80% of the endocrine population are insulin producing β-cells (Cabrera et al., 2006; Steiner et al., 2010). The latter show a segregation from the other endocrine cells which are gathered primarily in the periphery of the islet. The second largest population is made up by glucagon secreting α cells which correspond to 10–20 % of the islet mass, followed by somatostatin producing δ cells which correspond to less than 10 % of the islet cells. Lastly, ε cells and pancreatic polypeptide (PP) cells releasing ghrelin and pancreatic polypeptide, respectively, contribute with less than 1 % under normal conditions (Steiner et al., 2010; Figure 1.2). However, it has been shown that the murine pancreas exhibits a high structural plasticity depending on the physiological state, e.g., pregnancy, chronic hyperglycemia or obesity, in order to adapt to the changing needs of blood glucose regulation (Dolenšek et al., 2015).

β-cells play a central role in the maintenance of glucose homeostasis due to the secretion of insulin. The blood sugar-lowering hormone insulin is produced by pancreatic β-cells and is encoded by the *Ins1* and *Ins2* genes in the murine genome (Wentworth et al., 1986). The peptide hormone is first translated as proinsulin consisting of a 21 amino acid residue A chain, 30 amino acid residue B chain and the C-peptide, a 31 amino acid polypeptide that connects the two chains. During post-translational processing in the ER, the A and B chains are oxidized and consequently connected by cysteine disulfide bonds. The proinsulin is subsequently transported into secretory granules, where the final insulin is processed by cleavage of the C-peptide off the A and B chain (Fu et al., 2013; Petersen and Shulman, 2018; Figure 1.3). The secretory granules containing insulin are released through a complicated mechanism dictated by nutrients, hormones and neurotransmitters in order to keep the circulating glucose levels in a narrow physiological range. Nevertheless, glucose, which enters the β-cell through GLUT2 transporters, is the most important trigger of insulin secretion (Gilon and Henquin, 2001; Drucker and Nauck, 2006; Newsholme et al., 2014; Marchetti et al., 2017). Elevated levels of intracellular glucose lead to an increase in intracellular ATP levels, due to its breakdown via glycolysis and oxidative phosphorylation. Rising ATP levels will in turn cause a closure of ATP-sensitive potassium channels (K_{ATP}) and a consequent membrane depolarization. Consecutively, voltage-dependent Ca^{2+} channels open and inflowing Ca^{2+} triggers the secretion of secretory granules into intra-islet capillaries that are connected through a basement membrane with the β-cells (Newsholme et al., 2014; Burganova et al., 2021). An action potential in the islets is usually induced when glucose concentrations rise above the threshold of 4 mM, which subsequently causes a biphasic insulin secretion with a rapid first peak and a later appearing, prolonged second peak (Dean and Matthews, 1970; Ohara-Imaizumi et al., 2004). The first phase of insulin secretion, also referred to as triggering pathway, is a rapid release of insulin granules located in close proximity to the plasma

membrane, which is promoted by the initial calcium influx. In the second phase, known as the metabolic amplifying pathway, an increased sensitivity to the given calcium influx causes the recruitment of intracellular insulin granules to the membrane, which in turn facilitates another phase insulin secretion until euglycemia is reached (Kalwatt and Copp, 2017; Figure 1.3).
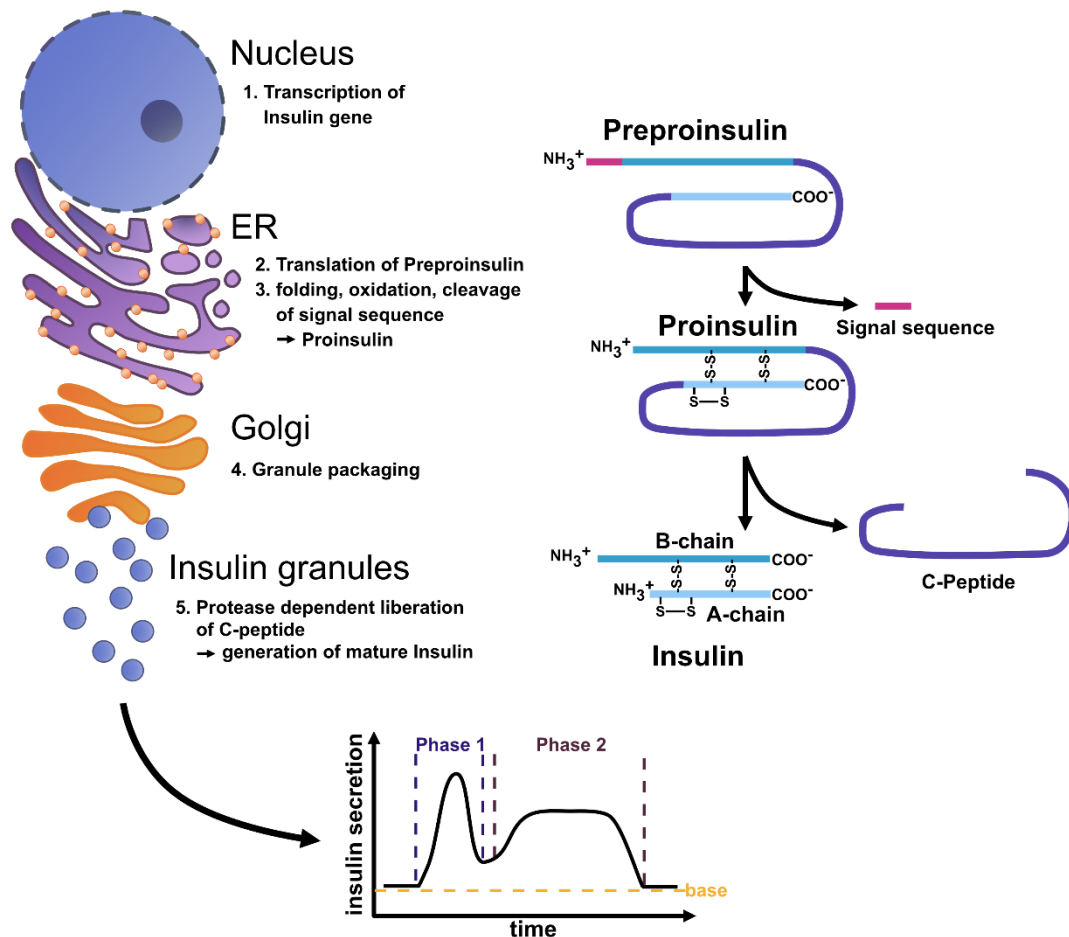
Figure 1.3: Biosynthesis and secretion of insulin. Upon transcription of the Ins1 or Ins2 gene in the nucleus, the mRNA is translated into the inactive precursor preproinsulin in the rough ER. Release of the signal peptide and folding as well as oxidation of the peptide causes the formation of proinsulin, which transits through the Golgi apparatus where it is packed into vesicles. Protease dependent liberation of the C-peptide results in the maturation of the insulin, which will be released in a biphasic manner upon arrival of metabolic signals.

In order to lower blood glucose levels, insulin binds in the target tissue to insulin tyrosine kinase receptors. This induces a receptor conformational change and auto-phosphorylation. Activation of the insulin receptor signaling triggers a phosphorylation cascade and eventually translocation of the GLUT-4 transporter to the cell surface to facilitate glucose uptake, as well as the activation of a transcriptional program supporting cell survival and growth (Fu et al., 2013). The actions of insulin after an increase of the blood glucose are crucial to promote an uptake of sugar into the cells for energy metabolism and to ensure normal tissue function. Moreover, keeping the blood glucose level in a narrow range prevents inflammation and

damage of the vascular system that could consequently lead to more severe diseases (Giacco and Brownlee, 2010; Karpińska and Czauderna, 2022).

Blood glucose homeostasis has to be ensured also during fasting states or conditions with high energy needs. This task is mainly carried out by the hormone glucagon, which is released by α-cells. Glucagon is a 29 amino acid peptide, catabolic hormone that opposes insulin actions. (Steiner et al., 2010; In't Veld and Marichal, 2010). In order to prevent hypoglycemia, α-cells take up circulating glucose via solute carrier family 2 member 1 (SLC2A1) to sense low glucose levels by a drop in the ATP/ADP ratio and a subsequent membrane polarization. The release of glucagon containing granules is, similarly to the β-cell mechanism, K_{ATP}-channel- and Ca^{2+}-dependent. At blood glucose concentrations under 5 mM, glucagon is secreted into the bloodstream via intra-islet capillaries to mobilize glucose from peripheral tissue (MacDonald et al., 2007; Quesada et al., 2008). At higher concentrations, increasing ATP levels lead to a membrane depolarization, which blocks glucagon release. Additionally, α-cell activity is also actively suppressed by insulin, the neurotransmitter γ-Aminobutyric acid (GABA) and Zn^{2+} ions (Franklin et al., 2005; Hellman et al., 2012).

Another hormone that participates in the modulation of the glucose homeostasis and insulin secretion is somatostatin. The 14-amino acid peptide hormone is produced by δ cells in the pancreas and was found to potently inhibit insulin, glucagon and pancreatic polypeptide release (Dubois, 1975; Brown et al., 1976). Somatostatin is known for its role in growth inhibition and is mainly produced by the hypothalamus. Therefore, the circulating blood somatostatin concentration was shown to be mostly independent from the pancreatic secretion, but somatostatin-induced regulation in islets was, in contrast, found to be strongly dependent on δ-cell action (Huising et al., 2018). Somatostatin is an important paracrine regulator of β-cell activity in islets. Its secretion is mainly induced by Urocortin 3, a peptide hormone that is co-released with insulin, but also by inputs from multiple other hormones, neurotransmitters, and nutrients. Therefore, δ-cells have a crucial function in the integration of diverse signals in order to avoid excess insulin secretion and to keep glucose levels in a physiological range (Li et al., 2007; DiGruccio et al., 2016). The hormone binds to somatostatin receptors 1 to 5 at neighboring target cells to induce G-protein-coupled receptor signaling. This negative feedback loop was found to be dysregulated in diabetes and suggests an essential role of somatostatin secretion in islet physiology (Huising et al., 2018).

The two cell types with the lowest contribution to the islet mass are ε-cells and PP-cells. ε-cells secrete the 28 amino acid peptide hormone ghrelin. The hormone is initially translated as the precursor preproghrelin that requires endoproteolytic and signal peptide cleavage in order to release mature ghrelin, which exists in an acylated or non-acylated state. Obestatin is a by-product of the cleavage of the ghrelin precursor (Sakataet al., 2019). All three products participate in processes such as regulation of Insulin release, cellular proliferation and growth

as well as improvement of insulin sensitivity (Dezakiet al., 2004; Granata et al., 2007; Sakata et al., 2019).

Lastly, pancreatic polypeptide is a 36-amino acid peptide produced by PP-cells (Kimmel, 1975). It plays an important role in the gut-brain-pancreas axis as it is associated with the reduction of appetite, exerts inhibitory functions in the gut and constrains glucagon secretion (Holzer, 2012; Aragón, 2015; Brereton, 2015).

Collectively, the pancreas is an organ that plays a central role in food digestion and energy metabolism. A multitude of cells such as acinar, endocrine and duct cells, but also arteries, veins, capillaries, lymph vessels, neural and stellate cells act in concert to ensure a tightly controlled function. Disruption of one or more parts can impair pancreas function and cause severe diseases such as diabetes, pancreatitis or cancer (Karpińska and Czauderna, 2022).

1.2. Diabetes mellitus type II and MODY: Causes, progression and treatments

Diabetes mellitus is a chronic metabolic disorder that is characterized by hyperglycemia and dysregulation of glucose, lipid and protein metabolism (DeFronzo, 2015). The International Diabetes Federation states that already 1 in 10 adults worldwide is living with diabetes and the prevalence is steadily rising. According to the World Health Organization, diabetes mellitus is one of the major causes of microvascular complications like blindness and kidney failure as well as macrovascular events, such as heart attacks and strokes. Up to 95 % of all diabetes patients are diagnosed with type 2 diabetes mellitus (T2DM), which is strongly promoted by a lack of physical activity and over-nutrition (Donath, 2014; DeFronzo et al., 2015). Thus, a healthy diet and maintaining normal body weight is an effective way to prevent or delay the onset of T2DM and all side effects of hyperglycemia (Nathan et al., 2007).

T2DM is usually preceded by a condition called pre-diabetes that is caused by the onset of insulin resistance in skeletal muscle, liver and adipose tissue. This phase is clinically defined by a slight increase of fasting glucose levels, impaired glucose tolerance, delayed first or second peak of insulin secretion and increased glycated HbA1c levels (Nathan, et al., 2007; Donath, 2014). Insulin resistance is often viewed as a result of chronic inflammatory processes caused by obesity, and adipose tissue was in this regard identified as main source of pro-inflammatory cytokines (Al-Ghamdi et al.,2022). The uptake of excessive nutrients into adipocytes causes stress in the ER and hypertrophy of the tissue, which in turn leads to increased cell death and hypoxia due to rapid tissue expansion. These processes are accompanied by the infiltration of macrophages that attempt to clear up the tissue from the apoptotic cells. All macrophages recruited to the adipose tissue show a classical proinflammatory phenotype and an active release of interleukins, such as IL-1β, which plays a

central role in the interruption of the insulin receptor substrate (IRS) signaling and, therefore, the induction of insulin resistance (Cinti et al., 2005; Donath and Shoelson, 2011). Inflammatory cues can impair Insulin signaling on different levels, for instance by upregulation of the negative regulator protein-tyrosine phosphatase 1B (PTP1B), direct IRS phosphorylation or IRS degradation via ubiquitination, which disrupts the signal transduction and causes decreased GLUT-4 translocation (Yaribeygi et al., 2018).

Insulin resistance can remain stable over a long period of time and may only slightly increase with age. Therefore, the transition from pre-diabetes to T2DM must be promoted by an additional factor, which is a progressive β-cell dysfunction. To overcome the effect of insulin resistance and as consequence of lasting hyperglycemia, β-cells initially increase their insulin secretion. In this phase, diabetes can still be efficiently counteracted by weight reduction and a diet that decreases the need for high insulin secretion. Otherwise, enduring hyperglycemia will harm islets and cause massive metabolic stress to the β-cells which will be followed by a rapid deterioration in their capacity for insulin secretion (Bonner-Weir and O'Brien, 2008). The reasons for the resulting β-cell dysfunction are diverse but inflammatory processes were determined as a crucial player of this process. For instance, lasting hyperglycemia increases glucose breakdown in the islet, which causes the production of high reactive oxygen species (ROS) in the mitochondria. ROS increases the cellular stress and activates the inflammasome and caspase 1 signaling. The subsequent IL-1β response triggers an infiltration of immune cells into the islets. Moreover, ER stress due to rapid insulin production, amyloid polypeptide deposition and obesity induced endocannabinoid production in the liver cause additional IL-1β secretion and immune cell recruitment (Harding and Ron, 2002; Hull et al., 2004; Robertson et al., 2004). The infiltration of the islet with proinflammatory immune cells will eventually lead to impaired β-cell survival as well as function. It is assumed that inflammatory processes in the islet promote β-cell dedifferentiation and loss of the β-cell identity, which results in decreased insulin production. T2DM will manifest when the insulin production is not sufficient anymore to overcome the insulin resistance (Böni-Schnetzler et al., 2008; Nordmann et al.,2017).

However, diabetic patients often have a history of the disease in their family and genetic analyses could determine hereditary factors that contribute to its establishment. Genome-wide association studies (GWAS) found more than 100 risk variants that are associated with T2DM (Dupuis et al., 2010, Scott et al., 2017). Most of them were identified in intronic regions, suggesting that they participate in the process of transcriptional regulation. Other loci could be directly linked to a gene which was associated with fasting glucose levels such as *ADCY5, PROX1, SLC2A2, GCKR* and others (Dupuis et al., 2010, DeFronzo, 2015). Nonetheless, a high genetic risk alone isn't an accurate predictor of T2DM development later in life. Studies indicated a direct link between increased BMI and insulin resistance that was rather independent from a low or high genetic risk. However, patients with a high genetic risk were

not able to compensate for insulin resistance and manifested T2DM more quickly (Lyssenko et al., 2008).

Therefore, T2DM is a multifactorial disease and genetic as well as environmental factors can increase the risk of chronic hyperglycemia establishment. Being overweight, physical inactivity, a habit of smoking and a genetic predisposition constitute the major risk factors and should be considered during treatment (DeFronzo, 2015). The basis of every T2DM therapy therefore includes the establishment of a healthier lifestyle but also glycemic control supported by medication. Available drugs are metformin which inhibits the hepatic gluconeogenesis, sulfonylurea which increase insulin secretion by blocking the inflow of potassium into the β-cell or the peroxisome proliferator-activated receptor (PPAR) agonist thiazolidinedione, which enhances insulin sensitivity by improving the glucose metabolism etc. The usage of insulin is implemented when all measurements mentioned before fail to attain glycemic control (Feingold, 2000). Nevertheless, these treatments do not constitute a cure and patients have a lower life expectancy due to vascular complications caused by T2DM. Better understanding how different aspects such as genetics, lifestyle and the immune system contribute to the onset of hyperglycemia and T2DM could help in the discovery of more advanced and personalized therapy for each patient (DeFronzo, 2015, Scott et al., 2017; Ling and Rönn, 2019).

A disorder often misdiagnosed as type 1 or type 2 diabetes is maturity onset diabetes of the young (MODY). It is caused by a maturation defect of the β-cells, or by mutations in enzymes involved in glucose sensing and, typically, has an early onset. MODY is a monogenic disorder with autosomal dominant inheritance usually causing haploinsufficiency (Vaxillaire et al., 1995). In contrast to type 1 or type 2 diabetes, there are no signs of autoimmune involvement or insulin resistance, and hyperglycemia is usually diagnosed before the age of 25. The most common types of MODY are caused by mutations in the genes *GCK, HNF1A, HNF4A* and *HNF1β*. As of today, 14 genes could be associated with MODY (Anık et al., 2015). However, it is a genetically heterogeneous condition without clear mutational hotspots within the genes (Santana et al., 2019).

A mild form of MODY is caused by defects in the *GCK* gene (MODY 2) which encodes glucokinase, an enzyme involved in the first rate-limiting step of glycolysis. Missense mutations can diminish catalytic activity, allosteric regulation, substrate specificity, enzyme stability or ATP binding ability. As a consequence, glucose metabolism is impaired and the glucose sensitivity of β-cells is reduced (Liang et al., 1995; Fajans et al., 2001). This can cause a mild increase in fasting glucose levels, or even a decrease due to hepatic overcompensation (Steele et al., 2010; Anık et al., 2015). It is treated by diet adaption only (McDonald and Ellard, 2013).

A more severe form of MODY is caused by a *HNF1α* mutation (MODY3). Up to date, more than 300 gene variants, which can cause a weakening of the promoter activity, impaired complex formation and DNA binding, were recorded (Valkovicova et al., 2019). *HNF1α* encodes a critical transcription factor for *INS* and *GLUT2* expression and regulates the expression of several other transcription factors in the process of β-cell differentiation during embryonic pancreas development. Thus, *HNF1α* mutation results in low fasting insulin levels and impaired glucose sensing. As a result, hyperglycemia can lead to micro- and macrovascular complications and requires to be tightly controlled (Pearson et al., 2003). MODY1, which is caused by defects in the *HNF4α* gene, results in comparable clinical symptoms as MODY3. *HNF4α* encodes for a transcription factor which regulates the expression of HNF1α (Yahaya and Ufuoma, 2020). Missense mutations in the gene can cause disruption of DNA, ligand or coactivator binding, decreased protein stability or dimerization ability, which eventually results in impaired insulin secretion response (Fajans et al., 2001; Pearson et al., 2005; Singh et al., 2019). Both, MODY1 and 3, are usually treated with sulfonylurea which stimulates glucose independent insulin secretion (McDonald and Ellard, 2013).

Another frequent type of MODY is caused by mutations in *HNF1β* (MODY5), which is expressed during early development of the pancreas, kidney, liver, and genital tract. Mutations in this gene can cause defects in all those organs and often lead to hyperglycemia independent renal failure and β-cell dysfunction (Wang et al., 2017). In order to prevent microvascular complications, insulin substitution is frequently employed to counteract hyperglycemia (McDonald and Ellard, 2013).

Other rare mutations causing MODY are found in genes encoding for pancreatic and duodenal homeobox 1 (*PDX1*), neurogenic differentiation 1 (*NEUROD1*), krüppel-like factor 11 (*KLF11*), insulin (*INS*), carboxyl ester lipase (*CEL*), paired box gene 4 (*PAX4*) and more. However, it is expected that several genes involved in MODY have not been discovered yet, and up to approximately 80 % of all MODY cases are initially diagnosed as type 1 or type 2 diabetes (Anık et al., 2015; Juszczak et al., 2016; Urbanová et al., 2018). Nevertheless, an early and accurate identification is crucial in order to apply the best treatment for the patient. The diagnosis of MODY relies substantially on family history and genetic testing. Therefore, further research to determine diagnostic biomarkers and additional types of MODY is necessary (Fajans et al., 2001).

1.3. Development and differentiation of the murine embryonic pancreas

The early embryonic pancreas develops from the innermost germ layer, the endoderm. Ectoderm, mesoderm and endoderm appear and segregate during gastrulation, during which nodal growth factor signaling is responsible for endodermal lineage commitment. As a consequence of subsequent developmental tissue remodeling processes, the endodermal epithelium transforms into the primitive gut tube, which will later on be regionalized into foregut, midgut, and hindgut (Zaret, 2008; Pan and Wright, 2011). From around E8.5 and onwards, sonic hedgehog (Shh) signaling is excluded from the area of the early pancreatic endoderm mainly through activin-βB and fibroblast growth factor 2 (FGF2) signaling, which originate from the notochord. (Hebrok et al., 1998). Inhibition of Shh allows the expression of pancreatic genes, such as *Pdx1*, but also Pancreas transcription factor 1 subunit alpha (*Ptf1a*) and SRY-Box Transcription Factor 9 (*Sox9*) are among the first appearing markers. Consequences of a missing expression of those transcription factors were investigated using knockout mouse models. Whereas neonatal *Pdx1* -/- mice suffer from pancreas agenesis, causes a loss of Ptf1a complete absence of exocrine tissue. Both genetic models are lethal after birth and the animals die within the first postnatal days. Inactivation of Sox9 in pancreas progenitors causes pancreatic hypoplasia and depletion of the progenitor pool. Thus, the pancreatic anlage is defined by the co-expression of Pdx1, Ptf1a and Sox9 (Jonsson et al., 1994; Krapp and Knöfler et al., 1998; Seymour et al., 2007). This area, which will later be evident by pancreatic bud outgrowth, consists of multipotent progenitor cells (MPC) that can give rise to all cell types of the pancreas (Romer and Sussel, 2015). Additional markers that are expressed in the MPCs are GATA Binding Protein 4/6 (Gata4/6), Foxa1/2, transcription factor 2 (Tcf2), one cut homeobox 1/2 (Onecut 1/2), hairy and enhancer of split 1 (Hes1), prospero homeobox 1 (Prox1), and motor neuron and pancreas homeobox 1 (Mnx1); however, these are less specific for the pancreatic fate and can be also detected in other regions during this developmental stage (Shih and Wang et al., 2013).

The period between E9 and E11, called primary transition, is characterized by expansion and rearrangement of the pancreas epithelium, which leads to the outgrowth of a dorsal bud at E9, whereas a ventral bud appears, locally separated, at around E9.5 (Edlund, 2002; Romer and Sussel, 2015). The following developmental program is guided by tightly controlled cues of FGF, Bone Morphogenetic Protein (BMP), Wnt, retinoic acid (RA), sonic hedgehog (Shh), and Notch signaling (Edlund, 2002, Zorn and Wells, 2010; Shih and Wang et al., 2013). Both buds intermingle with the surrounding mesenchyme and paracrine signaling, especially derived from the mesenchyme, notochord as well as endothelial cells, has a crucial impact on the early development by transmitting pro-proliferative cues (Bhushan et al., 2001;

Lammert et al., 2001, Edlund, 2002). Other signals from the surrounding tissue have to be suppressed in order to maintain a pancreatic fate. The ventral bud for instance, develops in close proximity to the liver and, in order to escape cues of that developmental program, a movement of the ventral lateral foregut endoderm is necessary to escape hepatic fate signaling (Bort et al., 2004; Pan and Wright, 2011). The primary transition is characterized by a rapid proliferation of the MPCs and the appropriate number of progenitor cells is generated, which will also define the ultimate organ size (Stanger et al., 2007). The primary transition is morphologically evident by the elongation of both pancreatic buds and the beginning of a branched tubular structure formation. A gut rotation initiates the eventual fusion of the dorsal and ventral pancreatic bud, which is completed at around E12.5 and marks the end of the primary transition (Shih and Wang et al., 2013).

The secondary transition begins at E12.5 when the MPCs take the first steps towards differentiation. As a consequence of lineage commitment and rearrangement processes, the tubular structure of the pancreas is remodeled into a highly branched network. Furthermore, the tip and trunk parts of the epithelium segregate due to the onset of MPC differentiation, a process that is actively shaped by Notch signaling. In the outer tip cell layer, Notch signaling is inhibited, allowing continued Ptf1a expression and the induction of c-Myc, and carboxypeptidase1 (Cpa1) expression. Tip cells will later differentiate into the acinar cells. Conversely, Notch signaling promotes the expression of NK6 homeobox 1/2 (Nkx6.1/6.2), Sox9, Tcf2, Onecut-1, Prox1 and Hes1 in the inner trunk compartment. Those cells will give rise to hormone producing endocrine and ductal cells. Active cross-repressive interactions of the transcription factors Nkx6.1/Nkx6.2 and Ptf1a allow the separation of the lineage restricted progenitors and repression of alternative developmental programs (Schaffer et al., 2010).

The acinar differentiation is shaped by the key regulator Ptf1a, which interacts with a basic helix-loop-helix E protein and a Recombination signal binding protein (Rbp) subunit, either Rbp-j or Rbp-jl, to form a hetero-oligomeric protein complex PTF1. Consequently, the active complex will bind to transcriptional enhancers to activate acinar gene expression and to guide the establishment of the acinar phenotype (Beres et al., 2006; Shih and Wang et al., 2013). The expression of Ptf1a and Rbp, on the other hand, is affected by the orphan nuclear receptor Nr5a2, which is a direct target gene of Ptf1a. Absence of Nr5a2 leads to incomplete acinar cell differentiation (Hale et al., 2014). Moreover, another central transcription factor of the acinar lineage is Mist1, which plays a dual role in the proliferation control of progenitor cells and in the coordination of the terminal differentiation (Jia et al., 2008). Most acinar cells have undergone differentiation by E15.5 and a subsequent expansion of the acinar cell pool relies, therefore, on proliferation of the differentiated cells (Shih and Wang et al., 2013).

MPCs in the trunk compartment become bipotent progenitors, which can give rise to either endocrine or ductal cells. In order to repress endocrine differentiation, Notch

signaling induces the expression of Hes1, a repressor of the pro-endocrine regulator Ngn3, in duct progenitors, which will in turn retain the expression of *Sox9*, *Tcf2*, *Onecut-1*, *Hes1*, *Prox1*, and *Glis3*. Even though those transcription factors define bipotent progenitors in earlier stages, they become restricted to the ductal lineage in the course of differentiation (Shih et al., 2012). The subset of MPCs inhibiting Notch signaling, and therefore maintaining Neurogenin3 (Ngn3) expression, proceed towards endocrine differentiation. Ngn3 loss of function was shown to cause a complete absence of all endocrine lineages in the pancreatic epithelium, as well as a loss of the expression of islet development regulators such as Isl1, Pax4, Pax6, and NeuroD in pancreas precursors (Gradwohl et al., 2000). As soon as bipotent progenitors have undergone endocrine commitment, they rapidly induce expression of the Ngn3 target gene *Snail2*, a transcription factor that facilitates tissue migration in a process called epithelial to mesenchymal transition. Consequently, cells with a high Ngn3 expression escape the trunk domain, in order to form islets (Pan and Wright, 2011). Interestingly, the segregation into different endocrine lineages seems to be temporally restricted. Experiments with temporally induced *Ngn3* expression in *Pdx1*^{+} cells showed that α cells appear preferentially at the earliest induction time point, whereas β- and δ-cells differentiated at later induction points and PP-cells were the last islet cell type to appear (Johansson et al., 2007). Furthermore, endocrine cells need to go through a network of transcriptional switches in order to promote one differentiation program whilst repressing another one. For instance, key determinants of β-cell commitment are Pax4, Pdx1 and Nkx6.1. A forced expression of those transcription factors would promote β-cell fate in endocrine progenitors, whereas Arx induction favors α-cell identity and a cross-inhibitory interaction of Arx and Pax4 stabilizes the different transcriptional programs (Collombat et al., 2003; Henseleit et al., 2005; Gannon et al., 2008). During the process of differentiation, endocrine progenitors still exhibit a certain plasticity and ectopic expression of key lineage transcription factors can cause a lineage switch (Collombat et al., 2007; Collombat et al., 2009; Yang et al., 2011). However, differentiated endocrine cells have limited lineage plasticity, suggesting that transcription factors in the final stages of endocrine development interact with chromatin modifying enzymes in order to silence genes belonging to different cell types, therefore stabilizing cellular identity (Yang et al., 2011; Shih and Wang et al., 2013). At the end of the secondary transition, the pancreas shows the topological morphology of the mature organ with highly branched ductal system, connecting to the acinar units and hormone producing cells arranged in islets (Shih and Wang et al., 2013). Tightly controlled repression and activation of transcription factors (Figure 1.4) is crucial in the course of progenitor differentiation into fully mature β-cells and many mechanisms involved in this process remain elusive (Theis and Lickert, 2019). Up to date, all attempts to recreate the process of β-cell differentiation under cell culture conditions have not provided cells that show the same functionality as primary β-cells. However, β-cell replacement by transplantation of *in vitro*

differentiated human embryonic stem cells (hESC) is a major hope in the treatment of severe diabetes and partial failure of the current differentiation procedures is due to a limited understanding of the underlying mechanisms. Thus, a better insight into the processes of β-cell differentiation could clearly benefit to improve protocols to generate functional mono-hormonal β-cells (Romer and Sussel, 2015).
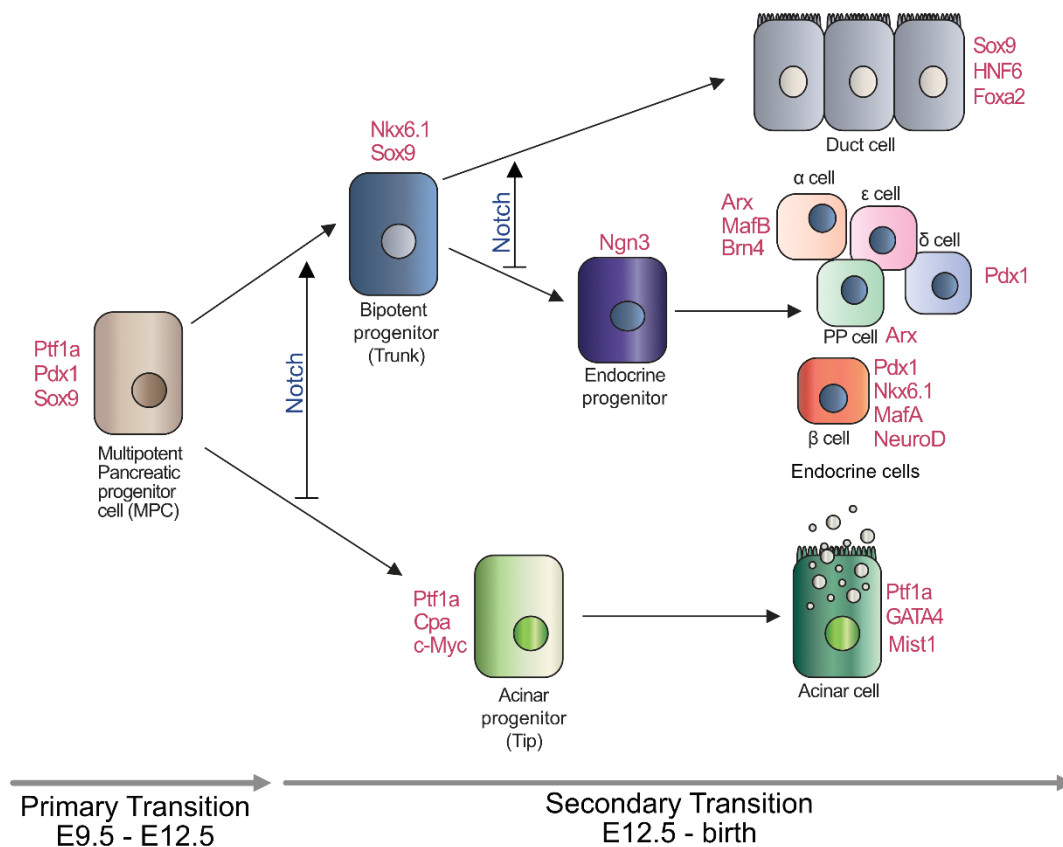
Figure 1.4: Differentiation processes in the embryonic development of the murine pancreas. The pancreas epithelium first appears around E9 consisting of MPCs characterized by the expression of Ptf1a, Pdx1 and Sox9. During the secondary transition, the tip and trunk domains segregate and active Notch signaling promotes formation of bipotent progenitors in the trunk compartment, which will later differentiate into the ductal or endocrine lineage. Progenitor cells in the tip domain repress Notch signaling and will eventually give rise to acinar cells. Final lineage commitment of all pancreatic cell types is guided by a complex transcription factor and signaling network.

1.4. Regulation and dynamics of epigenetic modifications in the process of β-cell differentiation

The role of epigenetic regulation in the process of differentiation has long been underappreciated but several studies suggest that the establishment of epigenetic modifications actively affects gene expression and stabilizes genetic programs. During the last few years, the importance of epigenetic regulation on transcriptional mechanisms has

gradually gained attention in the field of stem and progenitor cell maintenance and differentiation (Arnes and Sussel, 2015; Allis and Jenuwein, 2016).

The term epigenetics describes the changes in the phenotype of a cell that are caused by chromatin modification and rearrangement without altering the DNA sequence itself. The first mechanism involved in those processes is DNA methylation. Hereby, a methyl group is transferred onto the nucleotide cytosine to form 5-methylcytosine, a repressive chromatin mark (Figure 1.5). Methylation of DNA is followed by the recruitment of proteins which block transcription factor binding and therefore, inhibit gene expression (Moore et al., 2013). Regulation of DNA accessibility is further supported by a second mechanism contributing to epigenetic regulation, namely histone modifications. Histones are globular proteins that are
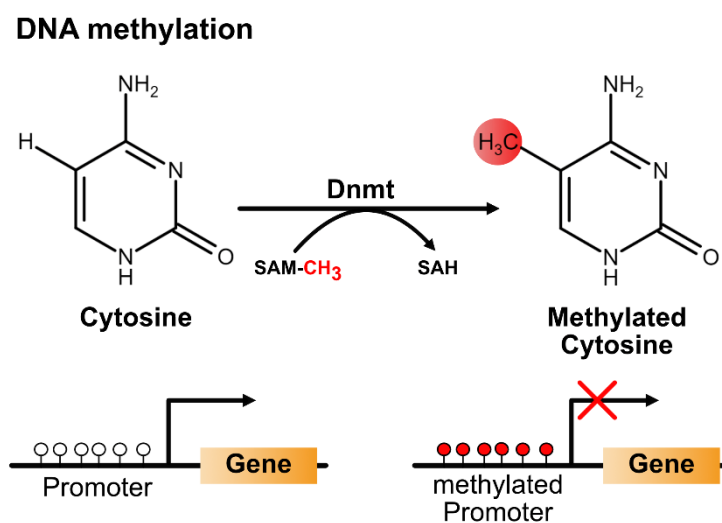
DNA methylation

Figure 1.5: DNA methylation. Methylation of the C5 position of cytosine is an epigenetic pattern generated by DNA methyltransferases (Dnmts). Dnmts use S-adenosylmethionine (SAM) as a methyl donor to catalyze the reaction and produce S-adenosylhomocysteine (SAH) as a byproduct. If the DNA methylation is located in a promoter region it is usually associated with transcriptional repression.

necessary for the packaging of DNA and can promote or restrict transcription through the recruitment of additional proteins. To that end, their N-terminal tails undergo posttranslational modification such as methylation, acetylation, phosphorylation, ubiquitination, ADP-ribosylation, sumoylation and glycosylation (Kaimala et al., 2022), which can be recognized by the so-called reader proteins. The type of histone modification determines the recruitment of diverse effector proteins that determine chromatin compaction, nucleosome dynamics, and transcription levels (Bannister and Kouzarides, 2011; Zhao and Shilatifard, 2019).

Histone modifications contribute actively as well as dynamically to the process of pancreas progenitor differentiation and β-cell identity (Campbell and Hoffman, 2016). Genome wide studies showed that promoter regions of lineage regulators in embryonic stem and progenitor cells carry bivalent histone marks which are activating (tri-methylation at the 4th

lysine of histone H3; H3K4me3) and repressive (tri-methylation at the 27th lysine of histone H3; H3K27me3; Figure 1.6).
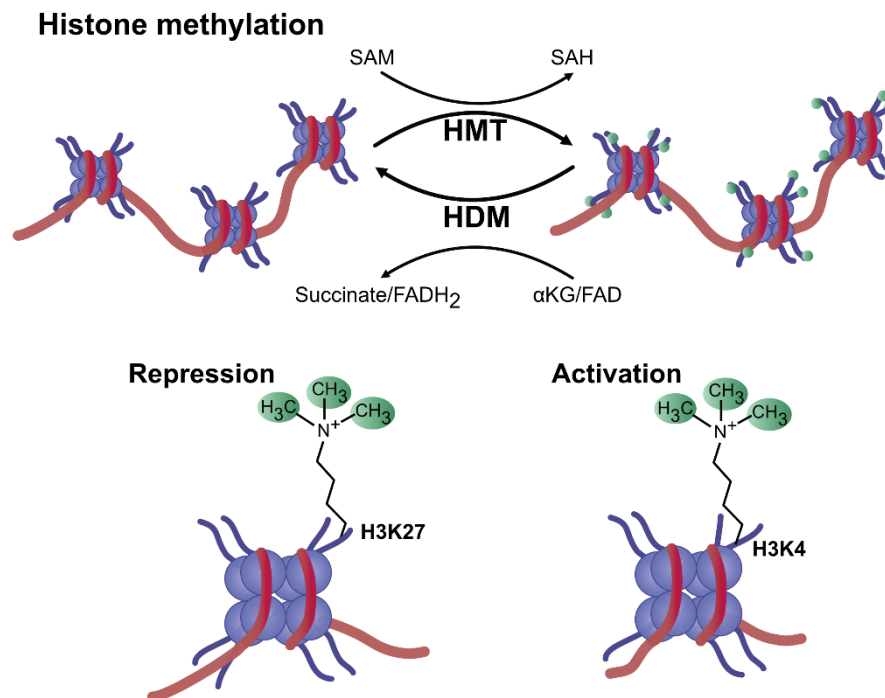
Figure 1.6: Histone methylation and demethylation. Catalysis of the addition or removal of methyl groups to the N-terminal tails of histones is either mediated by histone methyltransferases (HMTs) or histone demethylases (HDMs). HMTs use SAM as cofactor to transfer methyl groups to arginine or lysine residues of the histone tails. These post translational modifications can have a repressive or activating effect on the transcriptional activity, depending on the number and position of the methyl groups. Reversal of this reaction is catalyzed by HDMs. LSD1 domain demethylases utilize FAD and the Jumonji C domain demethylases α-Ketoglutarate (α-KG) to realize the reaction.

These counteracting histone marks leave the promoter in a poised state, which enables rapid activation and facilitates the switch between self-renewal and differentiation. In the endodermal tissue for instance, these epigenetic patterns are observed at promoter regions of Gata6 and Pdx1 (Mikkelsen et al., 2007). H3K27me3 histone demethylases such as Kdm6a (Utx) and Kdm6b (Jmjd3) can remove repressive histone marks, leading to the activation of poised genes. Kdm6a and Kdm6b are demethylases that play an important role in the process of early endodermal ESC differentiation. Kdm6b aids in this process by priming poised chromatin sites of the key endoderm lineage regulator Eomes, for later activation by Activin signaling. Simultaneous knockdown of Kdm6a and Kdm6b causes an impairment of endoderm differentiation, which can be rescued by sequential treatment with Wnt inhibitors. Thus, both proteins together modulate Wnt signaling in consecutive developmental stages, which shows that epigenetic processes contribute to the integration of signaling events (Kartikasari et al., 2013; Jiang et al., 2013). Epigenetic modifications can favor a genetic program of a specific lineage in ESCs, for instance hepatic cell fate is promoted by p300-dependent histone

acetylation. In order to avoid liver fate, p300 activity is reduced in early pancreas progenitors due to the restriction of BMP signaling (Xu et al., 2011). Early pancreas development is also regulated by and is dependent upon DNA methylation. Loss of Dnmt1, the most abundant DNA methyltransferase (Dnmt) in mammals, leads to pancreas agenesis due to cell cycle arrest of progenitor cells in the G2/M phase and subsequent apoptosis. Dnmts are responsible for the maintenance of gene silencing during development and a deletion in pancreas progenitors was shown to cause a de-repression of p53 followed by growth arrest (Georgia et al., 2013).

During later development, the pancreatic lineage is already established, and multipotent progenitors start, in the course of the secondary transition, to differentiate towards distinct pancreatic cell lineages. To that end, genetic programs related to rapid proliferation are silenced, while lineage specific functions are activated. During endocrine fate decision, repressive H3K27me3 domains, that are established by histone-methyltransferases, increase in number. A prominent enzyme catalyzing this reaction in pancreas development is the enhancer of zeste homolog 2 (EZH2), a component of the Polycomb Repressive Complex 2 (PRC2), which is involved in developmental gene silencing. EZH2 restrains the induction of endocrine differentiation by the addition of methyl groups to H3K27 to key endocrine and β-cell transcription factor genes and is therefore involved in the developmental timing of differentiation. A deletion of *EZH2* causes a premature differentiation as well as an increase in endocrine progenitors and eventually β-cells (Xu et al., 2014). Another epigenetic reader, that initially restrains endocrine commitment, is bromodomain extra-terminal protein (BET). BET binds to acetylated lysine tails and acts as a scaffold for the recruitment of transcription factors and chromatin organizers to modulate transcriptional activity. Inhibition of BET causes an increase in Ngn3 progenitors (Huijbregts et al., 2019). These two examples showcase the importance of timing in the course of differentiation and the active participation of epigenetic regulation in this process. EZH2 and BET initially block endocrine development to inhibit premature lineage induction and to precisely orchestrate developmental processes. As soon as endocrine fate is promoted, repressive histone marks need to be removed from key transcription factors of endocrine differentiation, a process in which histone demethylase JMJD3 is actively involved. This enzyme participates in the developmental transition from Ngn3 low to Ngn3 high progenitors (Yu et al., 2018). Subsequently, endocrine fate and lineage ratios are established, a process that strongly depends on the activity of histone deacetylases (HDACs). HDACs remove histone acetylation from lysine residues and induce a compaction of chromatin, which in turn represses RNA polymerase binding. More specifically, class IIa HDACs are considered critical developmental regulators due to their ability to stabilize cell fate decisions by shutting down genetic programs of alternative lineages (Park and Kim, 2020). During endocrine specification, expression of HDAC4, -5, and -9 is restricted to β- and δ-cells. Loss of HDAC5 and HDAC9 resulted in an increase of β-cell mass, whereas δ-cells numbers

increase dramatically in mice lacking *HDAC4* and *HDAC9*. Overexpression of the HDACs leads to a decrease in the respective lineages, which suggests that these histone modifiers

Histone acetylation
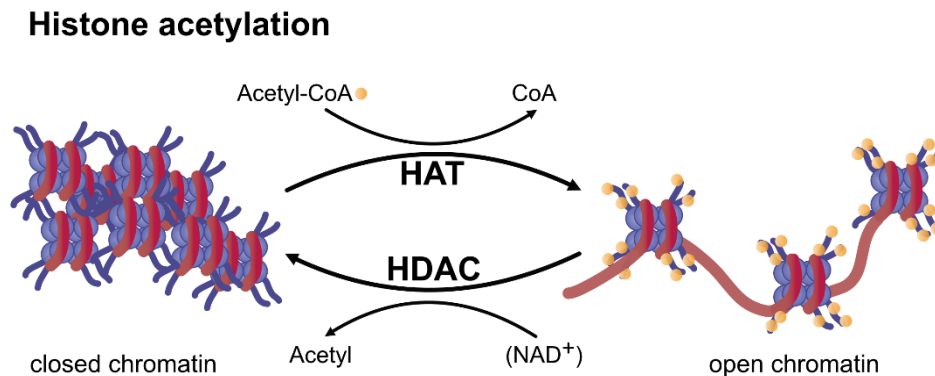
Figure 1.7: Histone acetylation and deacetylation. Histone acetyltransferases (HATs) or histone deacetylases (HDACs) catalyze either the addition or the removal of an acetyl group. HATs use acetyl-CoA as a cofactor to acetylate lysin residues on N-terminal histone tails. Acetylation removes the positive charge of the histones and are associated with chromatin de-compaction. The removal of acetyl modification from the histone tails is catalyzed by HDACs. Members of the sirtuins family need additionally an available pool of NAD$^+$ in order to catalyze the reaction.

actively control the establishment of endocrine lineage ratio, which in turn is regulated by the total level of HDAC expression (Lenoir et al., 2011). Simultaneously to the progressing islet cell maturation, *Ngn3* promoter domains display an increase of H3K27me3 marks, which is in concordance with Ngn3 downregulation in differentiating endocrine cells. Surprisingly, highly transcribed loci of islet hormones show only sparsely active histone modifications, which suggests the existence of another regulatory mechanism. It has been proposed that transcriptional regulation of islet lineage specific genes is controlled by epigenetic activation of key transcription factors such as *Pdx1* in β-cells (Bhandare et al., 2010; Kaimala et al., 2022). Moreover, β-cells show a high number of genes with monovalent epigenetic marks, which means that they carry either activating or repressive modifications. On the contrary, α-cells maintain many bivalent marks, which seems to give them a higher plasticity than β-cells (Bramswig et al., 2013). Even though mature β-cells might appear less plastic on an epigenetic level, their identity and functionality have to be actively maintained. Therefore, key lineage regulators recruit epigenetic effectors to preserve the transcriptional profile. For instance, α-cell fate is usually restrained in β-cells by Dnmt1-mediated hypermethylation of the *Arx* promoter and when this process fails, a conversion into α-cells and glucose intolerance is the consequence (Dhawan et al., 2011). In mature β-cells, this state of *Arx* repression is maintained by Nkx2.2 dependent Hdac1 and Dnmt3a recruitment, which keep this key α-cell fate regulator silenced. Accordingly, a disruption of this complex resulted in β- to α-cell conversion too (Papizan et al., 2011).

Collectively, all the above indicate a critical role of dynamic epigenetic regulation throughout the process of β-cell differentiation and in the maintenance of β-cell identity. Recent studies also suggest that epigenetic changes may be involved in the development of metabolic disorders like T1DM and T2DM (Kaimala et al., 2022). Transcriptional and epigenetic regulation are tightly interconnected and should be considered as intertwined in the process of differentiation.

1.5. The influence of metabolic adaption on stem and progenitor cell maintenance and differentiation

Due to the necessity of the availability of specific metabolites to set up epigenetic modifications, metabolic fluxes are, recently, receiving increasingly more attention. Several studies suggest an active role of metabolism in cell fate and epigenetic transitioning, rendering it an interesting subject in regenerative research.

Metabolic fluxes are dynamically regulated in order to facilitate nutrient utilization to generate biomass and energy, depending on the cells specialized function. In the very early embryonic development, blastomere cells rely on oxidative metabolism due to the abundance of maternal mitochondria. During the first round of cell divisions, mitochondria segregate and the copy number of mitochondrial DNA (mtDNA) per cell decreases rapidly. In this stage, the mitochondria are undeveloped with truncated cristae, and the initial oxidative period ends around the time of the implantation of the oocyte into the hypoxic uterine wall (Folmes et al., 2013). As a consequence, glycolysis is then primed in blastocyst cells by c-myc activation (Cao et al., 2015). The glycolytic breakdown of glucose can deliver a high amount of energy and NAD(P)H, from the parallel-running pentose phosphate pathway, to support rapid proliferation. Under a constant glucose supply, glycolysis fullfills energy demands as well as the need for nucleotide building block and overcomes the minimal oxidative capacity of the cells (Zhang et al., 2018). Interestingly, reprogramming of cells back to pluripotency includes a metabolic switch to a glycolytic metabolism, and inhibition of mitochondrial respiration promotes stemness (Folmes et al., 2011; Varum et al., 2009). Other studies have shown that block of glycolysis strongly reduces the proliferative capacity of ESCs (Kondoh et al., 2007). After this primary phase of ESC proliferation and tissue expansion, progressive downregulation of stemness genes and induction of differentiation follows, which is accompanied by the initiation of mtDNA replication (Chung et al., 2007). Promotion of mitochondrial maturation and biogenesis allows the metabolic switch from glycolysis towards oxidative phosphorylation. Differentiated cells have a lower demand for replication and anabolic reactions but are in need of a high amount of energy to fulfill lineage-specific functions. Therefore, they benefit from exploiting the more efficient oxidative metabolism (Figure 1.8), producing 36 ATP molecules per glucose, as compared to 2 ATP molecules from glycolysis (Tsogtbaatar et al., 2020). Part

of the mitochondrial metabolism is the TCA cycle, which is interconnected with other metabolic pathways, including oxidative phosphorylation and lipid oxidation. Moreover, it provides precursors of amino acids, intermediates for biosynthetic processes and the coenzymes NADH/FADH$_2$ (Martínez-Reyes and Chandel, 2020). The latter delivers electrons which are fed into the electron transport chain (ETC) of the oxidative phosphorylation to generate an electrochemical gradient by promoting the transport of protons from the mitochondrial matrix into the intermembrane space. Protons flow back down their electrochemical gradient through ATP synthase, which produces ATP (Tsogtbaatar et al., 2020). Mitochondrial metabolism is a major characteristic of differentiating cells and inhibition of the oxidative phosphorylation was even shown to impair ESC differentiation, whereas inhibition of key enzymes of glycolysis promotes myogenic differentiation (Zhang et al.,2011; Bracha et al., 2010).

A byproduct of the oxidative metabolism are ROS, which can, if not scavenged, act as a signaling molecule by modifying redox-sensitive target molecules. ROS signaling has been connected with differentiation induction via p38 MAPK signaling, whereas inhibition of ROS production reversed this effect (Crespo et al., 2010; Tormos et al., 2011). This mechanism could be directly linked to the mitochondrial metabolism by overexpressing the Uncoupling protein 2 (UCP2), which prevents glucose oxidation and consequently blocks hESC
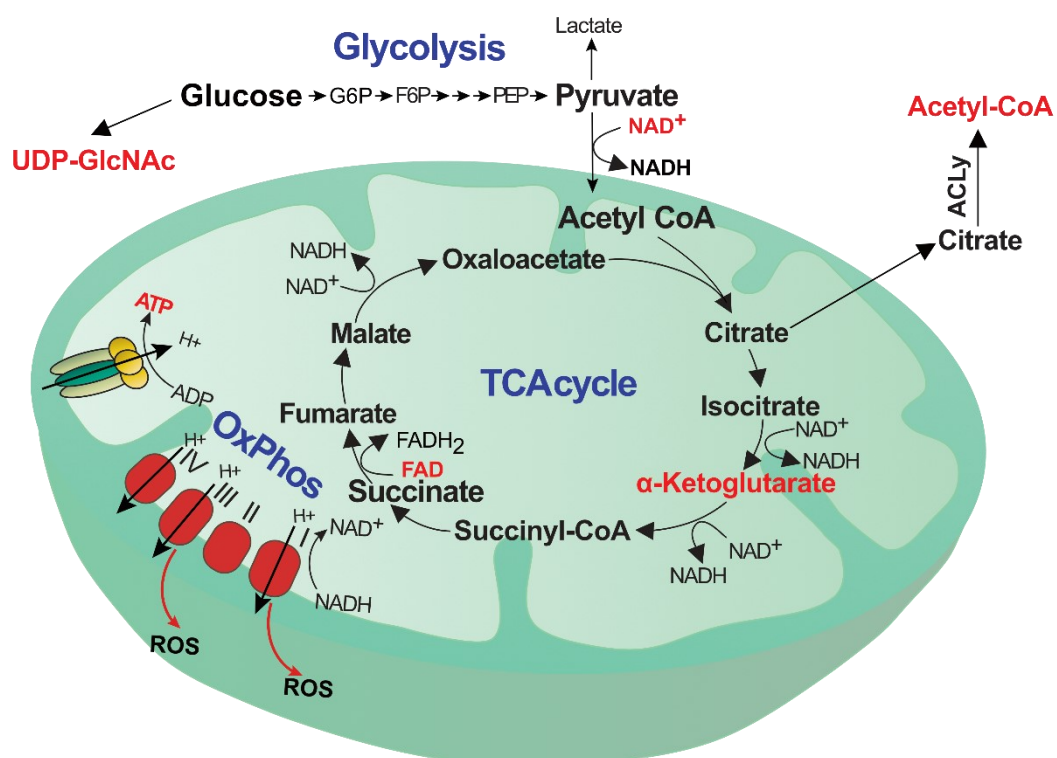
Figure 1.8: Glycolysis and oxidative metabolism. Dependence on glycolytic metabolism is a major characteristic of pluripotency due to limited oxidative capacity and high proliferative activity. Upon differentiation initiation, cells switch to the more efficient oxidative metabolism that also provides many cofactors necessary for epigenetic modifications, which are shown in red.

differentiation (Li and Stouffs et al., 2006; Zhang et al.,2011). Therefore, ROS might be a major regulator in the process of stem cell differentiation, directly linking it to the oxidative capacity of the cell. Interestingly, ROS produced in the initial phase of mitochondrial metabolism induction are scavenged by antioxidants, in order to avoid premature differentiation of mesenchymal stem cells. This indicates that ROS signaling is modulated on two levels: firstly by regulation of their production itself and secondly, by the action of scavengers (Tormos et al., 2011).

Another level on which the metabolism directs development is the provision of cofactors for chromatin and histone modifying enzymes (Figure 1.8). Several studies have shown that the establishment of epigenetic modifications relies on the availability of metabolites, such as α-ketoglutarate (αKG), S-adenosylmethionine (SAM), and acetyl-CoA, which in turn depends on the metabolic adaption associated with the specific cellular program. The TCA cycle metabolite αKG is a co-factor of histone demethylases (Figure 1.6), as well as DNA methyl cytosine hydroxylases, and therefore impacts the establishment of histone methylation marks and DNA methylation. Fluctuation of the α-ketoglutarate levels directly affect the process of ESC differentiation and a decline of the αKG concentration was found to be critical for the correct timing of differentiation (Hwang et al., 2016). Another critical cofactor in the process of differentiation is SAM, which is a methyl donor derived from the methionine metabolism (Figure 1.5 and 1.6). Inhibition of cellular SAM production blocks histone methylation in mouse ESCs (Shyh-Chang et al., 2013). An equally important histone modification is acetylation, which is considered as an activating mark that promotes transcription. Acetyl-CoA is thereby used as a cofactor by histone acetyltransferases (HATs), in order to set up the epigenetic modification patterns (Zhang et al., 2018; Figure 1.7). During development, acetyl-CoA levels are mainly regulated through the conversion of the TCA cycle intermediate citrate by the enzyme ATP citrate lyase (ACLy). Inhibition of this enzyme could be linked to a reduction of nuclear acetyl-CoA levels as well as ESC differentiation (Moussaieff et al., 2015). Moreover, ATP, UDP-N-acetylglucosamine (UDP-GlcNAc), FAD and NAD are additional cofactors necessary for the establishment of a correct epigenetic landscape and need to be provided by the cellular metabolism (Zhang et al., 2018).

Finally, the role of the metabolism during ESC differentiation is dynamic and adapts depending on the specialized function and needs of the cell. Metabolic fluxes were considered to be primarily orchestrated by cellular nutrient demands, though several studies point out a critical role of the metabolism in the timing of differentiation and establishment of the epigenetic landscape. Furthermore, metabolic switches are often one of the first signs of developmental transitions, indicating the importance of the availability of certain substrates in the process of stem cell differentiation (Folmes et al., 2013; Tsogtbaatar et al., 2020). Due to the strong impact that metabolite levels can have on lineage specification, more attention has been recently

directed towards a better understanding of metabolic cues and their effectors. The results of these investigations may support the establishment of cell differentiation procedures as well as culturing conditions, which could direct lineage selection by impacting epigenetic regulation. Gaining a better insight into the metabolic regulation of stem and progenitor cells could, therefore, assist in advancing the process of manufacturing appropriate cell to be utilized in cell replacement therapies (Tsogtbaatar et al., 2020).

1.6. Implications of the aldehyde dehydrogenase family in developmental processes

The aldehyde dehydrogenase (Aldh) family (EC 1.2.1.3) comprises a group of enzymes, which catalyze the oxidation and detoxification of endogenous or exogenous aldehyde substrates (Figure 1.9). Aldhs neutralize the highly reactive aldehydes by inactivation of the respective electrophilic carbonyl group and have consequently a cyto-protective function (Marchitti, 2008). Aldh activity is also pivotal in transformation and formation processes of essential cellular metabolites such as retinoic acid. Members of the Aldh family have a molecular mass of ca.
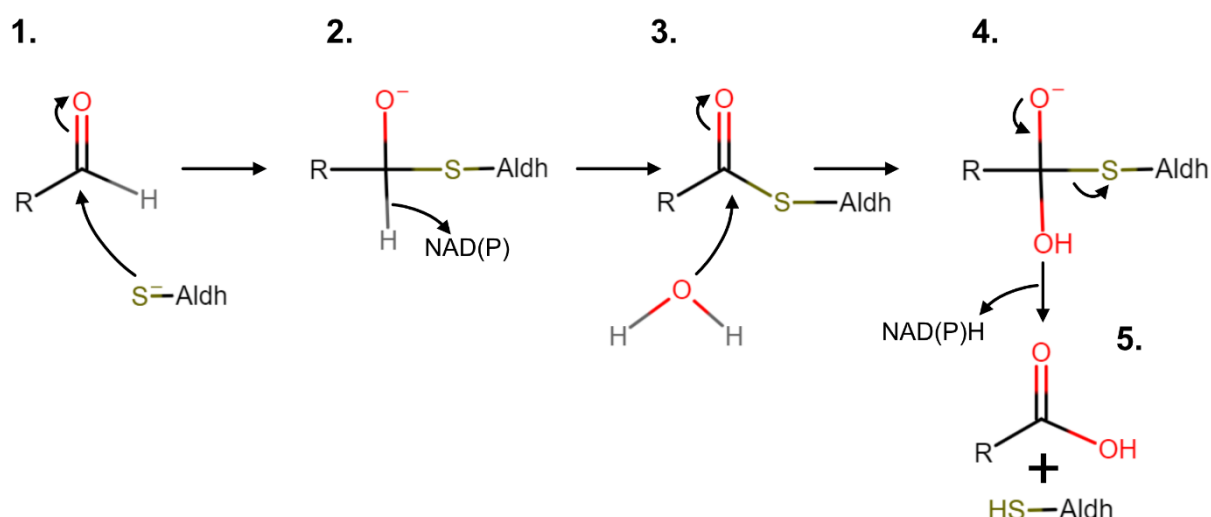
Figure 1.9: Aldh reaction mechanism. 1. Nucleophilic attack of the Aldh enzyme on the carbonyl of the aldehyde. 2. Hydride transfer to NAD(P). 3. Nucleophilic attack of H_2O on carbonyl. 4. Dissociation of reduced NAD(P)H. 5. Release of the carboxylic acid.

50–60 kDa and utilize NAD(P)$^+$ as an electron accepting cofactor (Shortall et al., 2021). Apart from the active substrate catalysis, the enzymes were shown to contribute to the maintenance of the redox state of the cell by the generation of NADH/NADPH and direct absorption of UV light through chaperone-like activity (Uma et al., 1996; Pappa et al., 2003; Estey et al., 2007).

Early studies found a distinct cell population in umbilical cord blood with high Aldh activity, which was harboring lineage committed hematopoietic progenitor cells (HPC). These HPCs showed a strong correlation between Aldh activity and colony-forming unit potency (Storms et al., 1999). Since then, multipotent progenitors enriched in Aldh activity were found

in several tissues such as the central nervous system, pancreas, skeletal muscles, salivary glands, melanocytes and intestine, suggesting that high Aldh activity is associated with progenitor cells and stemness (Vassalli, 2019). Two recent studies have proposed diverse functions in adult stem cells. The enzyme Aldh3a1 is enriched in human and mouse salivary gland stem cells where it contributes to the processes of differentiation and self-renewal. Deletion of the enzyme resulted in an aberrant tissue morphology of the three major salivary glands, mitochondrial dysfunction and impaired tissue regeneration after radiation. Moreover, loss of Aldh3a1 caused an accumulation of the ROS product 4-HNE due to the lacking detoxification process, which reduced cell survival (Viswanathan et al., 2022). Another example of Aldh involvement in stem cell physiology was examined in melanocytes. During regeneration, melanocyte stem cells in zebrafish activate an embryonic neural crest transcriptional program that induces Aldh2 expression. Consequently, a metabolic switch caused by Aldh2 delivers building blocks for nucleotide synthesis to generate progeny and deletion of the enzyme resulted in incomplete nucleotide biosynthesis (Brunsdon et al., 2022).

Nevertheless, the understanding of Aldh function in stem cell physiology is limited. Accumulating evidence suggests a fundamental role of Aldhs in the process of stem and progenitor cell differentiation, proliferation and survival, which was thought to be mainly regulated by Aldh dependent retinoic acid signaling but recent studies indicate the involvement of more complicated mechanisms (Jackson et al., 2011; Vassalli, 2019). Aldhs are also strongly associated with tumor-initiating ability and their expression is suggested as hallmark for cancer stem cells (Vassalli, 2019).

Accumulating evidence suggests that Aldh activity assists in the processes of stem and progenitor cell function and differentiation by different tissue and enzyme dependent mechanisms. Thus, understanding how Aldhs influence stem cell physiology and differentiation could benefit to current efforts in the topic of regenerative therapies.

1.7. Aldh1b1 as a marker for pancreas progenitors and its role in the process of differentiation

Aldh1b1 (Aldehyde Dehydrogenase 1 Family Member B1) is a mitochondrial enzyme of the Aldh superfamily, which is expressed in several organs including liver, small intestine, lung, heart, duodenum, kidney, stomach and pancreas (Marchitti, 2008; Stagos et al.,2010). In mice, the *Aldh1b1* gene is located on chromosome 4 and consists of two exons and one intron. The coding sequence is harbored in the second exon. Structural and functional analyses of the enzyme predict that it forms homotetramers and uses exclusively NAD, but not NADP, as a cofactor. Aldh1b1 is believed to play a central role in the alcohol metabolism and shows an intermediate K_M towards acetaldehyde. However, *in vitro* experiments suggested a clear

preference to medium-chain aldehydes and aromatic benzaldehyde (Stagos et al.,2010). To date, little is known about the physiological role of Aldh1b1.

Aldh1b1 was identified as an important regulator in the process of murine pancreas development, as recently shown by our research group (Serafimidis et al., 2008; Ioannou et al., 2013; Anastasiou et al., 2016). Its expression in the murine pancreas development is clearly detectable from E9.5 onwards and initially Pdx1-dependent as shown by the loss of Aldh1b1 expression in the Pdx1$^{-/-}$ pancreas. As pancreas development progresses, *Aldh1b1* expression is maintained in the tip and trunk compartments and its expression in the latter is Ngn3-dependent. RT-PCR analysis of all *Aldh* genes showed that *Aldh1b1* has the highest expression in the murine pancreas epithelium during secondary transition (Ioannou et al., 2013). Its expression is maintained in progenitor cells, but it is downregulated as cells differentiate (Ioannou et al., 2013; Anastasiou et al., 2016). By birth, the expression of the enzyme is mostly abolished and, in the adult, it is only retained in rare centroacinar-like cells (Mameishvili et al., 2019). Thus, *Aldh1b1* expression is restricted to pancreas progenitors, and it is not detectable in differentiated cells suggesting that it has a role exclusively in the process of progenitor maintenance and differentiation (Ioannou et al., 2013; Anastasiou et al., 2016).

A better understanding of the influence of Aldh1b1 on pancreas development, was achieved by using a loss-of-function mouse line (*Aldh1b1* null), which completely lacks *Aldh1b1* expression. Early pancreas development appeared normal in the absence of functional Aldh1b1, but during secondary transition, the *Aldh1b1* null pancreas showed a premature onset of differentiation, which was evident by an increase in the number of Ngn3$^+$ progenitors. Consistent with this finding, an increase in the expression of the markers C-Pep, DBA, Amylase, as well as the proliferation marker PH3, was found in the *Aldh1b1* null pancreas at 14.5 days post coitum (dpc).

Aberrant regulation of the endocrine differentiation during embryonic development in absence of Aldh1b1 was shown to result in islet defects, which were already evident at the first postnatal day (P1). RNA-seq analyses of P1 islets showed deregulation of transcription factors involved in β-cell maturation, such as *Pdx1*, *Nkx6.1*, *Mafa* and *Mafb,* as well as deregulation of several genes encoding vesicular and secretory granule proteins. Strikingly, the gene expression pattern was even more deregulated in the islets of 6-week-old mice, even though Aldh1b1 expression was already repressed in islets during embryonic development, suggesting a 'legacy effect' of the enzyme. There was also defective islet patterning since insulin expression was significantly reduced, accompanied by an increase in glucagon and somatostatin expression. As a consequence of the defective islet development, the response to glucose was strongly decreased in *Aldh1b1* null islets and the animals developed hyperglycemia with age (Anastasiou et al., 2016). Thus, Aldh1b1 seems to play an important

role in the process of differentiation timing and the absence of its activity leads to the generation of dysfunctional β-cells.

Aldh1b1 expression in the adult pancreas is restricted, as mentioned before, to the centroacinar-like cells, which have a progenitor identity. Those cells are mostly quiescent and self-renewing, but lineage-tracing experiments concluded that they contribute to the generation of all three pancreatic lineages. Centroacinar-like cells were identified to be involved in Kras-driven oncogenesis and genetic experiments could reveal that Aldh1b1 expression is a prerequisite in the development of Kras^{G12D}-induced pancreatic cancer indicating, therefore, a potential participation of Aldh1b1 in pancreatic intraepithelial neoplasia (PanIN) and pancreatic ductal adenocarcinoma (PDAC) development.

In summary, Aldh1b1 is a marker of pancreatic stem and progenitor cells and plays an important role in the process of pancreas development. Loss of Aldh1b1 function leads to the generation of dysfunctional β-cells and consequently hyperglycemia. This dissertation aims to gain a better insight into the Aldh1b1-dependent changes in the metabolism and differentiation process of progenitor cells to contribute to the understanding of the required mechanisms that drive the generation of functional β-cells.

2. Material and methods

2.1. Materials

2.1.1. Mouse strains

Strains used
C57BL/6JRj
Aldh1b1^{tm1lacZ}
Ins1^{Cre}/ROSA26^{LSLtdTomato}
Ins1^{Cre}/ROSA26^{LSLtdTomato}/ Aldh1b1^{tm1lacZ}
Pdx1^{Cre}/ROSA26^{LSL Aldh1b1}

Table 1: Mouse strains

2.1.2 Antibodies

Primary antibodies

Antigen	Origin	Used dilution	Supplier	Catalog number
CK19	Rabbit	1:100	CELL MARQUE	EP72
C-peptide	Rabbit	1:100	Cell Signaling	4593
E-Cadherin	Rat	1:400	Invitrogen	13-1900
E-Cadherin Alexa Fluor 488	Rat	1:100	Invitrogen	53-3249-82
Glucagon	Mouse	1:500	Sigma-Aldrich	G2654
IgG	Rat	1:200	Abcam	ab37361
Insulin	Mouse	1:1000	Sigma-Aldrich	I2018
Nkx6.1	Mouse	1:1000	DSHB (Madsen)	F55A10
PH3	Rabbit	1:500	Cell signaling	06-570
Ptf1a	Rabbit	1:3000	B. Breant, INSERM-Paris	
Sox9	Rabbit	1:1000	Chemicon (Sigma-Aldrich)	AB5535

Table 2: Primary antibodies used for immunofluorescence staining

Secondary antibodies

Origin/Antigen/Isotype	Conjugate	Used dilution	Supplier	Catalog number
Goat anti-rabbit IgG	Alexa Fluor 568	1:500	Invitrogen	A11011
Goat anti-rabbit IgG	Alexa Fluor 488	1:500	Invitrogen	A11070
Goat anti-mouse IgG	Alexa Fluor 568	1:500	Invitrogen	A11004
Goat anti-mouse IgG	Alexa Fluor 647	1:500	Invitrogen	A21235
Goat anti-mouse IgG	Alexa Fluor 488	1:500	Invitrogen	A11001
Goat anti-rat IgG	Alexa Fluor 488	1:500	Invitrogen	A11006
Goat anti-rat IgG	Alexa Fluor 647	1:500	Invitrogen	A21247

Table 3: Secondary antibodies used for immunofluorescence staining

2.1.3. Primers

Genotyping primers

Line	Primer sequence	PCR condition
Aldh1b1^{tm1lacZ}	5' ACACTGCAACAGGAGGACC 3' 5' TTCCCGTTATCTAGCGTCTCC 3' 5' GTCTGTCCTAGCTTCCTCACTG 3'	92 °C for 2 min 1 cycle 92 °C for 30 s 60 °C for 30 s 72 °C for 30 s 35 cycles 72 °C for 5 min
Ins1^{Cre}	5' AGAGACCATCAGCAAGCAG 3' 5' CGGACAGAAGCATTTTCCAG 3' 5' TCCAACGCCAAGGTCTGAAG 3'	94 °C for 3 min 1 cycle 94 °C for 45 s 55.9 °C for 45 s 72 °C for 30 s 30 cycles 72 °C for 7:30 min
ROSA26^{LSLtdTomato}	5' AAG GGA GCT GCA GTG GAG TA 3' 5' CCG AAA ATC TGT GGG AAG TC 3' 5' GGC ATT AAA GCA GCG TAT CC 3' 5' CTG TTC CTG TAC GGC ATG G 3'	94 °C for 2 min 1 cycle 94 °C for 45 s 56 °C for 45 s 72 °C for 30 s 40 cycles 72 °C for 5 min

ROSA26^{LSLAldh1b1}	5' GTTATCAGTAAGGGAGCTGCAGTGG 3'	94 °C for 1 min
	5' CTCGCGACACTGTAATTTCATACTG 3'	1 cycle
	5' GCCGGCAACATATTGTACAAAACCG 3'	94 °C for 45 s
		56 °C for 45 s
		72 °C for 30 s
		2 cycles
		92 °C for 45 s
		56 °C for 45 s
		72 °C for 30 s
		35 cycles
		72 °C for 7:30 min
Pdx1^{Cre}	5' CTGCCACGACCAAGTGACAGC 3'	94 °C for 3 min
	5' GCTAAGTGCCTTCTCTACACCTGC 3'	1 cycle
		94 °C for 30 s
		61 °C for 30 s
		72 °C for 45 s
		35 cycles
		72^{0}C for 7 min

Table 4: Primers and PCR conditions used for genotyping

qPCR primers

Gene	Primer sequence
Aldh1b1	5' GACCTGGACAAGGCCATCTA 3'
	5' CCTTAAAGCCTCCGAATGG 3'
β-Actin	5' TGGCTCCTAGCACCATGA 3'
	5' CCACCGATCCACACAGAG 3'
Pdx1	5' TCCACCACCACCTTCCAG 3'
	5' CAGGCTCGGTTCCATTCG 3'
Nkx6.1	5' CCTCCTACATCAAAGCGAACG 3'
	5' GCGGGAAATCAGCAAGACG 3'
Ptf1a	5' AACCAGGCCCAGAAGGTTAT 3'
	5' AAAGAGAGTGCCCTGCAAGA 3'
Sox9	5' AGGAGAACACCTTCCCCAAG 3'
	5' GTCCAGTCGTAGCCCTTCAG 3'
Krt19	5' TTGAGACAGAACACGCCTTG 3'
	5' CCTTCAGGCTCTCAATCTGC 3'
Amy	5' AACAATGTTGGTGTCCGTATTT 3'

	5' CAGACGACAATTTCTGACCTGA 3'
Mt-Rnr2	5' CCGCAAGGGAAAGATGAAAGAC 3'
	5' TCGTTTGGTTTCGGGGTTTC 3'
Mt-Nd1	5' CTAGCAGAAACAAACCGGGC 3'
	5' CCGGCTGCGTATTCTACGTT 3'
Hk2	5' GCCAGCCTCTCCTGATTTTAGTGT 3'
	5' GGGAACACAAAAGACCTCTTCTGG 3'
Mdh1	5' ATC GCA GAC CAC ATC AGA G 3'
	5' ACA GGG AAT GAG TAG AGC AG 3'
Mdh2	5' CCC AGG AAA CCA GGA ATG AC 3'
	5' TTC TGC TGT GAT GGG GAT G 3'
Idh1	5' CAG GCT CAT AGA TGA CAT GGT GG 3'
	5' CAC TGG TCA TCA TGC CAA GGG A 3'
Idh2	5' CCCTATTGCCAGCATCTTTGCC 3'
	5' CTTCTCCAGCGTCTGTGCAAAC 3'
Idh3β	5' TTCCTGGAGATGGAATTGGCCC 3'
	5' TCCACTTTCCTCCTGGTCCTTG 3'
Acly	5' TTC CTA GCA CAA AGA TGC CAT TGA 3'
	5' GTG GAG AAG ATT ACC ACC TCC A 3'
Slc25a1	5' GGA GAG GAC TAT TGT GCG GTC T 3'
	5' CCC GTG GAA AAA TCC TCG GTA C 3'

Table 5: qPCR primers

2.1.3. Culture Media

Medium type	Composition	Supplier	Catalog number
Spheroid culture medium	AdDMEM-F12	Gibco	12634010
	500 ng/ml RSPO1	Self-made	
	1.22 mg/ml Nicotinamide	Sigma-Aldrich	72340-250G
	1x B27	Gibco	17504001
	1x Penicillin-Streptomycin	Gibco	15140-122
	1x HEPES	Gibco	11560496
	1x GlutaMAX	Gibco	35050061
	1 µM Gastrin I	Abcam	ab141072
	0.2 mg/ml N-acetylcysteine	Sigma-Aldrich	A9165
	0.05µg/ml mEGF	R&D Systems	236-EG-200

	0.1µg/ml FGF10	R&D Systems	345-FG-025
	0.1µg/ml mNoggin	self-made	
	0.21 µg/ml A83-01	R&D Systems	2939/10
	10 µM ROCKi Y27632	Miltenyi Biotec	130-104-169
Flux Medium with U-C_{13} Glucose	SILAC Advanced DMEM/F-12	Life Technologies	A2494301
	0.7 mM L-Arginine monohydrochloride	Sigma	A6969-25G
	0.5 mM L-Lysine monohydrochloride	Sigma	L8662-25G
	4 mM L-Glutamine	Gibco	25030081
	17.5 mM U-C_{13} Glucose	Cambridge Isotope Laboratories	CLM-1396
	500 ng/ml RSPO1	R&D Systems	4645-RS-025
	1.22 mg/ml Nicotinamide	Sigma-Aldrich	72340-250G
	1x B27	Gibco	17504001
	1x Penicillin-Streptomycin	Gibco	15140-122
	1x HEPES	Gibco	11560496
	1x GlutaMAX	Gibco	35050061
	1 µM Gastrin I	Abcam	ab141072
	0.2 mg/ml N-acetylcysteine	Sigma-Aldrich	A9165
	0.05µg/ml mEGF	R&D Systems	236-EG-200
	0.1µg/ml FGF10	R&D Systems	345-FG-025
	0.1µg/ml mNoggin	R&D systems,	719-NG050
	0.21 µg/ml A83-01	R&D Systems	2939/10
	10 µM ROCKi Y27632	Miltenyi Biotec	130-104-169
Flux Medium with 1,2-C_{13} Glutamine	SILAC Advanced DMEM/F-12	Life Technologies	A2494301
	0.7 mM L-Arginine monohydrochloride	Sigma	A6969-25G
	0.5 mM L-Lysine monohydrochloride	Sigma	L8662-25G
	17.5 mM D-Glucose	Sigma	G7021-1KG
	4 mM 1,2-C_{13} Glutamine	Cambridge Isotope Laboratories	CLM-2001
	500 ng/ml RSPO1	R&D Systems	4645-RS-025
	1.22 mg/ml Nicotinamide	Sigma-Aldrich	72340-250G
	1x B27	Gibco	17504001
	1x Penicillin-Streptomycin	Gibco	15140-122
	1x HEPES	Gibco	11560496
	1x Glutamax	Gibco	35050061
	1 µM Gastrin I	Abcam	ab141072
	0.2 mg/ml N-acetylcysteine	Sigma-Aldrich	A9165

	0.05µg/ml mEGF	R&D Systems	236-EG-200
	0.1µg/ml FGF10	R&D Systems	345-FG-025
	0.1µg/ml mNoggin	R&D systems,	719-NG050
	0.21 µg/ml A83-01	R&D Systems	2939/10
	10 µM ROCKi Y27632	Miltenyi Biotec	130-104-169
Explant medium	DMEM high glucose	Life Technologies	21969-035
	1x N2 supplement	Life Technologies	17502-048
	1x GlutaMAX supplement	Life Technologies	35050-038
	1x Penicillin-Streptomycin	Life Technologies	15140-122

Table 6: Culture media for spheroid and explant culture

2.1.4. Buffers

ATAC buffers

Buffer	Composition	Supplier	Catalog number
ATAC-Resuspension buffer (RSB)	10 mM Tris-HCl pH 7.4	Biozol	GTX16364-1
	10 mM NaCl	Santa Cruz	sc-295833
	3 mM MgCl$_2$	Life Technologies	AM9530G
	0.1% NP40	Life Technologies	85124
	0.1% Tween-20	Sigma Aldrich	11332465001
	0.01% Digitonin	Promega	G9441
Washing buffer	ATAC-RSB		
	0.1% Tween-20	Sigma Aldrich	11332465001
Transposition mix	1x Tagment DNA (TD) buffer (Illumina)	Illumina	20034197
	1.5 µl transposase (Illumina)	Illumina	20034197
	1x PBS	Gibco	14190
	0.01% digitonin	Promega	G9441
	0.1% Tween-20	Sigma Aldrich	11332465001

Table 7: Buffers used in ATAC experiments

Cell lysis buffers

Buffer	Composition
Cell lysis buffer	100 mM NaCl
	20 mM Tris HCl pH 7.4
	10 mM EDTA
	0.5 % SDS

	0.2 mg/ml proteinase K
Tail buffer	200 mM NaCl
	100 mM Tris-HCl pH 8.5
	5 mM EDTA
	0.2 % SDS
	50 µg/ml Proteinase K

Table 8: Cell lysis buffers used for DNA isolation

Southern blot buffers

Buffer	Composition
ES cell lysis buffer	20 mM NaCl
	10 mM Tris/Hcl pH 7.5
	10mM EDTA pH 8
	0.5% Sarcosyl
Denaturation buffer	0.5 M NaOH
	1.5 M NaCl
Neutralization buffer	1.5 M NaCl
	1 M Tris/HCl, pH 7.2
2x SSC-buffer (pH 7)	0.3 M NaCl
	30 mM Sodium Citrate
Hybridization buffer	0.5 M sodium phosphate buffer, pH 7.2
	7% SDS
	10 mM EDTA

Table 9: Southern blot buffers

Single cell prep buffers

Buffer	Composition
Dissociation buffer E14.5	AdDMEM (Gibco)
	200 U/ml collagenase IV (Rockland)
	10% FCS (PAN Biotech)
	10% HBSS (Gibco)
	2 U/ml DNase (Promega)
Dissociation buffer P10	AdDMEM (Gibco)
	720 U/ml collagenase IV (Rockland)
	10% FCS (PAN Biotech)
	10% HBSS (Gibco)
	2 U/ml DNase (Promega)
Staining/Sorting buffer	PBS (Gibco)

	5% FCS (PAN Biotech)

Table 10: Buffers used for single cell preparations from tissue

Quenching buffers

Buffer	Composition
Flux quenching buffer	20% methanol
	0.1% formic acid
	3 mM sodium fluoride
	1 mM phenylalanine
	100µM EDTA
Untargeted metabolomics buffer	80% methanol

Table 11: Quenching buffers used for metabolome analyses

2.1.5. Kits

Kit name	Supplier	Catalog number
Illumina Tagment DNA Enzyme and Buffer Small Kit	illumina	20034197
DNA Clean and Concentrator-5 Kit	Zymo Research	D4013
MITO-ID Red detection kit	Enzo	ENZ-51007-0100
Quick RNA Microprep kit	Zymo Research	R1050
TAKARA BcaBEST Labeling Kit	TAKARA	6046
TUNEL Assay Kit-FITC	Abcam	ab66108
illustra MicroSpin G-50 columns	GE Healthcare	27-5330-01

Table 12: Kits

2.1.6. Chemicals

Reagent	Supplier	Catalog number
CellROX™ orange Reagent	CellROX™ orange Reagent	C10443
DAPI	Sigma Aldrich	10236276001
Dispase	STEMCELL technologies	07923
RQ1 RNase-Free DNase	Promega	M6101
DRAQ7	Biostatus	DR70250
EDTA	Sigma-Aldrich	03690-100ML

FastStart Essential DNA Green Master	Roche	06402712001
FCS	PAN Biotech	P30-3033
Matrigel, growth factor reduced	Corning	356231
MitoTracker Red CMXRos	ThermoFisher	M7512
Nextera™ DNA CD Indexes	illumina	20018707
Nylon membrane	Roche	11 417 240 001
PBS	Gibco	14190
Phenol/Chloroform/Isoamyl alcohol	Carl Roth	A156.2
ProLong Gold Antifade Mountant	Life Technologies	P36930
Proteinase K	Sigma	P6556-100MG
PrimeScript RT PRT	Takara	RR036B
Propidium iodide	Invitrogen	00-6990-50
Red Load Taq Master (5x)	Jena Bioscience	PCR-108L
RedSafe	HiSS Diagnostics	21141
RNase A	ThermoFisher	EN0531
Tissue-Tek O.C.T	Sakura	4583
TrypLE Express	Gibco	12604013

Table 13: Reagents

2.2. Methods

2.2.1. Mouse strains

All mouse strains used in the present study are listed in table 1 (Section 2.1.1.). Animal maintenance and experimentation were performed in accordance with international guidelines and subjected to ethical approval from the competent veterinary committees of TU Dresden.

2.2.2. Genotyping

Genomic DNA was isolated from either ear-punch tissue or tail. The tissue samples were digested using 0.2 ml tail buffer, containing 200 mM NaCl, 100 mM Tris-HCl pH 8.5, 5 mM EDTA, 0.2 % SDS and 50 µg/ml Proteinase K, for each tail and were incubated at 55 °C overnight. As soon as the tissue was completely digested, the DNA was purified by performing a phenol-chloroform-isoamyl alcohol (25:24:1) extraction, which allows the collection of ultra-pure genomic material. The DNA was washed first with absolute ethanol and subsequently with 70% ethanol. Upon carefully removing all ethanol remnants, the DNA was resuspended in 50 µl of ddH$_2$O. The extracted genomic material was then amplified in a standard PCR reaction using Red Load Taq Master and primers to the respective lineages (Section 2.1.3. Table 4), which was followed by an agarose gel (2% with RedSafe) electrophoresis separation. The separated PCR products could then be visualized under UV light.

2.2.3. Single cell suspension of the E14.5 pancreas

Embryonic mouse pancreata were dissected and isolated at an embryonic age (E14.5) in DMEM containing 10% FCS. Enzymatic digestion of the organ was conducted with dissociation buffer, containing AdDMEM, 200 U/ml collagenase IV, 10% FCS, 10% HBSS and 2 U/ml DNase, at 37 °C for 8 min. The digestion was inhibited with the addition of 2 mM Ethylenediaminetetraacetic acid (EDTA) for 10 min at room temperature. Thereafter, the pancreata were mechanically suspended by trituration with a 200 ml tip. The resulting single cells were pelleted at 400 rcf for 4 min and resuspended in phosphate buffered saline (PBS) containing 5% FCS for further processing.

2.2.4. Pancreas progenitor isolation by FACS

Single cell suspension of E14.5 embryonic pancreata was generated according to the procedure described in the previous paragraph. Cells were blocked for 15 min on ice with 12,5 µg/ml rat IgG to avoid unspecific antibody binding. Subsequently, progenitor cells were labelled using an anti-E-cadherin Alexa Fluor 488 conjugated antibody in a 1:100 dilution for 1 hr at 4

°C under gentle rotation. The suspension was pelleted at 400 rcf for 4 min and resuspended in PBS with 5% FCS to eliminate excess antibodies. Dead cells were marked by using the viability marker Propidium Iodide (PI) in a 1:100 dilution and E-cadherin positive pancreas progenitors were sorted into AdDMEM containing 10% FCS using either BD FACSMelody or BD FACSAria III.

2.2.5. Expansion of E14.5 pancreas progenitors

Pancreas progenitors were isolated as stated above and pelleted at 400 rcf for 4 min. Cells from one embryonic pancreas were resuspended in 50 µl growth factor reduced Matrigel and plated in a 96- well plate. Once the Matrigel was solidified, culture medium was added. The progenitor cells started expanding and forming visible spheroids already on the next day and were initially passaged 10 days after sorting and, subsequently, every 7 days. To this end, the spheroids were released from the Matrigel directly in the well by using Dispase for 40 min at 37 °C. The cells were transferred to a 1.5 ml tube and pelleted at 400 rcf for 4 min. Afterwards, the spheroid pellet was washed once in PBS and dissociated by adding 1x TrypLE Express for 10 min at 37 °C. The dissociation was stopped by adding AdDMEM and the cells were washed once more with AdDMEM and counted in a hemocytometer. The single cells were resuspended at 30000 cells/ 50 µl Matrigel and plated as a droplet in a 48 well plate. Culture medium was added after the Matrigel was solidified. Expanded progenitors were used at passage 3 (P3) for metabolic and gene expression experiments.

2.2.6. Metabolic flux analysis from expanded progenitors

Metabolic flux analysis was performed with expanded progenitors at P3, using 3 biological replicates of each genotype. In order to reach a sufficiently high cell number for the assay, cultured progenitor cells were plated with a density of 60 000 cells in 150 µl Matrigel and cultured for 5 days. NAC was removed from the culture medium 24 hours before the experiment. Afterwards, the experiment was performed using an adjusted culture medium (experimental medium), containing either U-C_{13}-Glucose or 1,2-C_{13}-Glutamine. In order to clear out either unlabeled glucose or glutamine, the wells were washed twice for 5 min at 37 °C with experimental medium. Subsequently, the cells were incubated in fresh experimental medium for 4h. The metabolite extraction was performed right after. To this end, the experimental medium was discarded, and the metabolites were extracted from the cells with the use of quenching buffer, containing 20% methanol, 0.1% formic acid, 3 mM sodium fluoride, 1 mM phenylalanine and 100µM EDTA. The extraction was conducted using 3x 250 µl quenching buffer, which was shortly added onto the Matrigel and immediately transferred to a low-binding tube on dry ice. The samples were stored at -80 °C until mass spectrometer

analysis was performed at the medical faculty of TU Dresden (Dr. Tiago Alves). The data was normalized to intracellular taurine and analyzed by performing MIMOSA (Alves et al., 2015).

2.2.7. Metabolite extraction from expanded progenitors for metabolome analysis

Metabolome analysis was carried out using expanded pancreas progenitors at P3. Prior to the experiment, 20 000 cells/well were plated in 50 µl Matrigel. Each biological replicate was split into 3 different wells to generate technical triplicates. NAC was removed from the culture medium at day 5 of P3 and the metabolites were extracted 24h later. For this, the cell culture medium was aspirated and the plate containing the expanded cells was transferred onto ice for 5 min to liquify the Matrigel. 1 ml cold PBS was added to each well and carefully mixed. The contents of the well were then moved into a 2 ml tube, which was kept on ice beforehand, and pelleted for 5 min at 4 °C and 300 rcf. Subsequently, the supernatant, containing the dissolved Matrigel, was discarded and the cells were lysed in 1 ml -80 °C quenching buffer (80% Methanol). The mixture was vigorously vortexed and kept at -80 °C for 20 min to support cell lysis. Following this incubation, the cell debris was removed, twice, by centrifugation at 14 000 rcf at 4 °C for 10 min. The quenching buffer containing the extracted metabolites was transferred into a safe lock tube and stored at -80 °C until the LC-MS/MS analysis was performed at the medical faculty of TU Dresden (Dr. Mirko Peitzsch). Measured MS/MS fragments were subsequently identified by their retention time and mass-to-charge ratio. Data processing and normalization was conducted using the software Progenesis QI Vers. 2.3. The data was log transformed, auto scaled and analyzed using MetaboAnalyst 5.0 (https://www.metaboanalyst.ca/).

2.2.8. Progenitor cell staining for ROS and MMP detection

ROS levels and MMP were analyzed in progenitor cells either directly after isolation from the E14.5 pancreas (procedure stated above), or after expansion in Matrigel. Expanded cells were dissociated into single cells by following the passaging protocol. Cells from one embryo, or approximately 100 000 expanded cells, were resuspended in PBS containing 5% FCS. Directly isolated cells required an E-Cadherin labeling (procedure as stated before) prior to the ROS or MMP staining to identify progenitor cells. Subsequently, CellROX orange, in a final concentration of 2 µM to detect intracellular ROS, or MitoTracker Red CMXRos, in a final concentration of 100 nM to detect the MMP, were added to the cell suspension. Both dyes were incubated in the dark at 37 °C for exactly 45 min. After this incubation, cells were pelleted at 400 rcf for 4 min and resuspended in PBS containing 5% FCS. Dead cells were marked with

the viability marker DRAQ7 in a 1:375 dilution. The fluorescence intensity was measured using the BD FACSCanto II and reanalyzed with FlowJo (BD Bioscience).

2.2.9. Progenitor cell staining for mitochondrial mass detection

A single cell suspension of freshly isolated or expanded cells was prepared as described in the section above and mitochondria were stained by following the instructions of the Mito-ID red detection kit. To this end, the cells were resuspended in 1x assay buffer, and the Mito-ID red dye was added in a final dilution of 1:10000 The dye was incubated in the dark at 37 °C for exactly 30 min. After this incubation, cells were pelleted at 400 rcf for 4 min and resuspended in PBS with 5% FCS. Dead cells were marked with the viability marker DRAQ7 in a 1:375 dilution. The fluorescence intensity was measured by using BD FACSCanto II and reanalyzed with FlowJo (BD Bioscience).

2.2.10. Analysis of the mtDNA/nDNA ratio by genomic qPCR

In order to determine the mitochondrial mass of E14.5 pancreas progenitors, expanded progenitors were lysed in 400 µl cell lysis buffer, containing 100 mM NaCl, 20 mM Tris HCl pH 7.4, 10 mM EDTA, 0.5 % SDS and 0.2 mg/ml proteinase K. The lysis was conducted for 3 h at 55 °C, and the mixture was cooled down to RT afterwards. 100 µg/ml RNase A was added for 30 min at 37°C to degrade present RNA. After this, the DNA was purified by performing a phenol-chloroform-isoamyl alcohol (25:24:1) extraction, allowing the isolation of high-quality DNA. After mixing and centrifugation of the sample at 12 000 rcf for 5 min, the isolated total DNA was collected in the aqueous phase and subsequently transferred into 600µl isopropanol, containing 7.5 M ammonium acetate. Inversion of the mixture caused the precipitation of the DNA, which was washed once in 70% ethanol and then resuspended in 20 µl of ddH$_2$O. The concentration of the DNA was determined by NanoDrop measurements and adjusted to 100 ng/µl. In order to quantify the samples, a qPCR reaction was performed, containing 1x FastStart Essential DNA Green Master, 10 pmol/ µl of the respective forward and reverse primers, ddH$_2$O and 1 µl cDNA per sample. Each condition was measured in triplicates by using the LightCycler 480. The detection of nuclear encoded gene *Hk2* was included to calculate the expression of the mitochondrial genes relative to the expression of the nuclear marker.

2.2.11. Quantitative polymerase chain reaction (qPCR) analysis

qPCR analyses were carried out using cDNA obtained from E14.5 expanded pancreas progenitors. To this end, cells were lysed and RNA was collected using the Zymo Quick RNA Microprep kit according to manufacturer's instruction. 2 µg of the isolated RNA was then used to perform cDNA synthesis, which was carried out using the 5x TAKARA PrimeScript RT

master mix. RNA and PrimeScript mix, already containing RTase, RNase Inhibitor, random 6 mers, Oligo(dT)-primer, dNTP mixture as well as reaction buffer, were diluted to 40 µl in ddH$_2$O and the reverse transcription reaction was carried out at 37 °C for 15 min. After this, the qPCR reaction was set up, containing 1x FastStart Essential DNA Green Master, 0.1 pmol of the respective forward and reverse primers, ddH$_2$O and 1 µl cDNA per sample. Each condition was measured in triplicates by using the LightCycler 480 (Cycling conditions: 95°C for 10 min, 40 cycles: 95 °C for 10 s, 60 °C for 10 s, 72 °C for 10 s). β- Actin was included as an internal standard to enable sample normalization.

2.2.12. Data analysis of qPCR results

The data was analysed with the classical ΔCt or ΔΔCt method. The mean of the Ct values of the triplicates and the respective standard deviation was calculated. The ΔCt was then determined by subtracting the Ct of the used standard from the Ct of the gene of interest. ΔΔCt is calculated by subtracting the mean ΔCt of the control sample (WT) from the ΔCt of the sample of interest. Finally, the fold change was assessed as $2^{-\Delta\Delta Ct}$.

2.2.13. Isolation of TdT$^+$ β-cells at P10

Pancreata from *Ins-Cre*$^{+/-}$/*TdTomato*$^{-/-}$ (/*Aldh1b1*$^{-/-}$) mice were dissected at the 10th postnatal day (P10). In order to achieve a tissue suspension, the pancreata were transferred into 1 ml cold HBSS with 1% BSA and carefully minced in a petri dish using a curved scissor. The tissue pieces were subsequently transferred into a 1.5 ml tube and 1 ml dissociation buffer, containing AdDMEM, 720 U/ml collagenase IV, 10% FCS, 10% HBSS as well as 2 U/ml DNase, was added for 10 min. Following the incubation, a triturate of the tissue using a 200 µL tip was performed to achieve a first dissociation of the tissue. The incubation and trituration step were repeated once more until the cell suspension appeared homogenous. The enzymatic reaction was inhibited by the addition of 2 mM EDTA, and the single cell suspension was finalized by another trituration step. The resulting single cells were pelleted at 400 rcf for 4 min and resuspended in PBS containing 5% FCS. Dead cells were marked with the viability marker 4',6-5 diamidino-2-phenylindole (DAPI) in a 1:1000 dilution and TdT$^+$ pancreas progenitors were sorted into AdDMEM containing 10% FCS using either BD FACSMelody or BD FACSAria III.

2.2.14. ATAC-seq analysis of E14.5 pancreas progenitors

ATAC-seq analysis was performed to investigate potential differences in the chromatin accessibility between WT and *Aldh1b1* null pancreas progenitors. To this end, 30 000 progenitor cells were sorted as described above and pooled to reach the necessary cell

number. The cells were pelleted at 500 rcf at 4°C for 5 min and subsequently resuspended and lysed in 50 µl ATAC resuspension buffer (RSB), containing 0.1% NP40, 0.1% Tween-20, and 0.01% Digitonin for exactly 3 min on ice. The lysis was washed out by the addition of 1 ml cold ATAC-RSB containing 0.1% Tween-20. Nuclei were pelleted at 500 rcf for 10 min at 4°C in a fixed angle centrifuge. The nuclei were resuspended in 50 µl of the transposition mixture, containing the chromatin modifying transposase, which was incubated with the extracted chromatin for 2 h at 37 °C and 1000 rpm. In this incubation period, the enzyme cut open the chromatin and inserted sequencing primers simultaneously into the genome. The processed DNA was extracted afterwards by using Zymo DNA Clean and Concentrator-5 kit. Next, a PCR reaction, containing 25 µM of two Illumina adapter (Nextera™ DNA CD Indexes), 1x NEBNext Master Mix and the transposed sample, was performed in order to amplify the fragmented and purified DNA by taking advantage of the previously inserted primer sequences (Cycling conditions: 72 °C for 5 min, 98°C for 30 s, 5 cycles: 98 °C for 10 s, 63 °C for 30 s, 72 °C for 1 min). 5% of this pre-amplified sample was use for a qPCR reaction, containing 25 µM of the two adapters utilized before, SYBR Green and 1x NEBNext Master Mix (Cycling conditions: 98°C for 30 s, 20 cycles: 98 °C for 10 s, 63 °C for 30 s, 72 °C for 1 min). The additional PCR cycle number necessary, was determined assessing the amplification plots of the qPCR. The remaining DNA was further amplified with the initial cycling conditions for the cycle number determined before and subsequently purified by using Zymo DNA Clean and Concentrator-5 kit. The final library was size selected with a 0.6x/1.3x SPR purification using AMPure XP beads. Paired-end sequencing of 2 WT and 2 *Aldh1b1* null samples with a depth of 50 million reads was performed on an Illumina NovaSeq 6000 system. Following the sequencing procedure, the reads were mapped to the mm10 mouse genome and differential accessibility analysis was carried out by the DESeq2 pipeline. GO analysis of the peak set was performed by using the GREAT online tool (http://great.stanford.edu/public/html/) and the motif enrichment was conducted with HOMER software.

2.2.15. RNA-seq analysis of pancreas progenitors and β-cells

RNA-seq was performed with directly from tissue isolated and pooled E14.5 progenitor cells or P10 β-cells (Isolated as described above). 40 000 freshly sorted cells were pelleted at 400 rcf for 4 min, the sorting buffer was aspirated, and the total RNA extracted using the Quick RNA Microprep kit, according to manufacturer's instruction. The concentration of the RNA was measured using the bioanalyzer and adjusted to the lowest concentration with RNase/DNase-free water. The mRNA was then enriched by a Poly-dT pulldown. Short read and paired-end sequencing of the mRNA library was performed using an Illumina multiplex system. Following the sequencing procedure, the reads were mapped to the GRCm39 mouse genome and differential expression analysis was carried out using the DESeq2 pipeline. Genes with

normalized counts > 100 within a 5% FDR cutoff were considered regulated. GO analysis of differentially regulated genes was performed using Enrichr (https://maayanlab.cloud/Enrichr/) and Heatmaps were designed with the online tool Morpheus (https://software.broadinstitute.org/morpheus/). Enriched gene sets were determined by GSEA 4.3.2 (UC San Diego and Broad Institute) and considered significantly enriched if the normalized enrichment scores had an FDR q-value below 0.25.

2.2.16. Explant culture of the embryonic pancreas

E14.5 embryonic pancreata were isolated and transferred onto permeable cell culture inserts. The inserts were moved subsequently into a 6-well plate containing explant medium to ensure medium exposure to the pancreatic explant. After 1 hour of equilibration, the media was exchanged and NAC was added for certain conditions. The explant was kept for 2 days in culture at 37 °C and 5% CO_2 atmosphere, while the medium was changed daily. After that, the explants were fixed in 4% Paraformaldehyde (PFA) for 30 min on ice, followed by a dehydration in 30% sucrose in PBS overnight at 4 °C. The explants were embedded in O.C.T. for cryo-sectioning and sectioned at 8 µm thickness. The sections on each slide were 32 µm apart, spanning the entire pancreatic tissue. The slides were stored at -80 °C for the next step of immunofluorescence staining.

2.2.17. Immunofluorescence staining of tissue sections

The explant sections were thawed from -80 °C to air dry until RT equilibration, prior to the staining procedure. The O.C.T. was then removed from the sections by washing with PBS for 10 min at RT, and postnatal sections were post-fixed in 4% PFA for 10 min at 4 °C. The tissue permeabilization was conducted subsequently, using 0.3% PBS-T (PBS + 0.3% TritonX-100). To minimize unspecific binding, the sections were blocked in 10% heat inactivated normal goat serum (NGS) or 5% bovine serum albumin (BSA) prepared in 0.3% PBS-T for 1 h at RT. The primary antibodies were added to the tissue sections in 0.3% PBS-T containing 1 % of the blocking serum and incubated overnight at 4°C in a humid chamber. On the next day, excess unbound antibodies were removed by PBS-T washing. Secondary antibodies were diluted in 1% serum in PBS-T and incubated on the tissue sections for 2h at RT. Unconjugated secondary antibodies were removed by washing with 0.3 % PBS-T, and the nuclei of the cells were stained using DAPI. Samples were mounted in Prolong gold and imaged using Apotome 2 (Zeiss).

2.2.18. Image analysis

The images obtained from explant immunofluorescence stainings were analyzed using the software Fiji ImageJ. In order to quantify the expression of the selected markers PH3, TUNEL, Ptf1a, Nkx6.1, Sox9, Ngn3, C-peptide, Glucagon and Cytokeratin-19 (CK19) the brightness and contrast of the images were adjusted, and masks were used (as stated in table 14) to determine the total fluorescent area of the markers.

Markers	Fiji mask
PH3	Otsu
DAPI	IsoData
E-Cadherin	Li
TUNEL	Otsu
Ptf1a	Otsu
Nkx6.1	Otsu
Sox9	Otsu
Ngn3	Otsu
C-peptide	Li
Glucagon	IsoData
CK19	IsoData

Table 14: Fiji ImageJ masked used for staining quantification

The total signal area average of three sections was calculated and divided by the corresponding total signal area for DAPI. Epithelial mitotic activity was quantified by division of the PH3 positive area by the epithelial DAPI area as marked by E-Cadherin co-staining. The fold change was calculated by division of the *Aldh1b1* null determined area by the area mean detected for respective markers and condition of the WT. The calculated values were compared using One-Way ANOVA ("analysis of variance") with post hoc Tukey test and pValues of <0.05 were considered statistically significant. Data are expressed as mean ± standard deviation.

2.2.19. Genomic Southern blot

The genomic Southern blot was performed to ensure a correct integration of the targeting vector into the ESC genome. ESC clones that were neomycin resistant, and therefore carried an integration of the targeting vector, were expanded. Subsequently, a subset of cells from successfully targeted clones was lysed by using ES cell lysis (20 mM NaCl, 10 mM Tris/Hcl pH 7.5, 10mM EDTA pH 8, 0.5% Sarcosyl buffer with 0.75 mg/ml Proteinase K and the DNA was purified by ethanol precipitation. 10 to 15 µg of the extracted DNA were used for an overnight EcoRI digest that would generate two fragments with 6 885 bp and 11 742 bp upon integration of the targeting vector into the correct position in ROSA26. The enzymatically digested DNA was loaded into a 0.7 % agarose gel containing ethidium bromide and separated

for 4-5 h at 130V in an electrophoresis chamber. Afterwards, the gel region of interest was excised under UV light and carefully transferred into a depuration solution containing 0.25 M HCl for 7 min. The solution was rinsed off completely and a denaturation of the DNA was followed in a denaturation buffer containing 0.5 M NaOH and 1.5 M NaCl for 30 min. The gel was subsequently transferred into a neutralization buffer (1.5 M NaCl, 1 M Tris/HCl, pH 7.2) for 30 min. The Southern blot, to transfer the DNA fragments from the gel to a positively charged nylon membrane, was performed overnight using capillary action. On the next day, the membrane was denatured in 0.4 M NaOH for 1 min, neutralized in 0.2 M Tris HCl, pH 7.5 and subsequently dried at 120 °C for 1 h in a hybridization oven to fix the DNA on the membrane. Next, the hybridization of the membrane with labeled probes was performed. To that end, the membrane was first soaked in 2x SSC-buffer, containing 0.3 M NaCl and 30 mM Sodium Citrate, and subsequently transferred into a glass bottle filled with 15 ml hybridization buffer (0.5 M sodium phosphate buffer, pH 7.2, 7% SDS, 10 mM EDTA). The membrane was rotated in a hybridization oven for at least 4h at 65 °C. In the meantime, the probe labeling using the TAKARA BcaBEST Labeling Kit was performed with 300 ng of template DNA according to manufacturer's instructions. In short, the probe was diluted in ddH$_2$O to a final volume of 12 µl, 2 µl of random primers were added and incubated for 3 min at 95 °C. The mix was cooled down on ice afterwards for 5 min. 1µl bca polymerase, 5 µl ^{32}p-dCTP, 2.5 µl dNTPs (without dCTP) and 2.5 µl 10x buffer (provided in the kit) were added and the labeling was performed for 4h at 300 rpm shaking and 55 °C. After this process was completed, the probe was purified using Illustra MicroSpin G-50 columns. This was followed by denaturation of the probe at 95 °C for 3 min and then standing on ice for 5 min. The labeled probe was added directly into the hybridization buffer in the glass bottle with the membrane and hybridization was carried out overnight at 65 °C. On the next day the membrane was washed for 30 min at 65 °C in 2x SSC with 0.1% SDS, followed by another 30 min wash in 0.2x SSC with 0.1% SDS. The last wash was performed in 0.1x SSC with 0.1% SDS for 30 min and the membrane was subsequently sealed and placed into a Phosphorscreen cassette overnight. The signal was detected using a Phosphoimager.

2.2.20. Statistical analysis

Statistical analysis was performed by using One-Way ANOVA ("analysis of variance") with post hoc Tukey test or unpaired t-test with Welch's correction. Data are represented as mean±SD of at least technical triplicates. Differences were considered significant when *p ≤0.05; **p < 0.005; and ***p < 0.0005. Statistical analysis and the representation of the respective data was carried out using Prism-GraphPad 9.

3. Results: Part 1

3.1. Aldh1b1 is a metabolic regulator of pancreas progenitors

Members of the aldehyde dehydrogenase family are primarily associated with the process of aldehyde oxidation and acetaldehyde clearance, whereas the latter reaction is mainly accomplished by the enzyme Aldh2 (Dingler et al., 2020). However, even though Aldh1b1 shares 75% peptide sequence homology with Aldh2, it shows the second lowest K_M for acetaldehyde of all aldehyde dehydrogenases (Stagos et al., 2010, Jackson et al., 2015). Earlier studies found that it exhibits a preference for the cofactor NAD^+ but not $NADP^+$ and additional catalytic activity towards some other aldehydes, like short- and medium-chain aliphatic aldehydes and aromatic aldehydes (Stagos et al., 2010). Besides the prominent role of Aldh family members in aldehyde oxidation, studies have identified additional functions in the redox balance of the cell and metabolic regulation. Nevertheless, as of today, little is known about the molecular functions of Aldh1b1 in differentiating cells *in vivo*. In the following chapter, I will try to elucidate the role of Aldh1b1 in the metabolism of pancreas progenitors and how inactivity of the enzyme affects progenitor cell differentiation.

3.1.1 Aldh1b1 loss-of-function promotes an increase in ROS and a reduction in mitochondrial mass

Aldh1b1 is a mitochondrial enzyme which is expressed in all pancreas progenitors, but not in differentiated pancreatic cells, thus, suggesting that it possesses an essential function in the mitochondrial metabolism of progenitor cells. Since the mitochondrion is considered a major producer of ROS and due to the known ability of some members of the Aldh family to control redox levels, I first assessed whether Aldh1b1 plays a similar function in pancreas progenitors (Viswanathan et al., 2022). To that end, an *Aldh1b1* knock-out mouse model was used, in which the coding sequence for *Aldh1b1* was replaced by a *lacZ* gene (Thesis Anastasiou, 2017). Progenitor cells from *Aldh1b1* null and WT mice were FACS isolated according to their E-Cadherin expression at E14.5 and stained with the CellROX dye in order to mark cellular oxidative stress. CellROX is a membrane permeable dye that does not emit fluorescence in its reduced state but releases a strong fluorescent signal after ROS-induced oxidation that was measured by flow cytometry. Aldh1b1 deficiency led to a significant 2-fold increase in fluorescence intensity (Figure 3.1 A,B), suggesting that Aldh1b1 reduces ROS levels in embryonic pancreas progenitors.
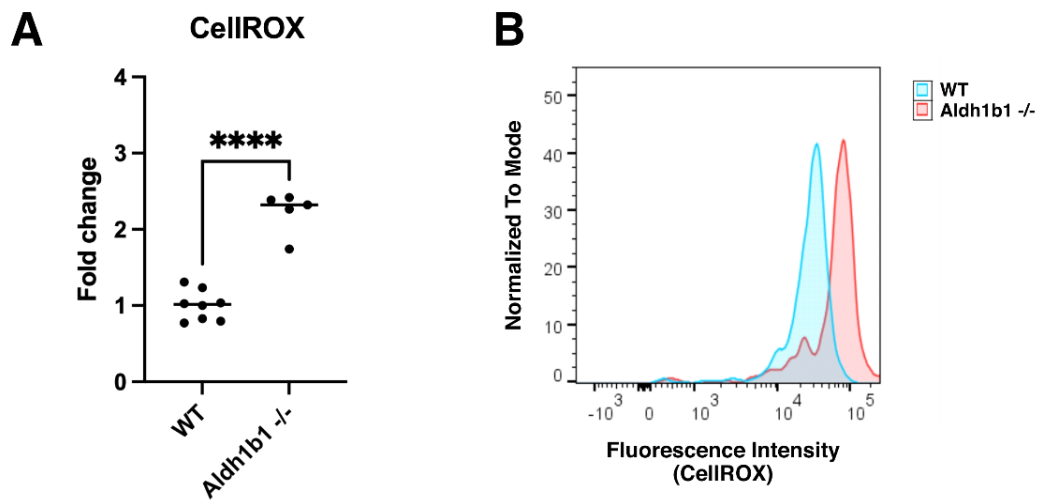
Figure 3.1: Detection of reactive oxygen species in E14.5 mouse pancreatic progenitors using flow cytometry analysis. (A) shows the median fluorescence of progenitor cells in distinct WT and *Aldh1b1* null embryos (n=8 and n=5, respectively). Here, a significant increase in ROS levels in *Aldh1b1* null progenitors was detected. (B) displays the distribution of the fluorescence intensity of all measured cells of two representative samples. Statistical analysis was performed using unpaired t-test with Welch's correction. Data were considered significant when *p≤0.05; **p≤0.01; ***p≤0.001; ****p ≤ 0.0001.

An increase of ROS levels in the cell frequently causes mitochondrial damage, dysfunction and a reduction of mitochondrial mass. The latter can be a consequence of an accumulation of DNA-modification, -strand breaks or -cross linking upon oxidative stress that consequently leads to the degradation of the mitochondrion (Ott et al., 2007). Thus, mitochondrial mass was determined next in the E14.5 pancreas progenitors to assess if an increase in ROS in the absence of Aldh1b1 affects mitochondrial mass. To this end, Mito-ID dye, that labels mitochondria regardless of their membrane potential, was used to stain WT and *Aldh1b* null progenitors. The differences in the fluorescence intensity were subsequently measured by flow cytometry and confirmed that loss of functional Aldh1b1 leads to a significant reduction in mitochondrial mass in embryonic pancreas progenitors (Figure 3.2 A,B).

Thus, Aldh1b1 seems to preserve mitochondrial mass by reducing the levels of ROS. These data are reminiscent of earlier studies on Aldh3a1 in salivary glands that showed a mitochondria protective effect of Aldhs supporting stem cell self-renewal (Viswanathan et al., 2022).
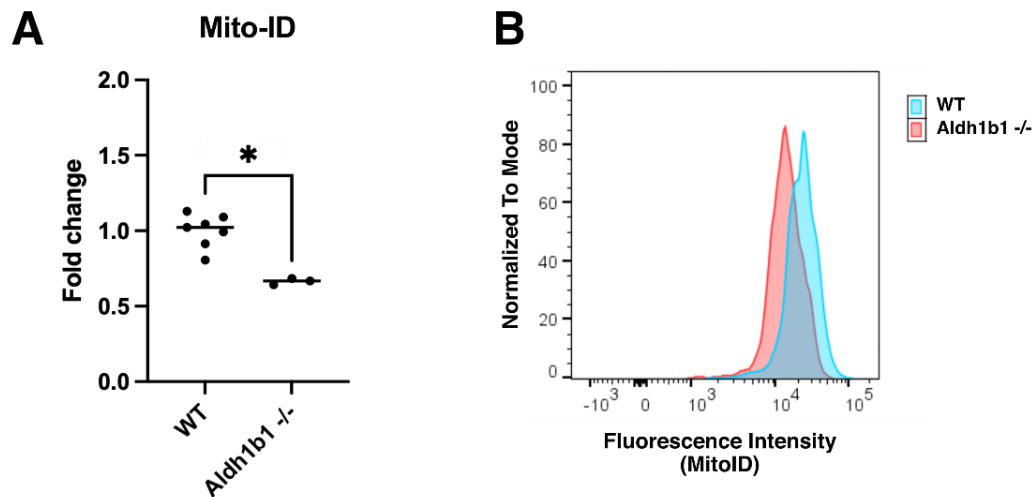
Figure 3.2: Detection of mitochondrial mass in E14.5 mouse pancreatic progenitors using flow cytometry analysis. (A) shows the median fluorescence of progenitor cells in distinct WT and *Aldh1b1* null embryos (n=7 and n=3, respectively). Here, a significant decrease in the mitochondrial mass in *Aldh1b1* null progenitors was detected. (B) displays the distribution of the fluorescence intensity of all measured cells of two representative samples. Statistical analysis was performed using unpaired t-test with Welch's correction. Data were considered significant when *p≤0.05; **p≤0.01; ***p≤0.001; ****p ≤ 0.0001.

In order to have a closer look on the functionality of the mitochondria in absence of Aldh1b1, the mitochondrial membrane potential (MMP) was determined by flow cytometry analysis. MitoTracker dye stains the mitochondrial membrane according to the electrical membrane potential. The MMP is established by the proton pumps in complex I, III and IV of the oxidative phosphorylation and is therefore a useful marker to detect possible mitochondrial dysfunction (Zorova et al., 2018). A decrease in measured fluorescence would indicate a reduced activity of the oxidative phosphorylation. However, this analysis did not detect a difference of the MMP in cells with Aldh1b1 deficiency in comparison with the WT, which suggests that *Aldh1b1* null pancreas progenitors have no mitochondrial dysfunction per se and appear to be able to compensate for the decreased mitochondrial mass (Figure 3.3 A,B).

This data suggest that Aldh1b1 loss of function is associated with a vast increase in ROS levels which lead, in turn, to a reduction of the mitochondrial mass. Since an elevation in intracellular ROS is often an effect of respiratory chain blockade of OXPHOS complexes I, III and IV, I looked into a possible change of the MMP but this was not evident (Smeitink et al., 2006). Exclusion of the possiblity that OXPHOS blockage is the reason for elevated ROS levels, creates the need for a more in-depth analysis of the metabolic profile of *Aldh1b1* null progenitor cells. To this end, an expansion of WT and *Aldh1b1* null progenitors was necessary to allow the detection of changes in the metabolism associated with Aldh1b1 loss-of-function.
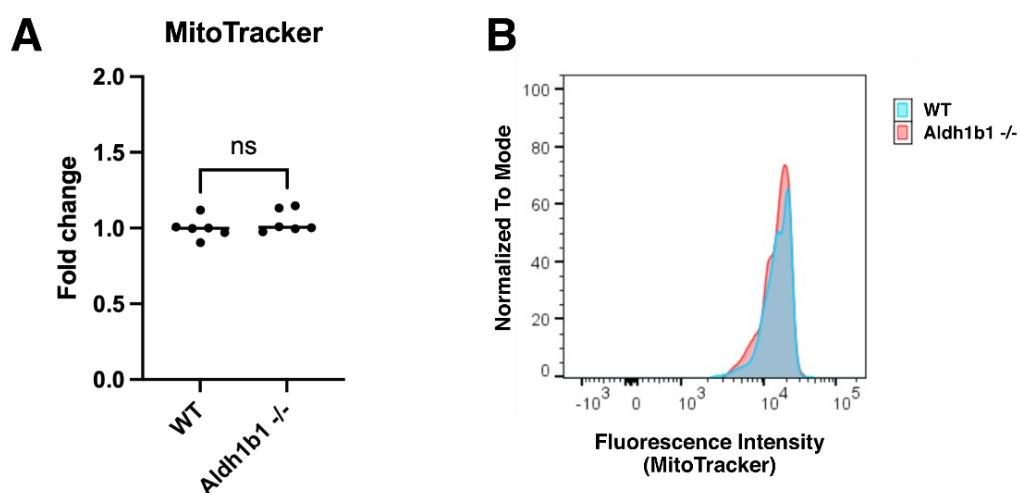
Figure 3.3: Detection of MMP from E14.5 mouse pancreatic progenitors using flow cytometry analysis. (A) shows the median fluorescence of progenitor cells in distinct WT and *Aldh1b1* null embryos (n=6 and n=6, respectively). Here, no significant change in the fluorescence intensity was detected. (B) displays the distribution of the fluorescence intensity of all measured cells of two representative samples. Statistical analysis was performed using unpaired t-test with Welch's correction. Data were considered significant when $*p \leq 0.05$; $**p \leq 0.01$; $***p \leq 0.001$; $****p \leq 0.0001$.

3.1.2. In vitro expansion of embryonic pancreas progenitors

Mass spectrometry-based metabolic analysis requires a relatively high number of progenitor cells, which exceeds the number of cells that can be isolated from a single embryonic pancreas, to enable reliable metabolic profiling. Thus, a 3D cell culture system was established, using a medium composition to sustain progenitor cell identity while supporting expansion. It has been shown that *Aldh1b1* null progenitors suffer from severe oxidative stress and fail to grow beyond passage 2 (P2) under non-reductive conditions (Ph.D. thesis Anastasiou, 2017). Therefore, the ROS scavenger N-acetylcysteine (NAC) was added in the medium in order to prevent oxidative damage and subsequent cell death. E-Cad⁺ progenitor cells were FACS isolated from E14.5 pancreata and subsequently embedded into Matrigel (Figure 3.4 A), a matrix mainly containing laminin, collagen IV, entactin and heparan sulfate proteoglycan. The usage of a 3D culture system enables a spatial organization and cell-cell or cell-extracellular matrix interactions, which should help maintaining the physiological properties of the progenitor cells. The cells grow as round and hollow spheres, called spheroids, due to their epithelial identity and polarity.

To ensure that the isolated cells retain their progenitor properties in the culture and over a certain number of passages, qPCR analyses were performed in passage 3 (P3) and passage 5 (P5; Figure 3.4 B). Stable *Aldh1b1* expression was detected at P3 and P5 in WT cells but, as expected, not in the *Aldh1b1* null progenitors. Furthermore, the expression of the progenitor markers Pdx1, Nkx6.1 and Sox9 as well as the differentiation markers CK19 and Amylase, were detected and maintained a stable expression over at least 5 passages. Thus,

under cell culture conditions and ROS scavenging, no differences in the expression of these markers could be detected between WT and *Aldh1b1* null progenitors.
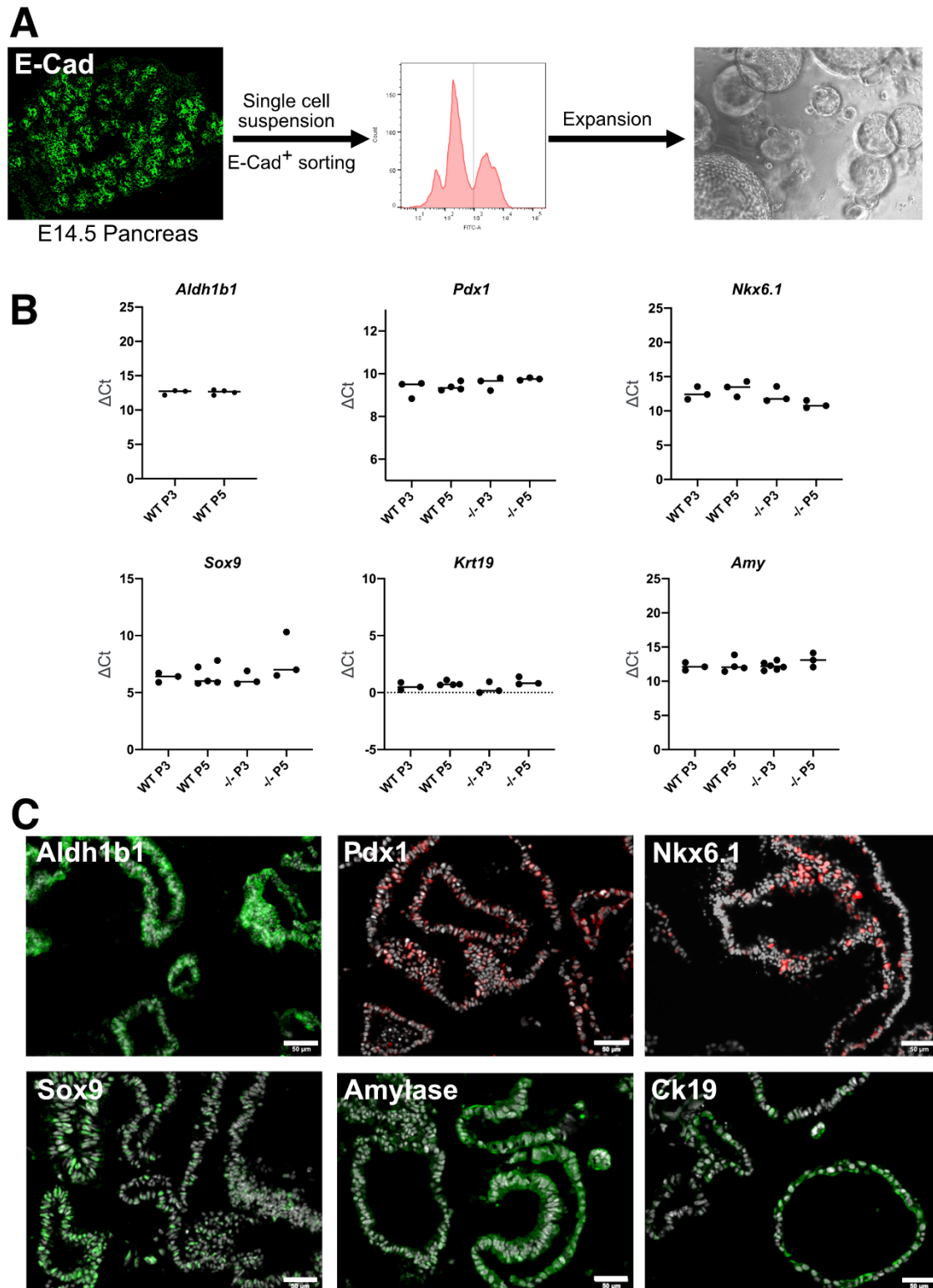
Figure 3.4: E14.5 pancreatic progenitor isolation and expansion. (A) Pancreas progenitor cells were isolated based on their E-Cadherin expression via FACS and expanded in a 3D culture system, in which they grew as spheroids due to their epithelial identity and polarity. (B) The progenitor cells show a stable expression of progenitor and differentiation marker in P3 and P5. (C) The marker expression could also be confirmed on the protein level via immunofluorescence staining, here shown for WT spheroids in P3. Scale bar = 50 µm.

Immunofluorescence staining was performed to confirm the expression of the selected markers at the protein level in P3 (shown for WT, Figure 3.4 C). The stable expression of progenitor and differentiation markers in the expanded progenitors confirmed that this culture system preserves progenitor properties of the cells. Moreover, the stable gene expression levels in P3 and P5 suggested that the cells did not dedifferentiate throughout the expansion, while maintaining a stable genetic program. Taken together, these observations confirmed that the expanded cells retained a progenitor identity and that this approach can be further used to investigate the Aldh1b1 associated metabolic profile.

3.1.3. Aldh1b1 regulates ROS levels and MMP in expanded pancreas progenitors

Isolated E14.5 pancreas progenitors displayed a significant elevation of ROS, but it remained unclear through which metabolic pathways Aldh1b1 affects oxidative stress in the cell. To conduct precise metabolomic analyses, it was necessary to expand the isolated E14.5 progenitor cells in culture using the spheroid culture system described above. The cell culture medium was supplemented with NAC to prevent oxidative stress induced cell death of *Aldh1b1* null cells after isolation, but the presence of NAC might mask the metabolic function of Aldh1b1. Thus, in the subsequent analyses, the compound was removed 24h prior to the experiments to recover the *in vivo* phenotype. In order to assess ROS levels and mitochondrial
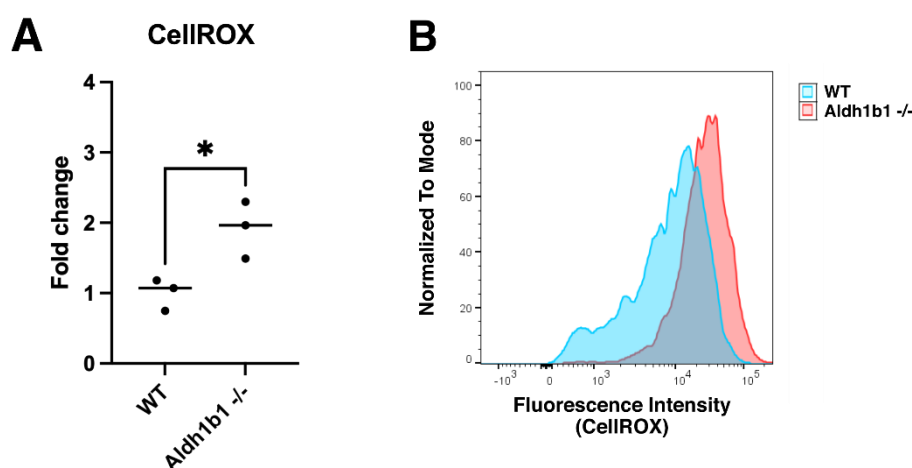
Figure 3.5: Detection of reactive oxygen species from expanded mouse pancreatic progenitors using flow cytometry analysis. (A) shows the median fluorescence of progenitor cells from distinct WT and *Aldh1b1* null embryos (n=3 and n=3, respectively). Here, a significant increase in ROS levels in *Aldh1b1* null progenitors was detected. (B) displays the distribution of the fluorescence intensity of all measured cells of two representative samples. Statistical analysis was performed using unpaired t-test with Welch's correction. Data were considered significant when *p≤0.05; **p≤0.01; ***p≤0.001; ****p ≤ 0.0001.

properties of the expanded cells, I repeated the flow cytometry experiments performed with the freshly isolated cells, using expanded cells in P3.

Consistent with the data obtained in the freshly isolated cells, expanded cells showed a significant increase of ROS levels. The difference in fluorescence intensity between WT and *Aldh1b1* null cells was less pronounced than that in freshly isolated cells and the range of measured fluorescence intensity was broader in the expanded cells (Figure 3.5 A,B).

The mitochondrial mass was first determined via flow cytometry analysis using Mito-ID dye, as described before for the freshly isolated cells (Figure 3.2 A,B), but no significant difference between WT and *Aldh1b1* null progenitors was detected under these cell culture conditions (Figure 3.6 A,B). In order to confirm this result, a genomic quantitative PCR was performed for the mitochondrial genes *mt-Nd1* and *mt-Rnr2*, encoding for ND1 and 16SrRNA,
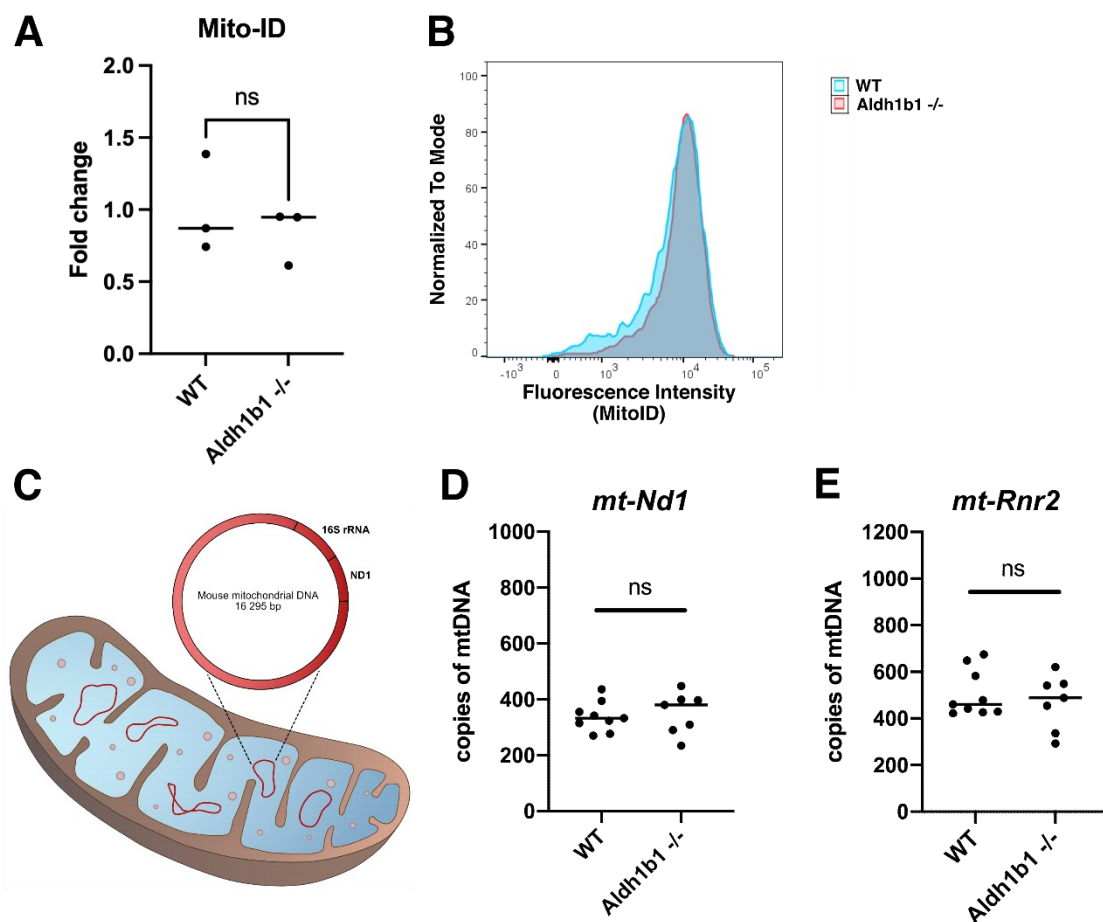
Figure 3.6: Determination of mitochondrial number from expanded mouse pancreatic progenitors using flow cytometry analysis and genomic qPCR. (A) shows the median fluorescence of progenitor cells from distinct WT and *Aldh1b1* null embryos (n=3 and n=3, respectively). The mitochondrial mass remained unchanged in *Aldh1b1* null progenitors in comparison to WT cells. (B) displays the distribution of the fluorescence intensity of all measured cells of two representative samples. The mtDNA copy number was determined by assessing two mitochondrial genes (C) but no difference was found in *Aldh1b1* null cells (n=7) compared to WT progenitors (n=9; D, E). Statistical analysis was performed using unpaired t-test with Welch's correction. Data were considered significant when *p≤0.05; **p≤0.01; ***p≤0.001; ****p ≤ 0.0001.

respectively (Figure 3.6 C). Both genes belong to a stable fraction in the mitochondrial genome which is less susceptible to deletions. The nuclear encoded gene *Hk2* was used for normalization in order to determine the relative mtDNA copy number between *Aldh1b1* null and WT progenitor cells (Tanhauser and Laipis, 1995; Quiros and Goyal, 2017). Using this assay, similar copy numbers for WT and *Aldh1b1* null expanded cells were found (Figure 3.6 D and E), therefore confirming the previous results from the Mito-ID flow cytometry analysis. Differences in the mitochondrial mass of the expanded cells compared to the freshly isolated cells could be caused by the prolonged exposure of ROS *in* vivo, leading to mitochondrial degradation (Frank et al., 2012). Withdrawal of NAC before the experiment increased the ROS levels of the progenitor cells but did not induce mitophagy suggesting that the decrease in mitochondrial mass might be a long-term effect of oxidative stress.

Finally, the MMP of expanded embryonic pancreas progenitors was determined via staining with MitoTracker and flow cytometry (Figure 3.7 A and B). In contrast to the freshly isolated cells, the expanded *Aldh1b1* null progenitors showed increased fluorescence staining compared to their WT counterparts. Taking into account the stable mitochondrial mass, these
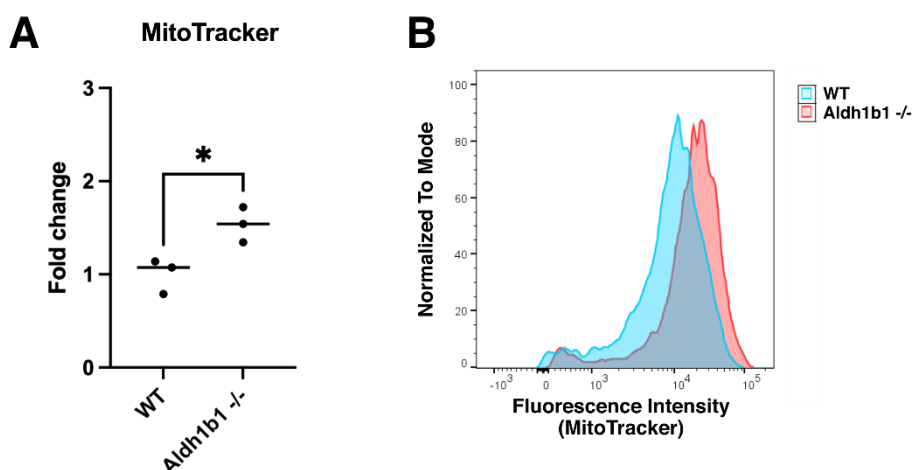
**Figure 3.7: Detection of MMP from expanded mouse pancreatic progenitors using flow cytometry analysis.** (A) shows the median fluorescence of progenitor cells from distinct WT and *Aldh1b1* null embryos (n=3 and n=3, respectively). The analysis showed a significant increase in median fluorescence intensity in *Aldh1b1* null cells. (B) displays the distribution of the fluorescence intensity of all measured cells of two representative samples. Statistical analysis was performed using unpaired t-test with Welch's correction. Data were considered significant when *p≤0.05; **p≤0.01; ***p≤0.001; ****p ≤ 0.0001.

results suggest an increased oxidative phosphorylation in the absence of Aldh1b1. Thus, the expanded progenitor cells remain dependent upon Aldh1b1 function to regulate ROS levels and, therefore, can be used to gain more in-depth insights into the Aldh1b1-dependent metabolism.

3.1.4. Loss of Aldh1b1 activity does not affect mitochondrial morphology

Members of the Aldh superfamily are associated with a cyto-protective function, due to their presumed role in aldehyde detoxification. A lack in the metabolism of certain aldehydes upon knockout of the respective enzyme, has been linked to an altered mitochondrial morphology and increased mitophagy due to aldehyde accumulation (Viswanathan et al., 2022).

In order to assess the mitochondrial morphology in the absence of Aldh1b1, electron microscopy with E14.5 expanded pancreas progenitors was performed. There was no evidence of increased mitophagy or structural defects, as shown by representative images of mitochondria of WT and *Aldh1b1* null progenitors (Figure 3.8). Both types of progenitor cells showed a range of mitochondrial morphology from small, rounded spheres, short tubules to elongated tubes (Figure 3.8). Thus, the mitochondrial architecture displayed no structural alterations that could imply functional limitations responsible for increased ROS levels.
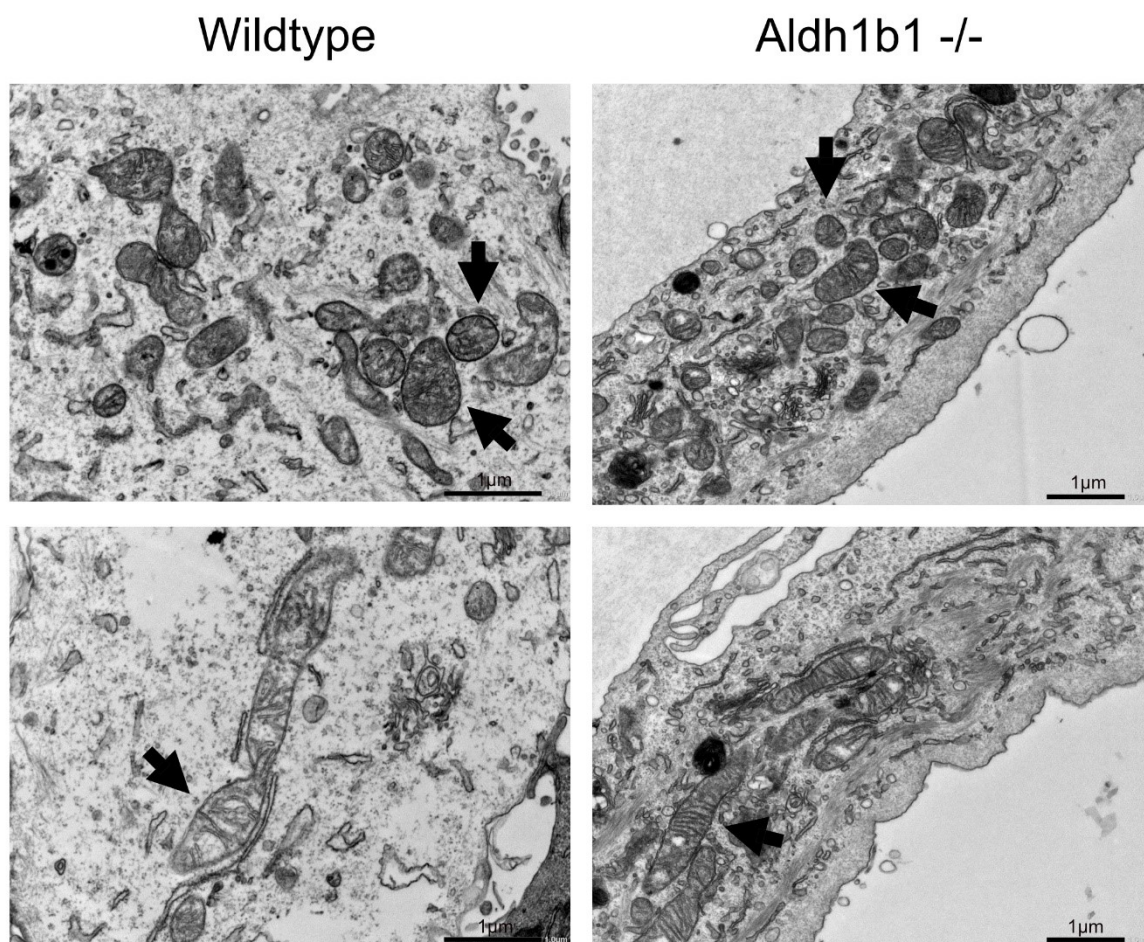
Figure 3.8: Assessment of the mitochondrial morphology. The mitochondrial morphology was examined by electron microscopy imaging of expanded WT and *Aldh1b1* null progenitor cells (n=3). Both cell types show a spectrum of different morphologies, which are highlighted by the arrows in these representative images. No signs of structural alternations or increased mitophagy were found.

Therefore, this analysis excluded the possibility of structural defects or underdeveloped mitochondria causing the elevated ROS levels.

3.1.5. Glucose tracing implicates Aldh1b1 function in lipid de-esterification

Metabolic reprogramming is an essential process during cellular differentiation. It is required for adapting to the changing energy needs and to ensure the production of metabolic intermediates that sustain the redox homeostasis and biosynthesis during different developmental stages. Additionally, certain metabolic fluxes are directly involved in the regulation of pluripotency and self-renewal, as well as timing of differentiation, and a disturbance of these fluxes could cause a desynchronization of developmental processes (McGraw and Mittal, 2010). It has been shown that *Aldh1b1* inactivation causes a premature differentiation in embryonic pancreas progenitors (Anastasiou et al., 2016) but how exactly Aldh1b1 regulates cell metabolism remains elusive and needs to be further investigated. To this end, expanded embryonic pancreas progenitors (3 biological replicates of each genotype) were incubated in a specific medium containing either uniformly labeled (U)-$^{13}C_6$-Glucose or 1,2-$^{13}C_2$-Glutamine tracers, which were incorporated by the cells and entered the cellular metabolism. The metabolites of the cells were extracted and analyzed by mass spectrometry and MIMOSA (Mass-Isotopomer Multi-Ordinate Spectral Analysis) in collaboration with Dr. Tiago Alves (TU Dresden, Medical Faculty). The detected patterns of incorporated ^{13}C facilitate a sensitive calculation of metabolic fluxes inside the cell. Each incorporated ^{13}C molecule increases the molecular mass of a given metabolite by 1 and allows the distinction of different
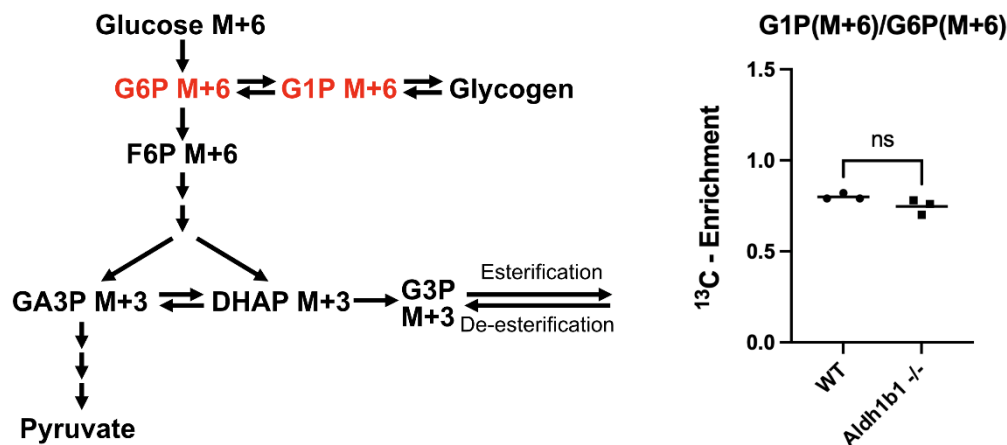
Figure 3.9: Contribution of metabolites deriving from glycogenolysis to the glycolysis. Minor reductions of the ^{13}C-enrichment of G1P compared to G6P indicated a rather low exploitation of the glycogenolysis in E14.5 pancreas progenitors. No differences between WT and *Aldh1b1* null progenitors was detected. The experiment was conducted with biological triplicates and statistical analysis was performed using unpaired t-test. Data were considered significant when *p≤0.05; **p≤0.01; ***p≤0.001; ****p ≤ 0.0001. G6P: Glucose-6-phosphate, G1P: Glucose-1-phosphate, F6P: Fructose-6-phosphate, GA3P: Glyceraldehyde-3-phosphate, DHAP: Dihydroxyacetone phosphate, G3P: Glycerol-3-phosphate.

labeling patterns. The analysis relies on the comparison of the ^{13}C enrichment of a given metabolite with the corresponding enrichment of its precursors, and therefore, determines the contribution of each precursor to the synthesis of the product. The enrichment patterns of E14.5 pancreas progenitors revealed an interesting metabolic profile and could determine some fundamental differences between the WT and *Aldh1b1* null metabolism. Using the U-$^{13}C_6$-Glucose tracer, which enters the cellular metabolism through the glycolytic pathway, allowed the assessment of the relative contribution of different fluxes to the generation of glycolytic metabolites.

A process that is connected to the upper glycolysis is the glycogenolysis/glycogenesis. Glycogen enters glycolysis as glucose-6-phosphate through the conversion of unlabeled glucose-1-phosphate. E14.5 progenitor cells showed a contribution of the glycogenolysis of approximately 20% into the generation of glucose-1-phosphate, suggesting a rather low reliance on glycolytic breakdown (Figure 3.9) and there was no difference between WT and *Aldh1b1* null in this respect. In the course of glycolysis, the hexose ring of glucose is split into two triose phosphate isomers dihydroxyacetone phosphate (DHAP) and glyceraldehyde 3-phosphate (GA3P), which are interconvertible by the action of triose-phosphate isomerase. DHAP can also be further converted into glycerol-3-phosphate (G3P), which is an important
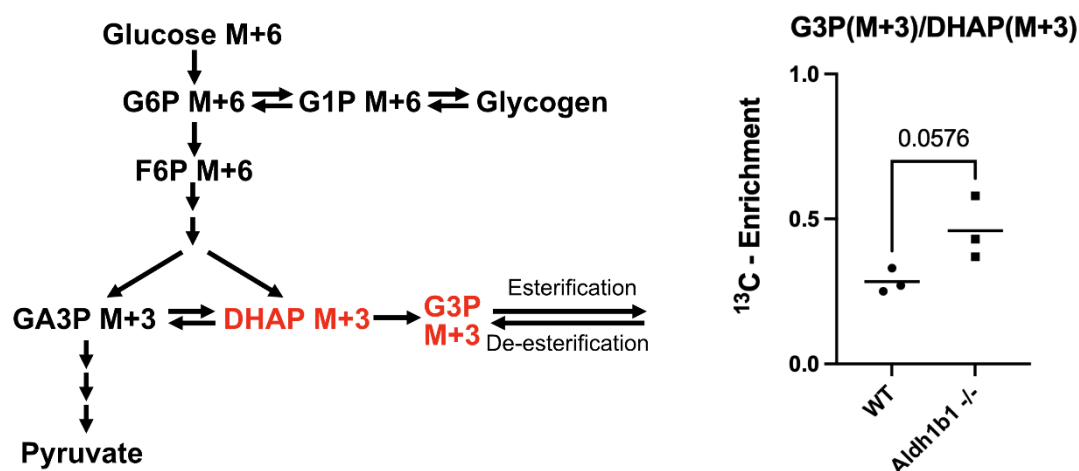
Figure 3.10: Contribution of the lipid de-esterification to the G3P pool. E14.5 WT and *Aldh1b1* null pancreas progenitors show a rather high reduction of the ^{13}C-enrichment of G3P, which indicates a very active de-esterification cycle. *Aldh1b1* null progenitors show a strong trend for a reduced rate of lipid de-esterification. The experiment was conducted with biological triplicates and statistical analysis was performed using unpaired t-test. Data were considered significant when *p≤0.05; **p≤0.01; ***p≤0.001; ****p ≤ 0.0001. G6P: Glucose-6-phosphate, G1P: Glucose-1-phosphate, F6P: Fructose-6-phosphate, GA3P: Glyceraldehyde-3-phosphate, DHAP: Dihydroxyacetone phosphate, G3P: Glycerol-3-phosphate.

precursor of the *de novo* synthesis of glycerophospholipids. In WT progenitor cells, a big fraction of the G3P was unlabeled, therefore suggesting that it was derived from glycerol breakdown through a very active lipid de-esterification process (Figure 3.10). *Aldh1b1* null

progenitors showed a strong trend of a reduced rate of lipid de-esterification and increased synthesis of G3P from the labeled glycolysis intermediate DHAP (M+3).
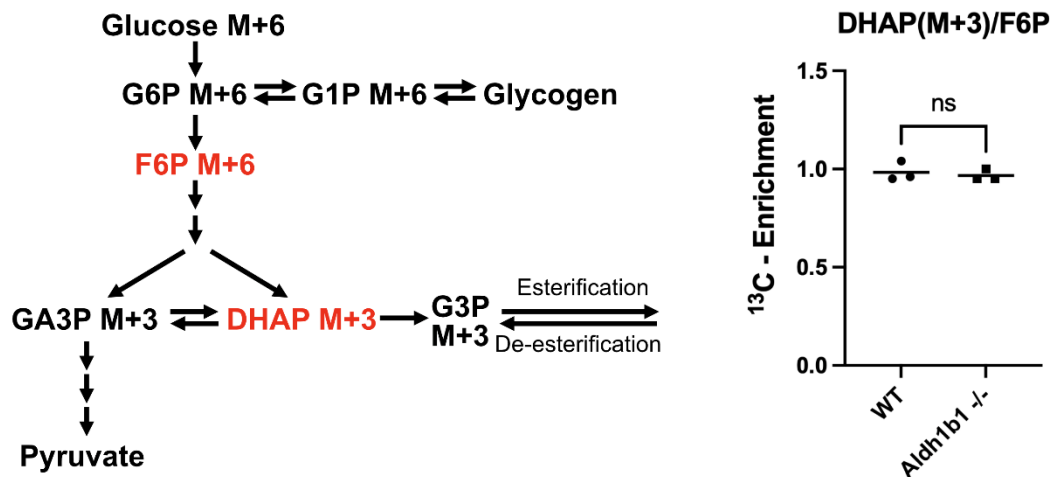
Figure 3.11: Contribution of glycolysis external fluxes to the pool of glycolytic triosephosphates. E14.5 WT and *Aldh1b1* null pancreas progenitors show no reduction in the ^{13}C-enrichment of DHAP compared to its precursor F6P, which indicates an inactivity of the glycerol phosphate shuttle. The experiment was conducted with biological triplicates and statistical analysis was performed using unpaired t-test. Data were considered significant when *p≤0.05; **p≤0.01; ***p≤0.001; ****p ≤ 0.0001.G6P: Glucose-6-phosphate, G1P: Glucose-1-phosphate, F6P: Fructose-6-phosphate, GA3P: Glyceraldehyde-3-phosphate, DHAP: Dihydroxyacetone phosphate, G3P: Glycerol-3-phosphate.

Next, the activity of the glycerol-3-phosphate shuttle was assessed, which could account for a reduction of the DHAP (M+3) / fructose-6-phosphate (M+3) ratio, but no external dilution of the labeled intermediates was detected (Figure 3.11). This suggested that this shuttle, which is responsible for a rapid transfer of NADH from the cytoplasm into the mitochondrion, is inactive in these cells.

Thus, even though glucose tracing revealed rather minor differences of the glycolytic fluxes between WT and *Aldh1b1* null pancreas progenitors, a dysregulation of the lipid metabolism caused by Aldh1b1 inactivation was detected.

3.1.6. TCA cycle metabolic tracing implicates Aldh1b1 in mitochondrial metabolism

Glycolysis is linked with the TCA cycle via the glycolytic end product pyruvate, which is transported through the mitochondrial membrane and subsequently decarboxylated by the enzyme pyruvate dehydrogenase (PDH), producing acetyl Co-A (Patel and Roche, 1990). The latter enters the TCA cycle through a condensation reaction with oxaloacetate catalyzed by citrate synthase (CS; Srere, 1969). Assessment of the contribution of glycolytic pyruvate to the
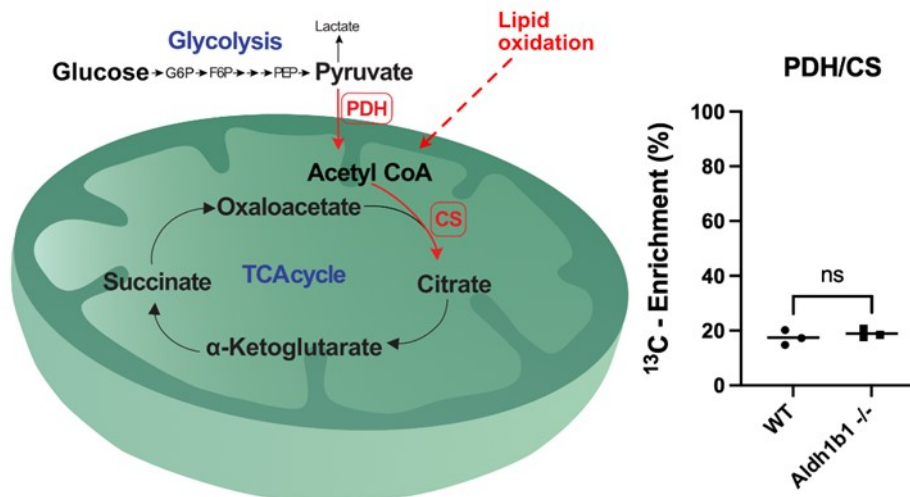
Figure 3.12: The contribution of glucose to the mitochondrial oxidation. The detected ^{13}C-enrichment of citrate was rather low and suggests a major external source contributing to the mitochondrial acetyl CoA pool. The experiment was conducted with biological triplicates and statistical analysis was performed using unpaired t-test. Data were considered significant when *p≤0.05; **p≤0.01; ***p≤0.001; ****p ≤ 0.0001.PDH: Pyruvate dehydrogenase, CS: Citrate synthase.

synthesis of citrate in E14.5 pancreas progenitors showed a rather low ^{13}C-enrichment of citrate of approximately 20% in WT and *Aldh1b1* null (Figure 3.12). This finding indicates a reduction of the labeling by an external acetyl-CoA source, most likely lipids. Thus, glucose is a minor source of TCA intermediates in these cells.

Another major source for TCA cycle intermediates is glutamine, which is a precursor of the TCA metabolite α-ketoglutarate. In order to assess its contribution to the mitochondrial fluxes, 1,2-[13]C$_2$-Glutamine isotopes were used. Glutamine is deaminated, in the mitochondrion or in the cytoplasm, to glutamate, which is further converted to α-ketoglutarate, a substrate of the mitochondrial TCA-cycle or citrate, respectively (Ablaet al., 2020). The E14.5 *Aldh1b1* null pancreas progenitor cells displayed a strong reduction of ^{13}C-enrichment, indicating that another unlabeled source contributed to the synthesis of glutamate (Figure 3.13). The significant decrease in glutamine conversion into glutamate that was detected in *Aldh1b1* null cells, suggested a potential block in the glutamine metabolism in *Aldh1b1* null progenitors.

Mitochondrial glutamate is further converted to α-ketoglutarate, which either contributes to the forward TCA cycle flux, which fuels OXPHOS, or it is converted to citrate by the reverse reductive carboxylation reaction catalyzed by Isocitrate dehydrogenase 2 (IDH2; Figure 3.14 A). The glutamate that stays in the cytoplasm is converted into citrate through another reverse reductive carboxylation reaction catalyzed by IDH1. Glutamate tracing, using 1,2-^{13}C-Glutamine, of the pancreas progenitor cells revealed a contribution of the reverse IDH (IDHr) reaction to the pool of citrate of app. 10% in WT cells, but this was significantly increased to

approximately 20% in the absence of functional Aldh1b1 (Figure 3.14 B). Cells usually exploit the IDHr reaction to maximize anabolic processes through citrate generation and to reduce mitochondrial respiration (Al-Khallaf, 2017). Changes in the relative expression of *Idh1* and
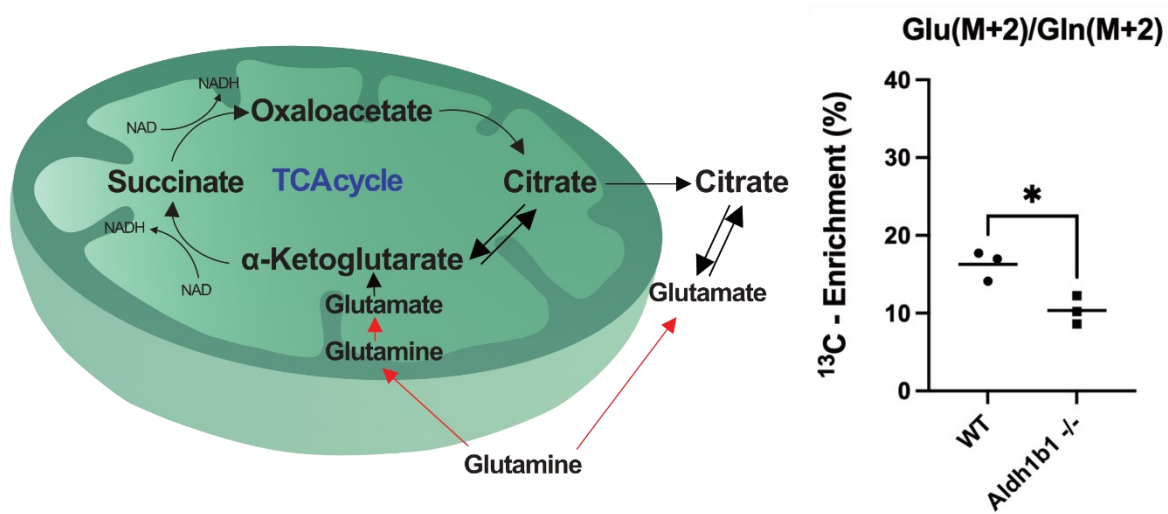
Figure 3.13: Analysis of the contribution of glutamine to the synthesis of glutamate. The ^{13}C-enrichment of glutamate compared to the enrichment of glutamine is significantly reduced in *Aldh1b1* null progenitor cells, implying a potential block in the conversion of glutamine driven by Aldh1b1. The experiment was conducted with biological triplicates and statistical analysis was performed using unpaired t-test. Data were considered significant when *p≤0.05; **p≤0.01; ***p≤0.001; ****p ≤ 0.0001.PDH: Pyruvate dehydrogenase, CS: Citrate synthase. Glu: Glutamate, Gln: Glutamine.

Idh2 in the *Aldh1b1* null progenitor cells would explain this finding but qPCR analyses did not detect such changes (Figure 3.14 C), implying a regulation independent from gene regulatory mechanisms.

Citrate is a precursor of acetyl-CoA, an important anabolic molecule, which participates in the synthesis of fatty acids (FA), glycerophospholipids, cholesterol as well as protein acetylation (Al-Khallaf, 2017). The majority of cellular citrate is produced through the condensation of oxaloacetate and acetyl-CoA catalyzed by citrate synthase (CS) in the mitochondrion. Mitochondrial citrate either contributes to the energy metabolism as a TCA cycle substrate or to anabolic processes via its transport to the cytosol and acetyl-CoA conversion, catalyzed by the cytosolic enzyme ATP citrate lyase (ACLy). Surprisingly, WT E14.5 pancreas progenitors showed a major contribution of about 90% of CS synthesized citrate to ACLy conversion but this contribution appeared reduced in *Aldh1b1* null progenitors (Figure 3.14 D). This was further supported by the finding that gene expression levels of *Acly* and the mitochondrial citrate transporter *Slc25a1* were significantly reduced (Figure 3.14 E). Therefore, Aldh1b1 loss-of-function results in a reduction of the TCA flow towards acetyl-CoA and this could impact the lipid metabolism and acetylation activity of the cell.
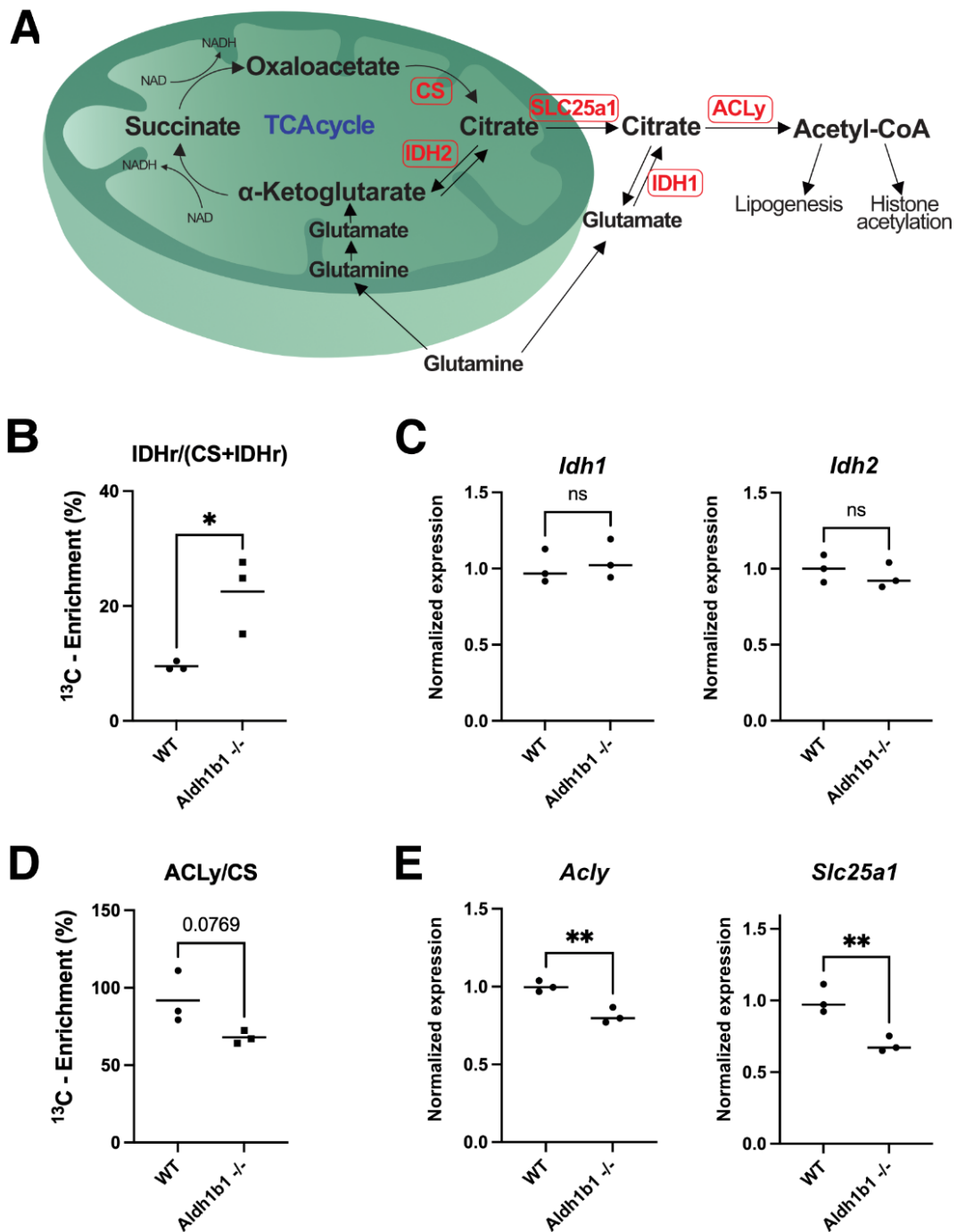
Figure 3.14: Flux analysis of the contribution of IDHr and ACLy. (A) Overview of reversed IDH reaction, citrate synthesis and breakdown to acetyl-CoA. (B) Contribution of the reverse IDH reaction to the citrate synthesis: *Aldh1b1* null progenitors show a significant increase of this reaction. (C) Gene expression analyses of cytoplasmic IDH1 and mitochondrial IDH2 show no difference between WT and *Aldh1b1* null expression. (D) Fraction of CS that breaks citrate into acetyl CoA: *Aldh1b1* Inactivation seems to cause a reduction in the generation of acetyl-CoA from citrate. (E) Quantitative PCR analyses show a decrease in the expression of *Acly* and the citrate transporter *Slc25a1*. The experiments were conducted with biological triplicates and statistical analysis was performed using unpaired t-test. Data were considered significant when *$p \leq 0.05$; **$p \leq 0.01$; ***$p \leq 0.001$; ****$p \leq 0.0001$. IDH: Isocitrate dehydrogenase, CS: Citrate synthase, ACLy: ATP citrate lyase.

57

ACLy catalyzes the generation of acetyl-CoA and oxaloacetate from citrate and coenzyme A in the presence of ATP. Oxaloacetate is subsequently transformed to malate which can re-enter the TCA cycle (Chypre et al., 2012). Since E14.5 pancreas progenitors were found to strongly exploit the ACLy reaction, a majority of the mitochondrial citrate is shuttled out into the cytoplasm to be consumed in this reaction, which in turn, creates an oxygen-independent loop between ACLy and CS (Figure 3.15 B). Calculation of the contribution of citrate, generated by the mitochondrial CS, to the oxygen-dependent TCA cycle, revealed a rather low TCA flux in WT progenitors, which was found to be significantly increased in absence of Aldh1b1 (Figure 3.15 A). This result suggests that the reduced conversion of citrate into acetyl-CoA, observed in the *Aldh1b1* null progenitors, promotes increased TCA-cycle activity (Figure 3.15 B).
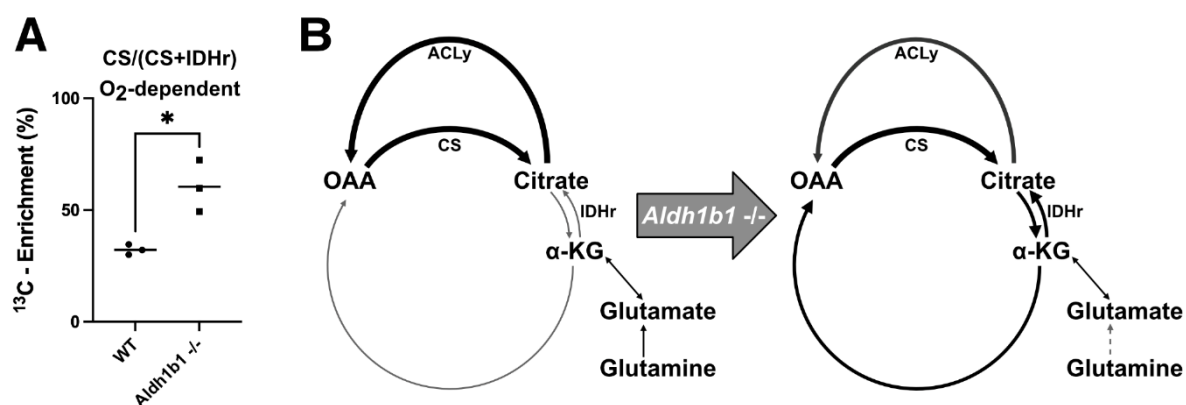
Figure 3.15: Oxygen-dependent and independent fluxes of E14.5 pancreas progenitors. A) Estimation of the contribution of citrate, derived from CS production to the TCA cycle showed a significant increase in *Aldh1b1* null pancreas progenitors. (B) Summary of the findings detected in E14.5 pancreas progenitors. *Aldh1b1* null displayed in comparison with WT progenitors a decreased conversion of glutamine into glutamate and an increase of the reversed IDH conversion from α-KG into citrate. Interestingly, the flux towards ACLy-dependent acetyl-coA production was detected to be reduced in *Aldh1b1* null progenitor cells. The experiments were conducted with biological triplicates and statistical analysis was performed using unpaired t-test. Data were considered significant when *$p \leq 0.05$; **$p \leq 0.01$; ***$p \leq 0.001$; ****$p \leq 0.0001$. IDH: Isocitrate dehydrogenase, CS: Citrate synthase, ACLy: ATP citrate lyase, OAA: Oxaloacetate, α-KG: α-ketoglutarate.

3.1.7. Untargeted metabolome analysis reveals metabolites affected by Aldh1b1 function

Metabolite tracing revealed differences in metabolic fluxes of *Aldh1b1* null pancreas progenitors compared to the WT and uncovered metabolic defects caused by Aldh1b1 inactivation. Additionally, ongoing tracing experiments will strengthen the statistical

significance of the experiments described above and will provide a more detailed picture of affected metabolic fluxes. In order to receive an unbiased overview of a broad range of potentially affected metabolites also outside the glycolytic and TCA cycle fluxes, metabolite concentrations were analyzed using an untargeted metabolomics approach in collaboration with Mirko Peitzsch in the TU Dresden Medical Faculty.

To this end, E14.5 pancreas progenitors were expanded, their metabolites extracted in 80% methanol, and then analyzed using ultra performance liquid chromatography (UPLC) with subsequent tandem mass spectrometry (MS/MS). This technique combines chromatographic separation of the metabolites with a subsequent detection of the mass-to-charge ratio of the molecules. The latter is achieved by an ionization of the metabolites, followed by an acceleration through a magnetic field, which implements the separation of the molecules according to their mass-charge-ratio. The advantage of using tandem mass spectrometry is a second ionization event that causes a fragmentation of the molecules in a predictable manner. This increases the specificity of the method and allows a more precise identification of metabolites. The detection is based on the charge of the fragments that creates a current at the detector and the information about the mass-charge-ratio is provided by the separation process.
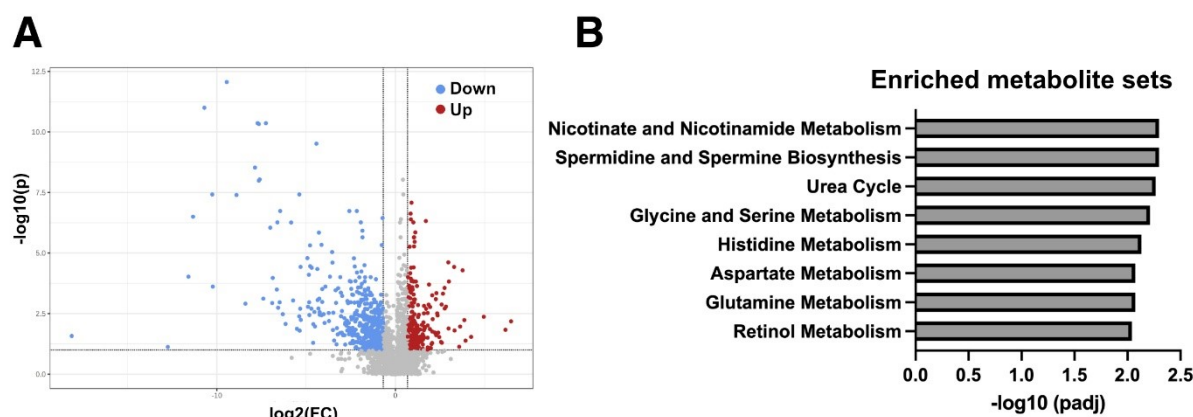
Figure 3.16: Untargeted metabolome analysis. (A) Volcano plot showing significantly regulated fragments of E14.5 *Aldh1b1* null pancreas progenitors comparted to the WT. 379 fragments were detected that showed a significant downregulation in absence of functional Aldh1b1 and 186 upregulated. The thresholds that were applied were set to a 1.6 FC and 5% FDR. (B) The metabolite set enrichment analysis of the experimental data was performed by using MetaboAnalyst 5.0. Metabolite sets with the highest p-values and enrichment scores were plotted.

Although the sensitivity of mass spectrometers has been improved throughout the last years, low cell numbers, as provided from the spheroid culture, are still challenging (Labib and Kelley, 2020). An additional complication was the extraction of the cells from Matrigel, which on one hand minimized the influence of Matrigel proteins on the analysis but on the other hand also increased the time of the metabolites at a temperature over -80 °C. This might have

caused a degradation of unstable metabolites, which in turn reduces the detectable spectrum of molecules.

The analysis determined significant differences in the metabolite profiles of WT and *Aldh1b1* null progenitors as there were 565 fragments detected with significantly altered concentrations in *Aldh1b1* null progenitors (Figure 3.16 A). 176 metabolites could be identified from the measured fragments and 61 metabolites were regulated in Aldh1b1 loss-of-function progenitors.

Since E14.5 pancreas progenitors display a notable increase in ROS levels in the absence of Aldh1b1 activity, it was investigated if a dysregulation in the biosynthesis of the tripeptide glutathione could be detected. Glutathione is a natural cellular antioxidant composed of the 3 amino acids glutamate, cysteine and glycine. However, no difference in the abundance
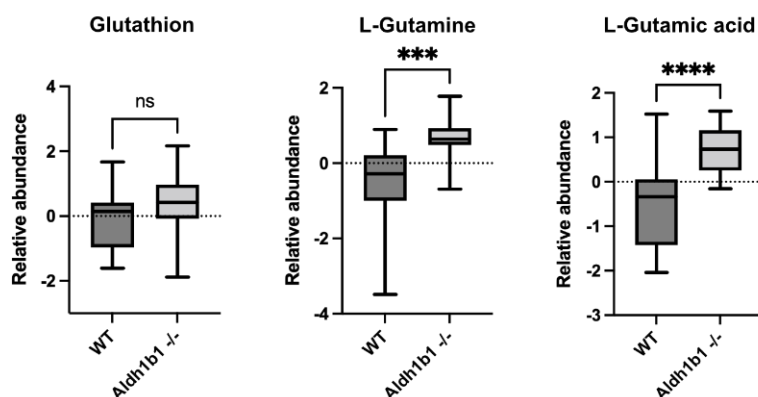
Figure 3.17: Representative metabolites that were detected using an untargeted UPLC-MS/MS approach, showing a differential regulation in *Aldh1b1* null pancreas progenitors. Shown are examples of metabolites from (A) glutamine metabolism, (B) methionine metabolism and (C) other progenitor cell related metabolites that show significantly different abundances in expanded *Aldh1b1* null progenitors. The data were analyzed using MetaboAnalyst 5.0. The data was log transformed and auto scaled. The experiments were conducted with WT and *Aldh1b1* null expanded progenitors (n=5 and n=3, respectively) in technical triplicates and statistical analysis was performed using unpaired t-test. Data were considered significant when *p≤0.05; **p≤0.01; ***p≤0.001; ****p ≤ 0.0001.

of glutathione was detected (Figure 3.17 A), suggesting that the ROS detoxification capacity is similar in WT and *Aldh1b1* null progenitors.

To identify other affected pathways, a metabolite set enrichment analysis of the experimental data was performed using MetaboAnalyst 5.0 (https://www.metaboanalyst.ca/). This analysis revealed significant enrichment in metabolic pathways of amino acids, as well as retinol, spermine and nicotinamide metabolism (Figure 3.16 B). L-glutamine and L-glutamic acid concentration showed a significant increase in *Aldh1b1* null progenitors. This might be a sign of a metabolic block (Figure 3.17 A), which could in turn be caused by biosynthesis pathways of other amino acids or citrate, that use glutamic acid as a precursor (Yoo, Yu and Sung et al., 2020).

Interestingly, the abundance of both, principal methyl donor, S-adenosylmethionine (SAM), and its demethylated form, S-adenosylhomocysteine (SAH) which is generated after DNA/RNA or protein methylation, was significantly increased in the absence of *Aldh1b1* (SAH; Figure 3.17 B). This suggested a potential increase in methylation (Parkhitko et al., 2019).

Spermine and Niacinamide, which are metabolites implicated in progenitor differentiation, cell fate and survival (Allmeroth et al., 2021; Zhang et al.,2021) also showed a significant downregulation in progenitor cells lacking Aldh1b1 activity (Figure 3.17 C).

Furthermore, vitamin A and glycerophosphocholine concentrations were increased in *Aldh1b1* null progenitors (Figure 3.18 B). Both metabolites are associated with retinoic acid metabolism, an important signaling molecule involved in the process of progenitor differentiation. Glycerophosphocholine, is a by-product of the retinyl ester synthesis (Figure 3.18 A), a storage form of vitamin A (Mata et al., 2004). An increase in the glycerophosphocholine abundance could therefore indicate a reduced presence of vitamin A derived retinoids in *Aldh1b1* null progenitors at E14.5.
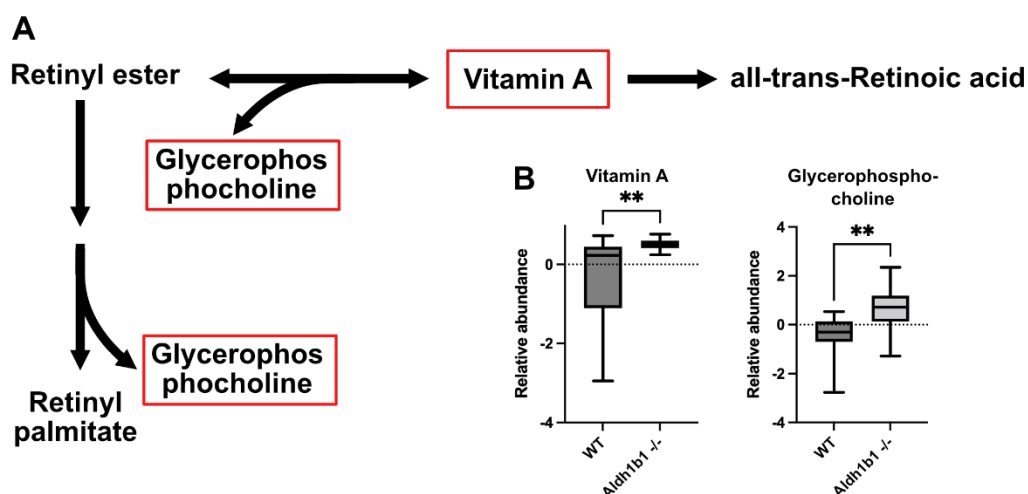
Figure 3.18: Untargeted UPLC-MS/MS analysis detected an increase in the concentration of vitamin A and glycerophosphocholine in *Aldh1b1* null progenitors. (A) displays the involvement of both metabolites progenitors in the retinol metabolism and (B) shows the abundance of vitamin A and glycerophosphocholine in WT and *Aldh1b1* null progenitors.

Therefore, inactivation of Aldh1b1 causes major perturbations in the progenitor cell metabolism, providing the basis to explain the changes in the processes of differentiation and cell fate observed in *Aldh1b1* null pancreas progenitors.

3. Results: Part 2

3.2. Aldh1b1 activity affects the gene expression of pancreas progenitors and postnatal β-cells

Aldh1b1 is expressed in all embryonic pancreatic progenitors and acts as a regulator of pancreatic progenitor differentiation and endocrine lineage specification (Ioannou et al., 2013, Anastasiou et al., 2016). *Aldh1b1* functional inactivation resulted in premature differentiation of progenitor cells during development and consequently in dysfunctional β-cells in the adult. In order to illuminate the processes that result in postnatal β-cell dysfunction, I examined the effects of Aldh1b1 loss-of-function on chromatin structure and gene expression.

3.2.1. Chromatin accessibility is reduced in *Aldh1b1* null embryonic pancreas progenitors

The findings presented in the previous chapter suggested that Aldh1b1 inactivity causes an aberrant metabolic profile in pancreas progenitors at E14.5. How exactly these defects affect progenitor differentiation and functionality of the postnatal β-cells remains to be elucidated. Earlier studies have shown that postnatal islets of *Aldh1b1* null mice exhibit a dysregulated gene expression at postnatal day 1 (P1), which is even more pronounced in islets of 8-week-old mice (Anastasiou et al., 2016). In order to comprehend how Aldh1b1 deficiency, and hence the concomitant metabolic dysregulation during embryonic development, affect postnatal gene expression and functionality of β-cells, a closer look into the chromatin accessibility of E14.5 pancreas progenitors was deemed necessary. A defective implementation of epigenetic marks could result in insufficient genetic silencing or activation, which would persist into adulthood. The Assay for Transposase-Accessible Chromatin sequencing (ATAC-seq) is an approach used to determine potential differences in chromatin accessibility, a property directly connected to the epigenetic state of the WT and *Aldh1b1* null embryonic pancreas progenitors. This technique uses a hyperactive Tn5 transposase loaded with NGS adapters, thus enabling simultaneous fragmentation and tagging of open chromatin. Subsequent amplification and purification of the tagged DNA fragments, allows for sequencing and mapping to a reference genome. The number of reads assigned to a region in the genome is a direct measure of accessibility. Performing ATAC-seq in E14.5 pancreas progenitors revealed a surprising exclusive reduction of the chromatin accessibility in *Aldh1b1* null progenitors (Figure 3.19 A). Differential peaks were found predominantly in close proximity to transcription start sites (Figure 3.19 B). These findings constituted strong evidence for a reduced accessibility of DNA-binding proteins to the promoter region of specific genes in the absence of Aldh1b1 activity.

Representative consensus peak sets illustrating the reduced peak size in *Aldh1b1* null pancreas progenitors, are displayed in Figure 3.19 C. Subsequently, I conducted gene ontology (GO) analysis of relevant affected genes in order to determine if they could be associated with certain biological functions (Figure 3.20 A). The top ranked biological functions of the gene sets were all linked to processes of chromatin organization and modification as well as protein acetylation. Thus, the aberrations observed in the chromatin accessibility in *Aldh1b1* null pancreas progenitors, could indeed affect chromatin properties later on.

Motif analysis of the differential peak set revealed an enrichment of Krüppel-like factor and specificity protein (Klf/Sp) binding sites (Figure 3.20 B) in the affected regions. The Klf/Sp family is a group of highly related C2H2 zinc finger class transcription factors, whose DNA-binding-domain preferentially binds to CACC elements and guanine-cytosine-rich regions. They contribute as transcriptional activators or repressors in several cellular processes including stem cell maintenance, progenitor cell differentiation and proliferation (Presnell et al.,
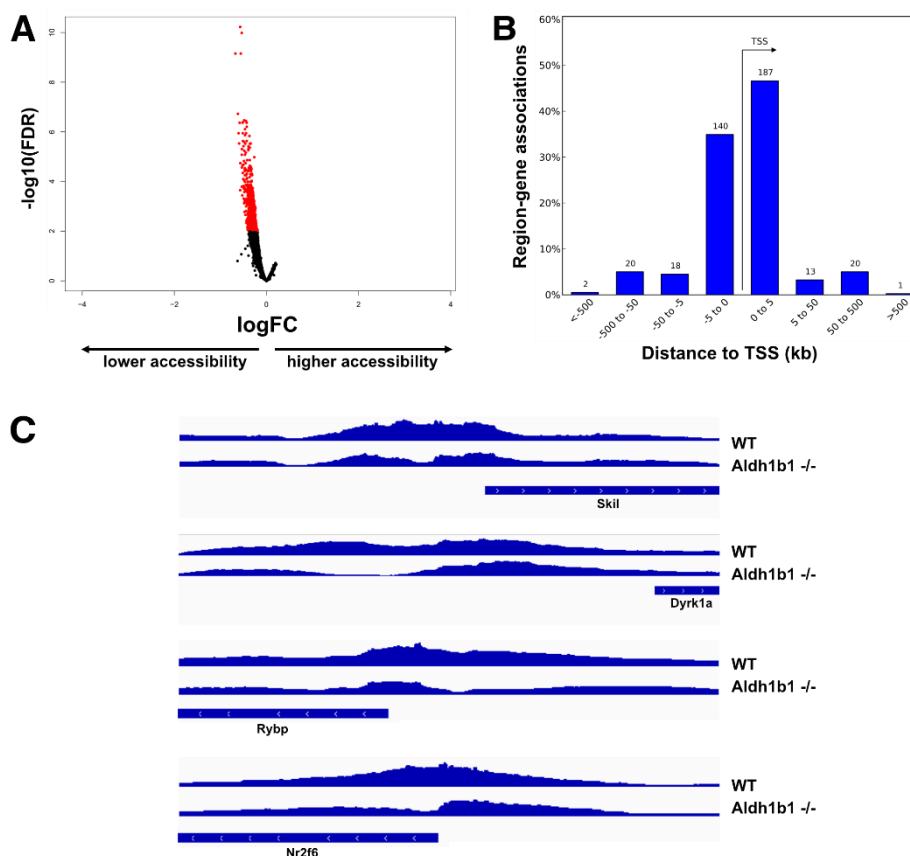
Figure 3.19: ATAC-seq of E14.5 pancreas progenitors. (A) *Aldh1b1* null (n=2) progenitors display a reduced chromatin accessibility compared to the WT (n=2). Red data points represent significant peaks (FDR < 0.01). (B) The majority of differential peaks was found in close proximity to the TSS. In (C), a representative peak set is shown that illustrates the reduced peak size in *Aldh1b* null progenitors. The peaks were called using MACS algorithm and DESeq2 analysis of the 2 WT and 2 *Aldh1b1* null samples was performed to identify differential peaks.

2015). Another enriched motif corresponds to Nuclear respiratory factor 1 (Nrf1) binding sites. This transcription factor is involved in the regulation of cellular respiration and metabolism.

In summary, loss of Aldh1b1 activity appears to cause a reduction of the chromatin accessibility in pancreas progenitors. Affected regions are mainly located close to the
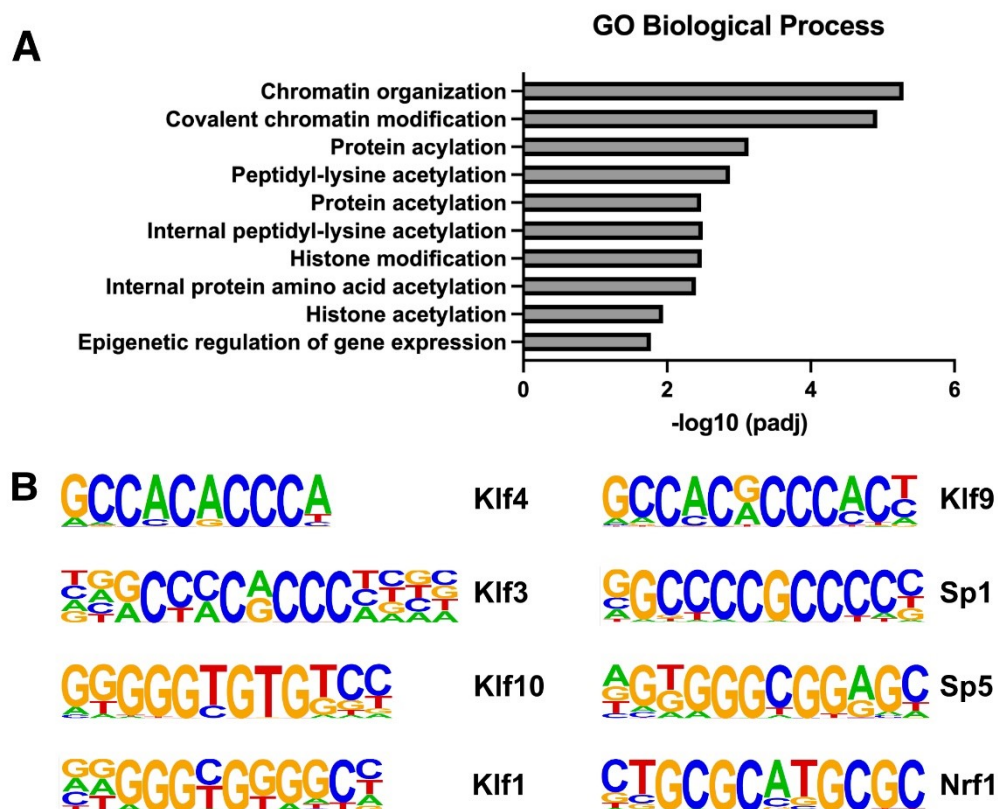
Figure 3.20: GO and motif analysis of a selected ATAC peak set. (A) GO analysis was performed using GREAT tool. Genes associated with the affected chromatin sites in *Aldh1b1* null progenitors were top ranked in biological functions that are linked to processes of chromatin organization and modification as well as protein acetylation. (B) HOMER motif analysis revealed an enrichment of Klf/Sp binding sites in the affected chromatin regions.

transcription start site, where reduced accessibility could interfere with the binding of important differentiation regulators. Nevertheless, whether these changes in the chromatin landscape translate into transcriptional changes, needs to be investigated.

3.2.2. Identification of early differentially expressed genes in *Aldh1b1* null pancreas progenitors

Transcriptional activation directly depends on the accessibility of promoters, enhancers and silencers and it is, therefore, strongly linked to absence of nucleosomes in those regions. Nucleosome remodeling can affect the rate of transcription initiation of a wide range of genes. In order to assess whether the observed changes in the accessibility of the DNA in *Aldh1b1* null E14.5 pancreas progenitors were translated into transcriptional changes, an RNA-seq

experiment was performed from of 3 WT and 5 *Aldh1b1* null samples. The analysis allowed the determination of early changes in the gene expression of *Aldh1b1* null pancreas progenitors. However, at this stage, fold changes were rather low and the analysis, relied exclusively on a cutoff with 5% False Discovery Rate (FDR). This analysis identified 1122 differentially expressed genes od which 655 were upregulated and 467 downregulated (Figure 3.21 A). The RNA-seq analysis revealed an upregulation of important progenitor markers, linked to processes of the trunk compartment differentiation, such as *Sox9*, *Onecut-1*, *Prox1*, *Glis3, Hnf1b* and *Mnx1*. Although the expression of the aforementioned markers of progenitor differentiation was increased, some genes expressed in terminally differentiated endocrine cells, such as *Ins1, Ins2* and *Adcyap1r1,* were downregulated in *Aldh1b1* null progenitors (Figure 3.22 A), whereas the expression of others, such as *Gcg* or *Ghrl* did not change. Moreover, performing gene ontology analysis (GO) using the determined differentially regulated genes, disclosed a general dysregulation of genes involved in epithelial proliferation (Figure 3.21 B and 3.22 D). Thus, Aldh1b1 inactivation leads to a defective expression of progenitor and endocrine markers at E14.5 as well as a dysregulation of marker genes involved in epithelial proliferation.
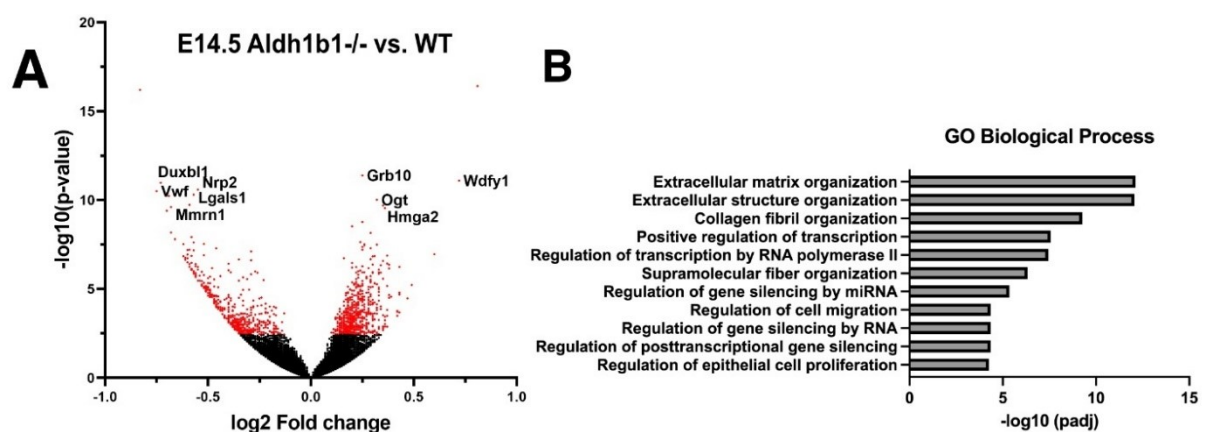
Figure 3.21: Differential expression analysis of E14.5 pancreas progenitors. (A) The volcano plot shows 1012 significantly regulated genes in *Aldh1b1* null β-cell compared to the WT (FDR 5%), the *Aldh1b1* gene was excluded in this plot for representative reasons. (B) Gene ontology (GO) analysis of differentially expressed genes revealed a dysregulation of genes involved in extracellular matrix organization, transcription regulation, cell migration and proliferation. GO analysis was performed using Enrichr. Differential gene expression analysis was performed by running DESeq2 of 3 WT and 5 *Aldh1b1* null samples.

In order to exclude the possibility that other family members of the Aldh family were upregulated in order to compensate for Aldh1b1 inactivation, the gene expression of all detected Aldh members was controlled for differentially regulation. None of these genes showed a significant upregulation and *Aldh1a2* was even downregulated in the absence of Aldh1b1 (Figure 3.22 A). Moreover, no dysregulation of genes encoding for enzymes involved in glycolysis or TCA cycle was detected and no regulation of genes involved in oxidative damage response or ROS detoxification was observed either. Interestingly, numerous

members of the SLC protein group were dysregulated in *Aldh1b1* null progenitors compared to the WT (Figure 3.21 E). SLC is a superfamily of transporter proteins, which transfer a plethora of substances across cellular membranes and act as metabolic gatekeepers (Colas et al., 2016). Affected SLC proteins belong to all kinds of carriers, which could, therefore, interfere with a wide variety of primarily metabolic processes.
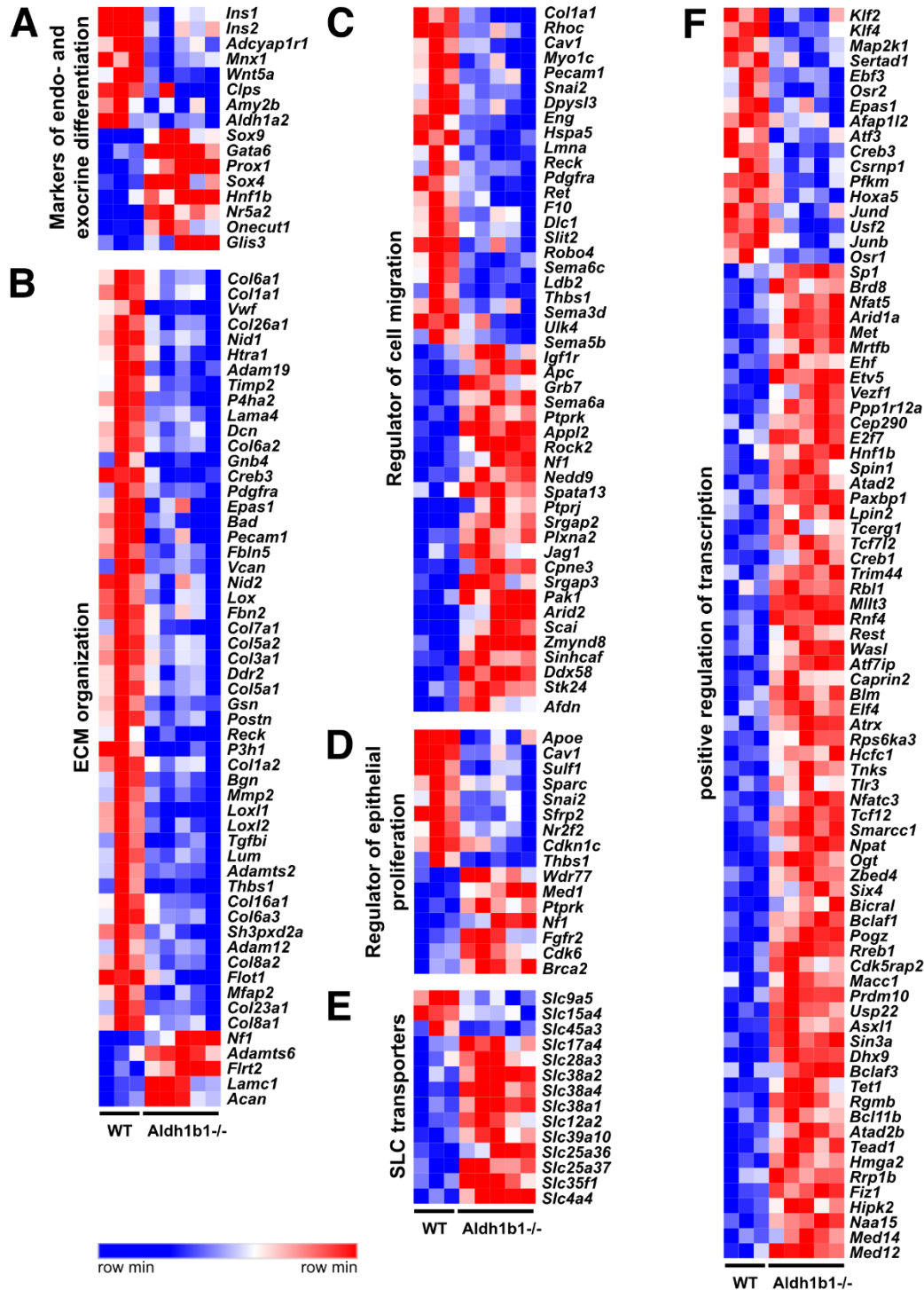
Figure 3.22: Z-score heatmaps of early differentially regulated gene sets in *Aldh1b1* null progenitors: A-E: Gene sets that show a dysregulation in E14.5 *Aldh1b1* null pancreas progenitors. Differential gene expression analysis was performed by running DESeq2 of 3 WT and 5 *Aldh1b1* null samples. The heat maps were designed using Morpheus.

GO analysis found a strong enrichment of dysregulated genes in the process of extracellular matrix (ECM) organization (Figure 3.21 B). The ECM provides essential cues that are required for the regulation of differentiation, morphogenesis as well as tissue homeostasis and it is required for physical scaffolding (Frantz et al., 2010). The majority of the differentially regulated genes involved in the establishment of the ECM were found to be downregulated in absence of Aldh1b1 (Figure 3.22 B), indicating reduced interaction with neighboring cells as well as a lower integration rate of specific extracellular signals. Furthermore, the results of the GO analysis suggested an enrichment of differentially expressed genes which are associated with cell migration (Figure 3.21 B), a process that is often employed by cells which participate in morphogenetic programs (SenGupta et al., 2021). *Aldh1b1* null pancreas progenitors exhibited a dysregulation of many genes associated with this process (Figure 3.22 C). Lastly, several differentially expressed genes involved in transcriptional regulation were upregulated in *Aldh1b1* null pancreas progenitors indicating an increase in transcriptional activity (Figure 3.21 B and 3.22 F). Hence, Aldh1b1 inactivation causes a number of early defects in the pancreatic gene expression, which might lead to developmental defects of the progenitor cells and could affect the maturation as well as functionality of the differentiated cells later on.

3.2.3 RNA-seq analysis of *Aldh1b1* null β-cells reveals an altered gene expression profile at P10

Aldh1b1 is a mitochondrial enzyme, but its expression is ablated in differentiated β-cells. Nevertheless, *Aldh1b1* loss-of-function during early embryonic development resulted in a defective insulin secretion postnatally (Anastasiou et al., 2016). To assess if the transcriptional dysregulations, observed at E14.5, persisted in β-cells, RNA-sequencing of P10 β-cells was performed.

To this end, an *Ins1*[Cre] knock-in line (Thorens et al., 2015) was used and intercrossed with *ROSA26*[LSLtdTomato] mice, in order to label *Ins1* expressing β-cells with TdTomato (TdT). First, the recombination efficiency was determined by insulin immunofluorescence staining at P1 and P25 and revealed that approximately 95% to 100% of all Ins^{+} cells were TdT[+] at both stages (Figure 3.23 A). Additionally, no ectopic TdT expression was detected. Experiments were performed using murine β-cells from P10 pancreata to capture the gene expression at the earliest postnatal age that also allowed the collection of a decent cell number. A single cell suspension of the collected pancreata was prepared by performing collagenase digestion. TdT[+] β-cells were isolated using FACS and were further processed for RNA-sequencing (Figure 3.23 B).
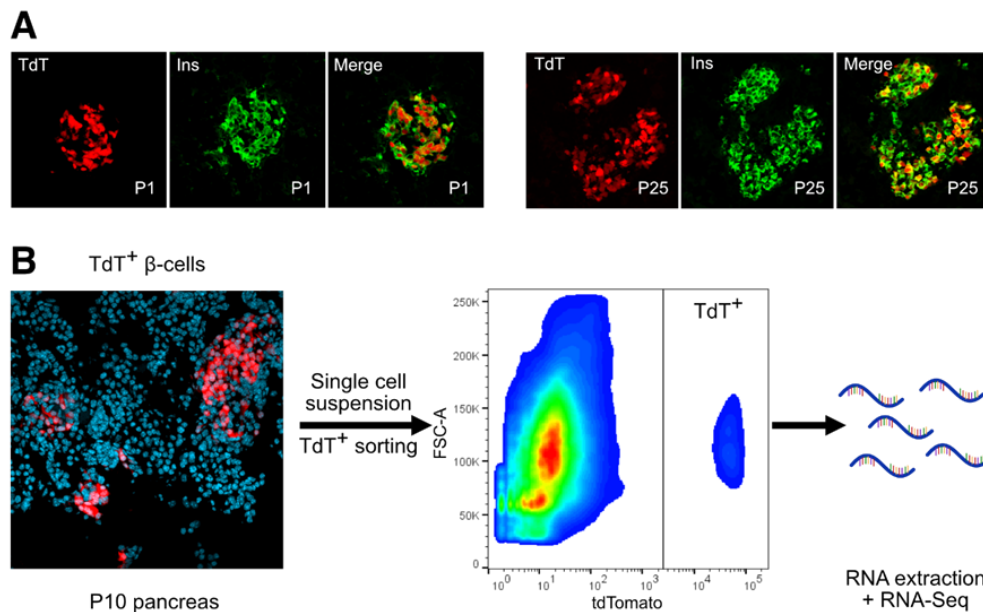
Figure 3.23: Isolation of Tdt⁺ β-cells. Murine β-cells were labeled by Ins1-Cre induced TdT expression. (A) The recombination efficiency was determined at P1 and P25 by immunofluorescence staining of insulin and revealed that approximately 95% to 100% of all Ins⁺ cells were also TdT⁺. No ectopic TdT expression was detected. (B) β-cells were FACS isolated and lysed to collect RNA.

Analysis of P10 β-cell RNA-seq data, using 3 biological replicates of each genotype, was performed using a 5% FDR cutoff. This analysis identified persisting but minor dysregulation of 304 genes in *Aldh1b1* null postnatal β cells, from which 219 genes were upregulated and 85 downregulated (Figure 3.24 A). Interestingly, gene set enrichment analysis (GSEA) suggested an enrichment of regulated genes in *Aldh1b1* null β-cells that are involved in glutathione metabolism and oxidative damage response (Figure 3.24 B). This indicated the existence of continuous oxidative stress in postnatal β-cells. GO analyses revealed a dysregulation of differentially expressed genes that are involved in mitosis (Figure 3.24 C). Genes associated with processes such as mitotic spindle organization, sister chromatid segregation, G1 to S phase transition as well as DNA metabolic processes were mainly upregulated in *Aldh1b1* null β-cells (Figure 3.25 A-D), such upregulation is usually associated with increased cell division. Thus, P10 β-cells, which differentiated in the absence of functional Aldh1b1, seem to display an increased proliferation activity.

GSEA analysis also suggested a regulation of genes involved in the biosynthesis of ribosomal proteins as well as genes involved in PPAR signaling (Figure 3.24 B), both processes have implications in proliferative activity (Jorgensen et al., 2002; Vivas et al., 2011; Reza and Yuan, 2021). Consistent with the findings in the E14.5 progenitors, no deregulation in the gene expression of enzymes involved in glycolysis and TCA cycle was detected. However, transcription of the gene encoding for the enzyme ACLy was significantly down
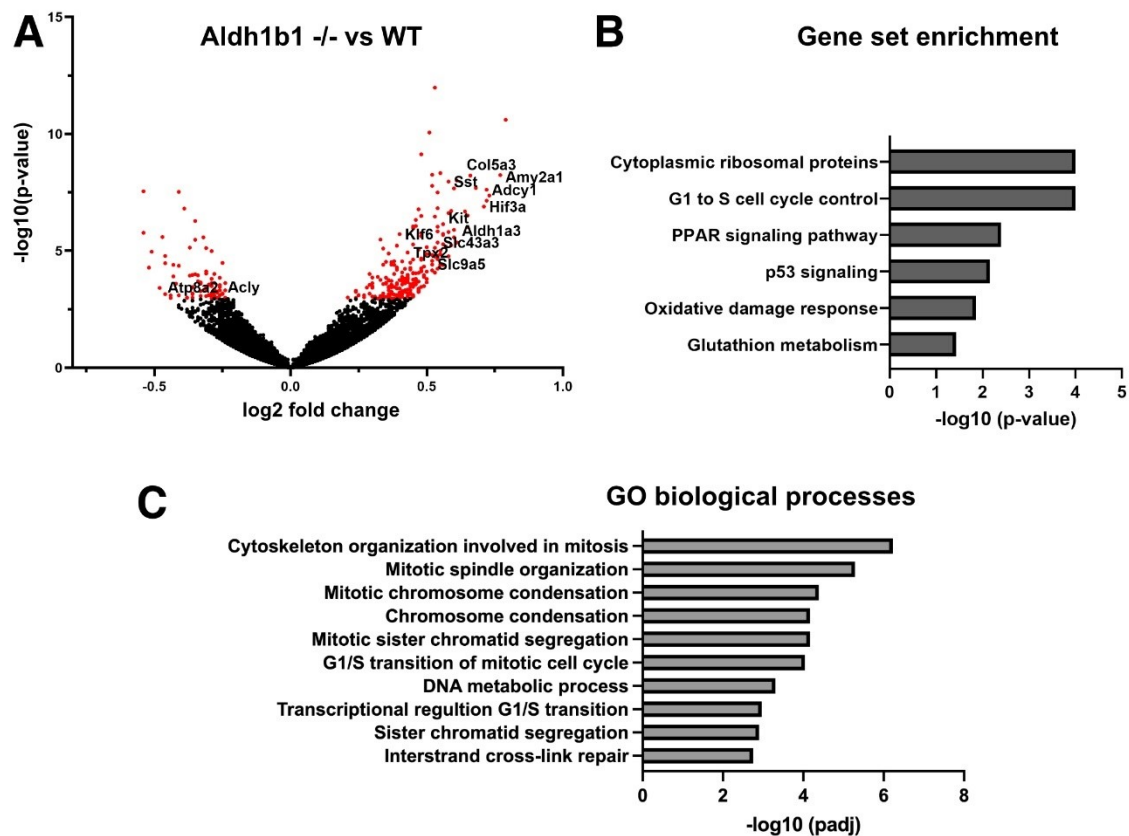
Figure 3.24: Differential expression analysis of P10 β-cell. (A) The volcano plot shows 304 differentially regulated genes in *Aldh1b1* null β-cells compared to the WT (FDR 5%). (B) GSEA of differentially expressed genes. (C) GO analysis of differentially expressed genes revealed a global dysregulation of gene set involved in the process of mitosis. Differential gene expression analysis was performed by running DESeq2 of 3 WT and 3 *Aldh1b1* null samples.

regulated in *Aldh1b1* null β-cells (Figure 3.24 A). ACLy showed already a downregulation in E14.5 expanded progenitor cells and this might be associated with a decreased conversion rate of citrate (Chapter 3.1.6, Figure 3.14). This result suggested that *Aldh1b1* null β-cells carry a persistent metabolic defect. Lastly, an upregulation of genes linked to β-cell dedifferentiation, such as *Amy2a1, Sst, Aldh1a3* as well as *Klf6,* was detected in *Aldh1b1* null cells (Kim-Muller et al., 2016; Dumayne et al., 2020; Figure 3.24 A). Taken together, transcriptional differences of P10 *Aldh1b1* null β-cells in comparison with their WT counterpart are rather small but suggested an increased β-cell proliferation as well as persisting oxidative stress and an upregulation of genes that are associated with β-cell dedifferentiation in young *Aldh1b1* null mice.
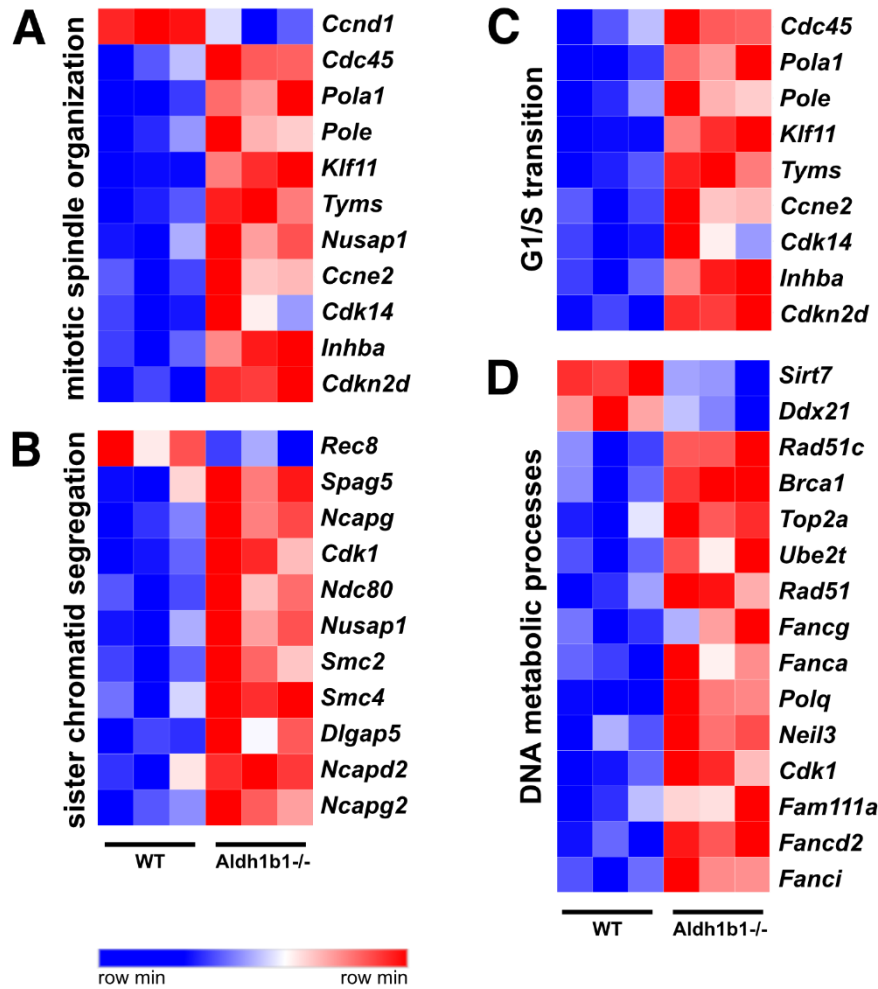
Figure 3.25: Z-score heatmaps of differentially regulated genes in *Aldh1b1* null β-cells. An upregulation of genes associated with cytoplasmic ribosomal proteins (A), cell cycle control (B), PPAR signaling (C) as well as GPCR signaling (D) was detected in P10 *Aldh1b1* null β-cells. Gene sets were considered significantly enriched if the normalized enrichment scores had an FDR q-value below 0.25. Differential gene expression analysis was performed by running DESeq2 and the heat maps were designed using Morpheus.

3.2.4. ROS scavenging reverts the *Aldh1b1* null progenitor phenotype *in vitro*

Previous studies have observed a premature differentiation of *Aldh1b1* null pancreas progenitor cells *in vivo* at E14.5, documented by the increase of Ngn3 expression, a transcription factor inducing endocrine lineage differentiation. Moreover, the differentiation markers C-Peptide, Amylase, DBA as well as the proliferation marker PH3, were also found to be significantly increased (Anastasiou et al., 2016). According to the epithelial PH3 expression, E14.5 was determined as the peak of *Aldh1b1* null pancreas progenitor proliferation, with an almost 3-fold increase compared to the WT.
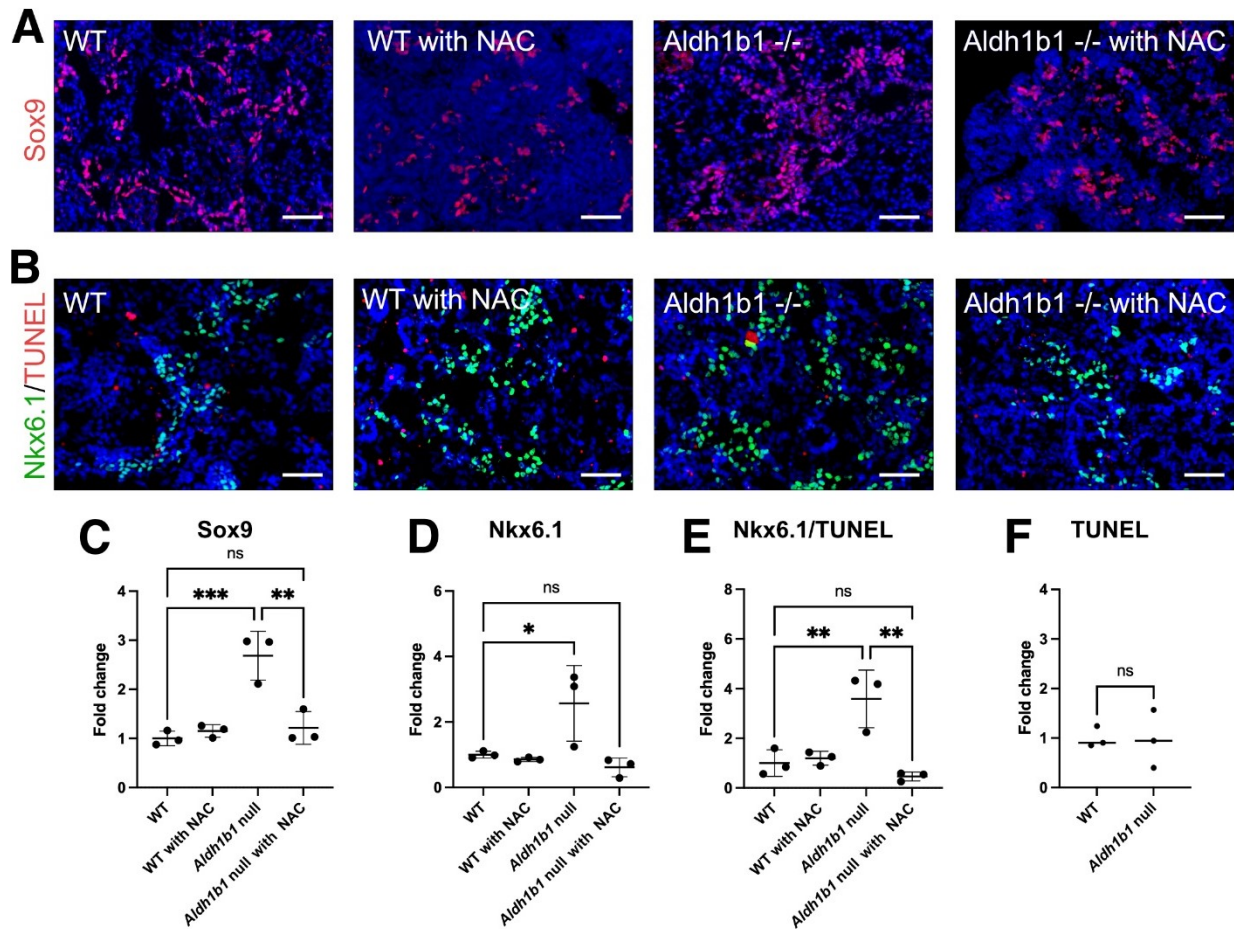
Figure 3.26: Quantification of Sox9⁺, Nkx6.1⁺ and TUNEL⁺ cells in cultured WT and *Aldh1b1* null E14.5+2d explants. *Aldh1b1* null pancreata show, compared to the WT, an increase in Sox9⁺, Nkx6.1⁺ and Nkx6.1⁺/TUNEL⁺ cells, which is reverted by NAC treatment. There was no effect observed in WT explants treated with NAC in comparison with the untreated control. The quantification was performed with biological triplicates and statistical analysis was performed using unpaired t-test with Welch's correction. Data were considered significant when *p≤0.05; **p≤0.01; ***p≤0.001; ****p ≤ 0.0001. Scale bar = 50 μm.

In order to be able to determine the effect of different compounds on progenitor cell differentiation, an explant culture system was established, which allows to follow the progenitor differentiation *in vitro*. To this end, the murine pancreata were isolated at E14.5, when most cells were still in a progenitor state, and transferred onto plate inserts, on which the explants were cultured at the air-liquid interface. The explants can remain in culture for up to 6 days to assess different time points of progenitor cell differentiation. Furthermore, the culture system allows the substitution or withdrawal of compounds in order to determine their effects on differentiation. Here, I focused on a 2 days culture (E14.5+2d) to detect early changes in the transcription factor expression.

Firstly, differences in the expression of the progenitor markers Sox9, Nkx6.1 and Ptf1a and differentiation markers C-Peptide, Glucagon and CK19 as well as PH3, were observed performing immunofluorescence staining and subsequent quantification, in WT and *Aldh1b1* null explants. Then, the effect of NAC treatment on pancreas progenitor differentiation was determined by adding the ROS scavenger from E14.5. Differences between the distinct conditions were determined by immunofluorescence staining followed by quantification. After 2 days in culture, Sox9, a transcription factor initially expressed in bipotent progenitors and later retained in the ductal epithelium, exhibited a significant increase in *Aldh1b1* null explants. However, explants treated with NAC showed no significant difference in Sox9+ cells compared to the WT control, whereas ROS scavenging did not affect Sox9 expression in the WT (Figure 3.26 A,C). Nkx6.1, a transcription factor, which is firstly expressed in bipotent progenitors and later on restricted to β-cells, was analyzed next (Shih and Wang et al., 2013). A significant increase of Nkx6.1+ cells in *Aldh1b1* null explants, in comparison to WT pancreata was observed, and abolished after NAC treatment. The WT explant control cultured with NAC showed no difference as compared to WT without treatment, suggesting that ROS scavenging did not affect Nkx6.1 expression (Figure 3.26 B,D). Additionally, co-staining of Nkx6.1 and TUNEL, as well as TUNEL alone, were quantified to detect potential differences in cell death. *Aldh1b1* null progenitors showed a significant increase in Nkx6.1+/TUNEL+ cells at E14.5 + 2d compared to WT (Figure 3.26 B,E), whereas total TUNEL staining of the whole pancreas did not reveal differences between WT and *Aldh1b1* null (Figure 3.26 F). However, the number of Nkx6.1+/TUNEL+ cells decreased upon NAC treatment and reverted to WT levels (Figure 3.26 B,E). Lastly, no difference was detected in the appearance of the master regulator of acinar differentiation Ptf1a in *Aldh1b1* null cells, when compared to the WT (Figure 3.27 A,E).

As already mentioned, the peak of proliferation in *Aldh1b1* null pancreata occurs at E14.5 and declines to the WT level afterwards (Anastasiou et al., 2016). Accordingly, quantification of PH3+ cells in the epithelium of E14.5+2d explants showed, no significant differences between WT and *Aldh1b1* null progenitor cells, suggesting a limited proliferation activity (Figure 3.27 B,F). The expression of terminal differentiation markers was then assessed to investigate for potential differences in the differentiation process of *Aldh1b1* null progenitors. To this end, Ins+ and Gluc+ cells, for endocrine differentiation (Figure 3.27 C,G,H), and CK19, for ductal differentiation (Figure 3.27 D,I) were quantified, but no differences between WT and *Aldh1b1* null could be observed at this time point.
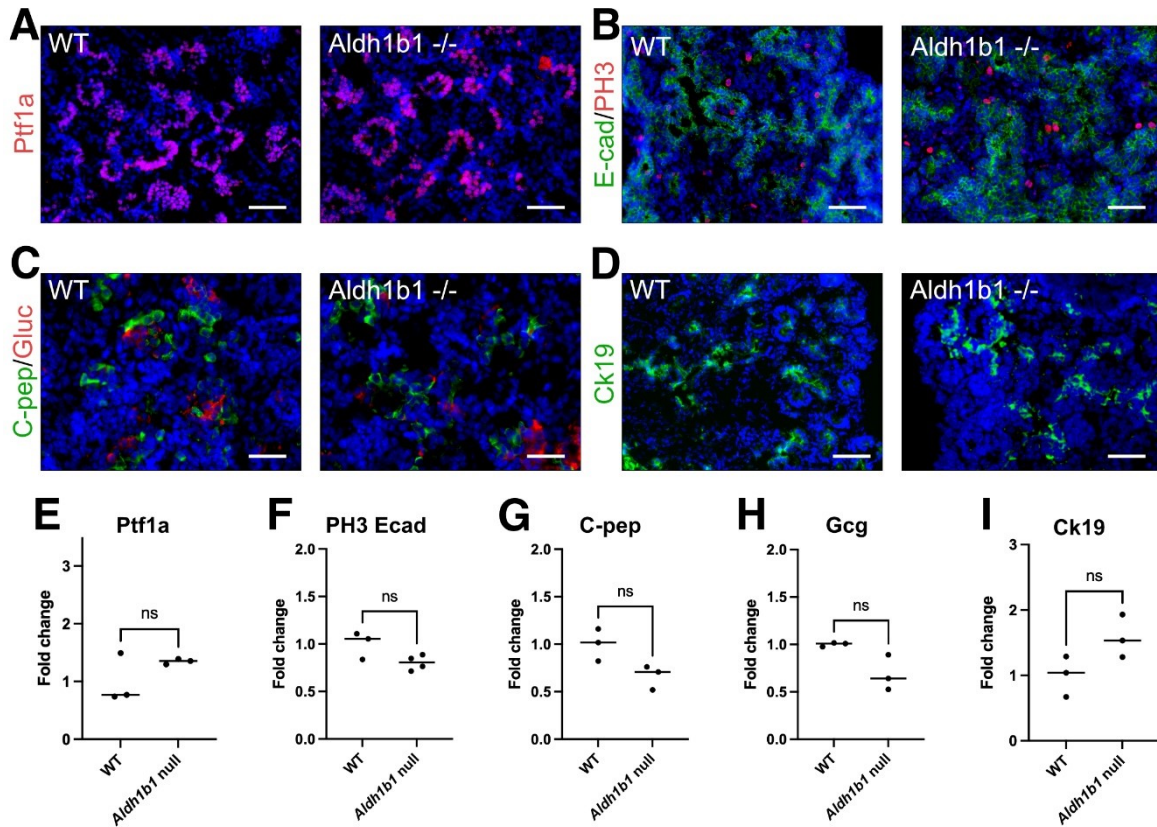
Figure 3.27: Quantification of Ptf1a$^+$, PH3$^+$, Ins$^+$, Gluc$^+$ and CK19$^+$ cells in cultured WT and *Aldh1b1* null E14.5+2d explants. *Aldh1b1* null pancreata show no significant increase in Ptf1a$^+$, PH3$^+$, Ins$^+$, Gluc$^+$ and CK19$^+$ cells after 2 days in culture. The quantification was performed with biological triplicates and statistical analysis was performed using unpaired t-test with Welch's correction. Data were considered significant when *p≤0.05; **p≤0.01; ***p≤0.001; ****p ≤ 0.0001. Scale bar = 50 μm.

In conclusion, these data suggest a defective expression of the key transcription factors of the endocrine and ductal lineage, Sox9 and Nkx6.1, in *Aldh1b1* null explants at E14.5+2d, as well as an increase of apoptotic Nkx6.1$^+$ cells. Quantification of terminal differentiation markers did not show any differences between WT and *Aldh1b1* null explants at that time point. Interestingly, all observed effects caused by Aldh1b1 inactivation were reverted upon ROS scavenging with NAC, suggesting a central role of ROS in the establishment of the *Aldh1b1* null phenotype.

3.2.5. Generation of the *ROSA26$^{LSL\ Aldh1b1}$* conditional *Aldh1b1* gain-of-function mouse strain

During pancreas development, Aldh1b1 is exclusively expressed in progenitor cells, suggesting that it may help maintain the progenitor state. However, it is not known whether continuous expression would affect differentiation or cell fate. Therefore, we aimed to create a mouse strain that would allow for the conditional continuous expression of *Aldh1b1*. To that end, a *ROSA26* targeting construct was created carrying a transgene for the conditional

expression of *Aldh1b1* under the control of a constitutive, strong promoter. The coding sequence of *Aldh1b1*, was inserted in intron 1 of the ROSA26 locus and followed in frame by T2A, a self-cleaving peptide, and the coding sequence of eGFP. The bovine growth hormone poly A signal (bGH pA) was added at the end of this bicistronic transgene. EGFP will mark cells with induced Aldh1b1 expression and T2A will mediate the separation of the proteins during translation. A transcriptional stop codon and a neomycin-resistance gene, flanked by loxP sites, were placed upstream of the Aldh1b1-T2A-eGFP transgene to prevent its continuous expression and allow for the selection of ES clones with successful integration. Recombination using a Cre-driver would allow the conditional activation of the transgene. The transgene was flanked by homology arms using the appropriate ROSA26 sequences (Figure 3.28).
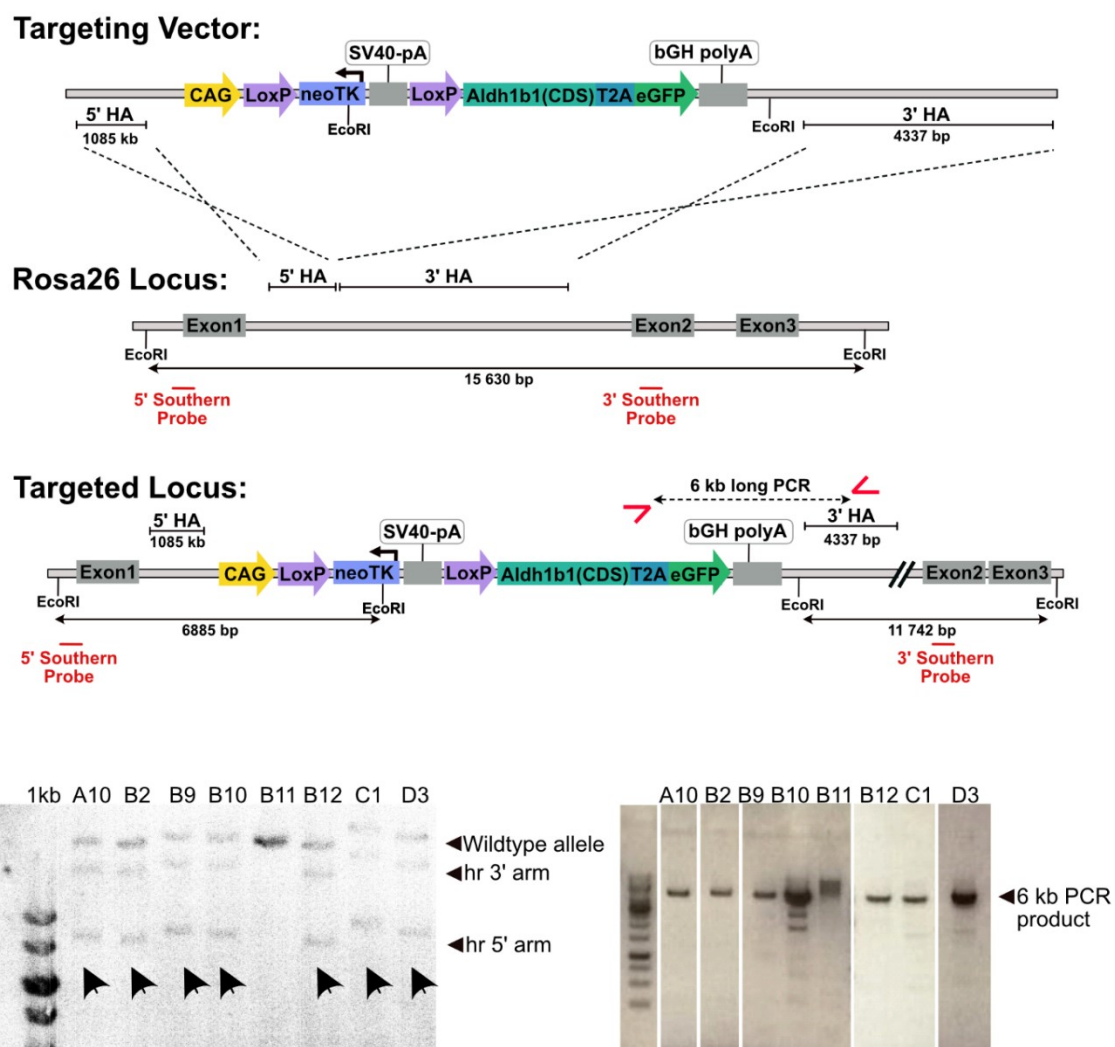
Figure 3.28: Design and generation of a *ROSA26^lslAldh1b1* conditional *Aldh1b1* gain-of-function mouse strain. (A) Scheme of the targeting vector and the targeting strategy into the *ROSA26* locus. The recombination led to an insertion of the construct in-between exon 1 and exon 2 of *ROSA26.* Correct insertion was proven by long rang PCR and southern blot which are shown in (B) and (C) for representative clones.

The designed construct was incorporated in mouse embryonic stem cells by the MPI-CBG transgenic facility via electroporation and homologous recombination mediated insertion. Recombined cell clones were selected by neomycin resistance and were then tested for the correct insertion of the construct into the *ROSA26* locus by long-range PCR of the 3' homology arm (Figure 3.28) and Southern blot in collaboration with Dr. Rayk Behrendt in the TU Dresden Medical Faculty. In order to detect whether the homology arms show a correct insertion, the DNA of the clones, which produced a correct long PCR product was EcoRI digested and subsequently separated by length with agarose electrophoresis. The DNA was blotted on a positively charged nylon membrane and this was followed by hybridization with ^{32}p-dCTP labeled Southern probes (Figure 3.28). The hybridized Southern blot of correctly targeted clones showed two DNA fragments, of 11 742 bp and 6885 bp in length, as indicated in the drawing of the targeted allele in Figure 3.27 B, whereas the untargeted allele showed just one fragment of 15 630 bp in length. The correctly targeted clone B10 was selected for injection in murine blastocysts, in the MPI-CBG transgenic facility, and gave germline transmission. To determine the functionality of the transgene, continuous expression of Aldh1b1 in a Pdx1-Cre dependent manner was induced. To that end, intercrossing with a Tg$^{Pdx1-Cre}$ line was performed in order to remove the LSL cassette and induce the expression of the Aldh1b1-T2A-eGFP transgene in pancreas progenitors. Immunohistochemical analyses revealed extensive expression of the GFP-reporter at E14.5 (Figure 3.29 A) and P1 (Figure 3.29 B), indicating that
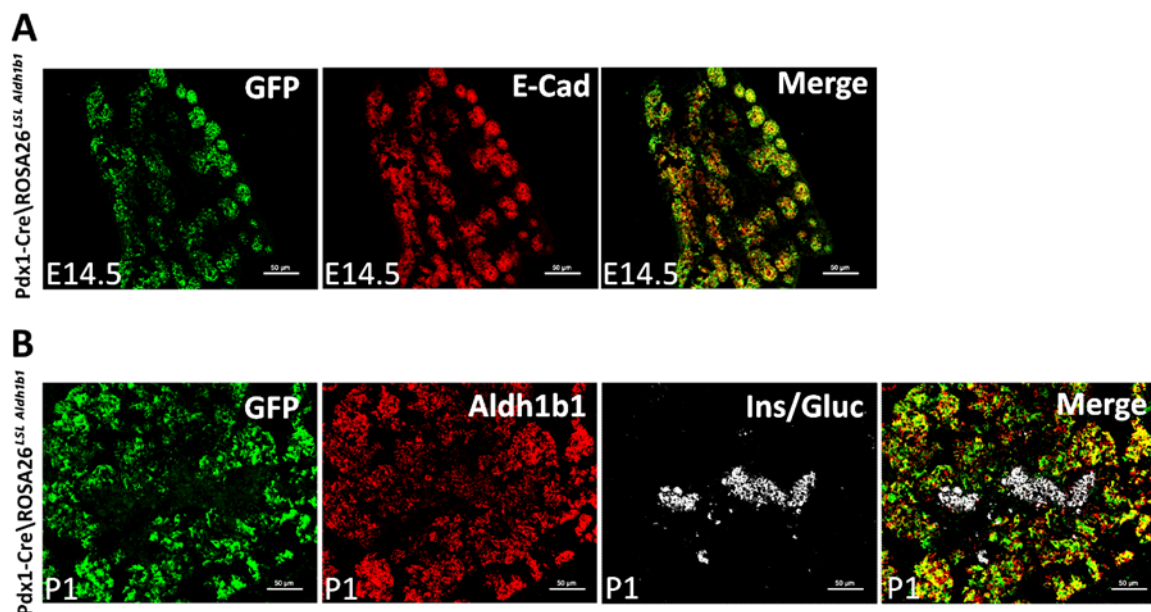
Figure 3.29: Immunofluorescence staining of the *ROSA26^lslAldh1b1* conditional ***Aldh1b1* gain-of-function mouse strain at E14.5 and P1.** Continuous expression of *Aldh1b1* was achieved after intercrossing with *Tg^Pdx1-Cre*. The co-expression of GFP in recombined cells confirms an exclusive activation of the transgene in E-Cadherin positive pancreas progenitors at E14.5 (A) and a continuous expression at P1 (B). Continuous expression of Aldh1b1 induced by a Pdx1-cre driver seems not to overlap with Insulin/Glucagon expression. n=3. Scale bar = 50 µm.

pancreas progenitor cells underwent recombination. Further analysis at E14.5 confirmed co-expression of GFP exclusively with E-cadherin, demonstrating specific induction of continuous Aldh1b1 expression in pancreas progenitors. Moreover, immunofluorescence staining at P1 showed persisting Aldh1b1 expression in the pancreas and a co-expression of GFP. The results of the immunofluorescence staining indicated that the Aldh1b1 gain-of- function transgene functions as expected and can be used for the induction of continuous Aldh1b1 and GFP co-labeling after intercrossing with a Cre-recombinase driver mouse line. Interestingly, the large majority of insulin and glucagon expressing cells were GFP negative in pancreas tissue sections at P1 (Figure 3.29 B). This result indicated that continuous *Aldh1b1* expression might inhibit endocrine differentiation and underlines the importance of timely *Aldh1b1* downregulation in differentiated cells. However, how exactly a strict regulation of Aldh1b1 expression regulates pancreas progenitor maturation, is a matter that needs to be investigated further.

4. Discussion

High Aldh activity has been widely reported in stem as well as progenitor cells and has been often associated with stemness preservation but also differentiation (Allahverdiyev et al., 2012). The latter aspect was often attributed to the involvement in RA synthesis, a metabolite that is essential in many different specification events during embryonic development. Recent studies suggest diverse functions of Aldh enzymes in stem- and progenitor cells, such as oxidative stress protection, aldehyde detoxification and participation in the regulation of the cellular metabolism (Gudas and Wagner, 2011; Pappa et al., 2003; Viswanathan et al., 2022; Brunsdon et al., 2022). Aldh1b1 is a mitochondrial member of the Aldh superfamily that is involved in pancreas progenitor differentiation and β-cell maturation. Its expression is tightly controlled during pancreatic development and is limited to progenitor cells. Absence of Aldh1b1 during embryonic pancreas development was shown to cause a differentiation burst at around E14.5, which was evident due to a strikingly increased expression of lineage markers. Late β-cells, that differentiated in the absence of functional Aldh1b1, gradually developed hyperglycemia and were glucose intolerant as a result of impaired insulin secretion (Anastasiou et al., 2016). However, the enzymatic function of Aldh1b1 in pancreas progenitors and how it ultimately affects gene expression and β-cell functionality remained elusive.

4.1. *Aldh1b1* inactivation causes high levels of ROS in pancreas progenitors

In this study, I presented evidence that Aldh1b1 inactivation caused an increase in ROS levels in E14.5 pancreas progenitors. This finding might explain the previously shown premature differentiation and proliferation observed in *Aldh1b1* null progenitors, which could be driven by ROS-induced stimulation of the cell cycle (Kirova et al., 2022). Furthermore, several studies have shown that ROS is an important inducer of progenitor cell differentiation due to its ability to modify target molecules and activate signaling cascades (Crespo et al., 2010; Tormos et al., 2011). The main source of ROS is the mitochondrial oxidative phosphorylation, where it is released as a byproduct from the complexes I, III and IV (Zorova et al., 2018). Viswanathan et al. presented a study in 2022, in which deletion of Aldh3a1, caused an accumulation of its cytotoxic presumed substrate 4-hydroxynonenal, which in turn disrupted mitochondrial function and morphology. Examination of mitochondrial appearance ruled out mitotoxic effects in pancreas progenitors lacking Aldh1b1 activity, thus, excluding major morphological defects as reason for high ROS levels. Assessment of the MMP, as a marker for electron transport chain activity, revealed no difference between WT and *Aldh1b1* null pancreas progenitors, but taking into account that progenitor cells lacking functional Aldh1b1 possess significantly reduced mitochondrial mass suggests that the oxidative phosphorylation activity per mitochondrion is increased compared to the WT. The high ROS production in *Aldh1b1* null cells is therefore

seemingly not caused by a complete block in the mitochondrial respiration nor by increased overall electron transport chain usage. Another possible reason for elevated ROS levels could be defective cellular scavenging mechanisms. Differentiating cells often have a reduced antioxidant system due to their usage of ROS signaling to initiate differentiation (Khacho and Slack, 2018) and this may increase their susceptibility to perturbations in the antioxidant defense mechanisms. However, the performed metabolome analysis could not detect any differences in the glutathione metabolism of WT and *Aldh1b1* null cells. Moreover, RNA-seq analysis did not reveal any differentially expressed genes, associated with oxidative damage response or glutathione detoxification, suggesting that E14.5 *Aldh1b1* null pancreas progenitors lack gene regulatory mechanisms to respond to and control oxidative stress. A process that might be exploited by pancreas progenitors to regulate ROS levels, e.g. to modulate ROS signaling, is reverse electron transfer at mitochondrial complex I, which is a physiological electron leak, producing high amounts of ROS (Scialò et al., 2017; Wright et al., 2022). Here, a reduced pool of coenzyme Q due to a stronger usage of the oxidative phosphorylation in *Aldh1b1* null progenitors could enhance the production of ROS. This hypothesis could be tested by the usage of reverse electron transfer inhibitors, such as rotenone or metformin, which should lower ROS levels and rescue the *Aldh1b1* null phenotype, if OXPHOS complex I is the origin of oxidative stress in absence of functional Aldh1b1.

4.2. Reduced ACLy activity in *Aldh1b1* null pancreas progenitors could affect histone modifications and ROS levels

Targeted flux analysis using isotope tracers is an important, state of the art, tool to measure and identify changes of reaction rates in central metabolic pathways. Isotope tracing experiments of glycolytic fluxes indicated a reduced rate of lipid de-esterification in absence of Aldh1b1 activity, suggesting decreased lipolysis activity in *Aldh1b1* null progenitors but no major perturbation of the glycolysis was observed. Moreover, glucose seemed to be a minor source of TCA intermediates in E14.5 pancreas progenitors.

Examination of TCA cycle fluxes in absence of Aldh1b1 activity uncovered striking differences in the glutamine metabolism. The conversion rate of isotopic glutamine to glutamate was reduced in absence of Aldh1b1, which might suggest a metabolic block at this level. This finding was in agreement with the observed increase in relative glutamine and glutamate abundance detected by the untargeted approach. Glutamine as well as Glutamate are essential metabolites in the process of progenitor cell differentiation due to their role as precursors of several amino acids and contribution to the synthesis of nucleotide biosynthesis. Several studies have shown that a block in the glutamine metabolism can redirect or abrogate differentiation and alter cell specification (Sumikawa et al., 2022; Martano et al., 2019, Oburoglu et al., 2014). Dysregulation of the glutamine metabolism, caused by Aldh1b1

inactivity, could, therefore, impact the differentiation program and lineage allocation of pancreas progenitors. Furthermore, glutamine tracing revealed an exploitation of the reversed IDH reaction in pancreas progenitors. This reaction is a reductive carboxylation of α-ketoglutarate to the product isocitrate and, finally, acetyl-CoA. This reaction is often exploited by cancer cells, to enable the production of acetyl-CoA from glutamine as a precursor for lipid synthesis and histone acetylation under hypoxic conditions (Filipp et al., 2012; He et al., 2022). Interestingly, in WT progenitor cells, approximately 10% of the glutamine-derived α-ketoglutarate was converted to isocitrate by exploiting reverse IDH reaction, even under normoxic conditions. This observation suggests that the progenitor cells have a great need of carbon building blocks for acetyl-CoA synthesis. In *Aldh1b1* null progenitors was an increase in this IDH-mediated reaction observed, which could derive from a compensatory mechanism due to a reduced ACLy conversion of citrate. As a mitochondrial enzyme, Aldh1b1 could also be involved in the process of balancing forward and reverse reaction and deletion of *Aldh1b1* would result in a dysregulation.

The enzyme ACLy is the main producer of cytosolic acetyl-CoA and plays consequently a central role in processes of cellular energy production, lipid synthesis and protein acetylation. The conversion of citrate to acetyl-CoA was strongly favored over the conversion to α-ketoglutarate in E14.5 progenitors, which repeatedly points out the reliance of these cells on this reaction for the synthesis of acetyl-CoA. Aldh1b1 inactivity caused a reduction of ACLy mediated conversion of citrate and qPCR analysis showed a significant downregulation of the ACLy gene. Previous studies showed a direct effect of ACLy downregulation on histone acetylation and lipid synthesis, which indicated that *Aldh1b1* null pancreas progenitors might also be affected by reduced histone acetylation (Zhao et al., 2016). A decrease in activating histone modification would, in turn, affect chromatin organization as well as transcriptional activation and interfere the differentiation process of embryonic pancreas progenitors.

Additionally, reduction of ACLy conversion in *Aldh1b1* null cells increased the rate of citrate converted to α-ketoglutarate, which is then further converted in the oxygen-dependent fluxes of the TCA-cycle. This observation is consistend with the previously detected increase in MMP in *Aldh1b1* null progenitor cells. Thus, the observed reduction of ACLy-dependent citrate conversion might indirectly affect ROS levels in *Aldh1b1* null pancreas progenitors. Indeed, studies performed with epithelial cancer models have already associated ACLy depletion with an increase in mitochondrial ROS production (Migita et al., 2013).

4.2. Changes in the metabolome profiling of *Aldh1b1* null pancreas progenitors

Using untargeted metabolomics facilitated a global detection of molecules in E14.5 pancreas progenitors and revealed a dysregulation of many metabolites that have essential functions in differentiating cells. The analysis found an accumulation of vitamin A and

glycerophosphocholine in *Aldh1b1* null pancreas progenitors, suggesting a block in the biosynthesis of retinoic acid in these cells. This finding was consistent with the transcriptional downregulation of *Aldh1a2,* an enzyme responsible for the conversion of retinol into retinoic acid, detected in the RNA-seq analysis. Retinoic acid signaling controls multiple developmental processes and is dynamically regulated in differentiating cells. A depletion of retinoic acid signaling in developing pancreas progenitors was shown to impair endocrine and β-cell differentiation (Öström et al., 2008). Thus, a premature downregulation could affect cellular differentiation programs in pancreas progenitors.

Furthermore, the polyamine spermine, but not spermidine, was significantly reduced in *Aldh1b1* null progenitors. Previous studies have suggested that the availability of polyamines determines the rate of protein translation during differentiation, cell fate and self-renewal (Heby, 1981; Allmeroth et al., 2021). Downregulation of specific polyamines, such as spermine could, therefore, affect translational efficiency and consequently the differentiation program. Moreover, the metabolite niacinamide that is known to drive differentiation and to regulate cell cycle progression in progenitor cells was found to be significantly less abundant in progenitors lacking Aldh1b1 activity (Meng et al., 2018; Nasr et al., 2020). These findings indicate that *Aldh1b1* null pancreas progenitors might display a premature downregulation or dysregulation of metabolites involved in progenitor cell differentiation. This aspect most likely resulted from the premature beginning of differentiation, which changed the timing of the process.

4.3. *Aldh1b1* null pancreas progenitors show a distinct chromatin accessibility and RNA expression profile at E14.5

Progenitor cell differentiation is a process that strongly depends on the regulation of gene expression, also through changes in chromatin accessibility. During embryonic development, cell type associated epigenetic patterns will be applied to ensure the maintenance of the specific genetic program of the differentiated cell. E14.5 pancreas progenitors showed a strong metabolic flux towards acetyl-CoA synthesis, which would result in increased acetylation. The reduction in the rate of this reaction would suggest a decrease in activating histone acetylation marks in *Aldh1b1* null pancreas progenitors and, indeed, assessment of the chromatin accessibility revealed a reduction of open chromatin. A drop in cellular acetyl-CoA concentrations has been directly associated with a change in the epigenetic status of the cell (Galdieri and Vancura, 2012) and histone acetylation is widely associated with transcriptional activation (Utley et al., 1998), making the genes available for the binding of the transcriptional machinery. Thus, reduction in the accessibility in *Aldh1b1* null progenitors most likely derives from a reduction in activating histone marks. Untargeted metabolome analysis detected an increase in the concentration of the methionine cycle intermediates SAM and SAH in *Aldh1b1* null progenitors, which are substrate and product of methylation reactions. This indicates an

increase in these reactions, which would contribute to the reduced chromatin accessibility, due to the involvement of DNA methylation in genetic silencing. Affected regions in the genome were mainly associated with biological functions pertaining to chromatin organization as well as processes of protein acetylation. The decreased accessibility in *Aldh1b1* null progenitors might consequently reduce the expression of histone modifiers, which would further impair the establishment of a lineage specific and maintaining epigenetic profile. The differentially accessible regions in the genome were enriched with Klf/Sp binding sites, which are transcription factors playing key roles in processes like stem cell renewal, progenitor cell differentiation, proliferation, embryonic development and metabolism (Presnell et al., 2015). Especially Klf4 and Klf1 have been linked to terminal differentiation in other tissues (McConnell et al., 2007; Miller and Bieker, 1993). Transcription factors of the Klf/Sp family are highly conserved and bind to many target genes dispersed over the genome. Affected chromatin regions were also enriched in binding motifs of Nrf1, a transcription factor involved in metabolic regulation. Nrf1 has been described as an important regulator in the process of glucose sensing in β-cells and controls the transcription of genes linked to cellular respiration, differentiation as well as lipid metabolism (Zheng et al., 2015; Tsujita et al., 2014). Collectively, changes in the chromatin accessibility in *Aldh1b1* null cells affect binding sites of regulators that guide cellular differentiation and the establishment of chromatin modifications, which implicates a progressive dysregulation of the epigenetic patterning.

Next, I investigated whether early changes in the gene expression were detectable in E14.5 *Aldh1b1* null progenitors, and this revealed a starting dysregulation of the transcriptional activity. Deletion of *Aldh1b1* expression has been implicated with a premature differentiation in E14.5 progenitor cells (Anastasiou et al., 2016), which might be associated with the observed dysregulation of many genes relevant for tip/trunk and epithelial differentiation. However, although *Aldh1b1* null cells differentiate earlier, they show a downregulation of endocrine genes, including *Ins1* and *Ins2*, whereas no change in the expression of duct markers was observed. These findings indicated that the premature differentiation impairs early β-cell development.

The observed dysregulation in the expression of genes encoding for SLC proteins implies also an impact on metabolic processes. SLC transporters are regulated according to the need of the cell which depends on cell type and lineage associated function as well as environmental factors. A dysregulation of their expression is often associated with the development of metabolic diseases such as T2DM (Colas et al., 2016). During development, a dynamic nutrient distribution assists the process of differentiation. Interestingly, the transcription factors of the Klf/Sp family and Nrf1 are known to regulate the expression of certain SLC proteins (Tsujita et al., 2014; Hou et al., 2022).

Furthermore, differentially expression of genes that are involved in the organization of the ECM and migration regulation suggests an increase in tissue rearrangement processes in *Aldh1b1* null progenitors. Pancreas organogenesis is a process that is shaped by epithelial reorganization, which is accompanied by ECM remodeling (Shih et al., 2016). In order to migrate, cells have to reduce their contacts with neighboring cells, which is in many cases achieved by a degradation of ECM proteins (Lamouille et al., 2014). A prominent example of cell migration in the developing pancreas is the delamination of endocrine cells, which usually occurs from E16.5 on (Wu et al.,2021). Nevertheless, premature differentiation of the progenitor cells might have accelerated this process. *Aldh1b1* null progenitors also displayed an upregulation of many genes involved in positive transcriptional regulation, which is consistent with the increase in proliferation and differentiation that has been observed in the E14.5 pancreas in absence of Aldh1b1 activity (Anastasiou et al.,2016).

4.5. Aldh1b1 inactivity during pancreas progenitor differentiation results in some mild dysregulation of gene expression in P10 β-cells

The precise timing of differentiation is crucial to maintain a correct balance between proliferation and differentiation activity of progenitor cells. A premature onset of differentiation can cause exhaustion of the progenitor cell pool and a dysregulation in the lineage ratios of the differentiated cells (Kim et al., 2015; Lenoir et al., 2011). Aldh1b1 was discovered as a regulator of the timing of pancreas progenitor differentiation and could, therefore, affect the identity of differentiated β-cells. However, performing RNA-seq analysis determined only weak changes in the transcriptional activity of *Aldh1b1* null P10 β-cells, even though a defective gene expression and chromatin accessibility has already been seen in E14.5 progenitors. An upregulation of genes associated with different mitotic processes suggests an increase in β-cell proliferation in *Aldh1b1* null mice, which is coherent with the increase in proliferation observed in *Aldh1b1* null islets (Anastasiou et al.,2016). Interestingly, the induction of β-cell proliferation has been implicated with β-cell dysfunction or an insufficient supply of insulin in young rodents (Montanya et al., 2000; Nir et al., 2007), which might indicate an insufficient insulin secretion of β-cells that differentiated in absence of Aldh1b1 activity. Moreover, *Aldh1b1* null β-cells show a strong upregulation of the transcription factor Klf6, which is involved in the regulation of proliferation-inducing genes. An upregulation of Klf6 has been reported in the context of insulin resistance, where it controls β-cell proliferation as a protective mechanism to avert β-cell dedifferentiation (Dumayne et al. 2020).

RNA-seq analysis revealed an upregulation of the genes *Amy2a1, Sst* and *Aldh1a3*, which might be the result of an incipient dedifferentiation. Especially Aldh1a3 upregulation has been described as a marker of failing β-cells in diabetic mice (Kim-Muller et al., 2016; Son et al., 2023) but also stress-induced upregulation of somatostatin has been determined as a

marker of changing β-cell identity (Jeffery et al., 2021). Nevertheless, *Aldh1b1* null β-cells did not show a reduced expression of ins1 or ins2. Previous studies performed with *Aldh1b1* null islets have shown an impaired insulin secretion in 20-week-old mice, which started showing an onset of hyperglycemia with 12 weeks (Anastasiou et al.,2016), suggesting that the gene expression of P10 β-cells displays a very early picture of an incipient β-cell dysfunction. Anastasiou et al., 2016 described some early changes in the gene expression of P1 *Aldh1b1* null islets, which weren't detected in this study at P10. The reason for this is most likely that islets comprise many different cell types, such as endocrine, exocrine, mesenchymal, endothelial or stellate cells with different genetic programs. This can on one hand cause masking of some β-cell specific changes but on the other hand show specific effects of *Aldh1b1* inactivation on other cell types, whereas I presented β-cell changes.

Hence, a shift in the timing of progenitor cell differentiation in absence of Aldh1b1 activity affects the postnatal gene expression of β-cells even at a young age of the mice. The defects observed might be a consequence of prolonged oxidative stress or an incomplete establishment of the β-cell identity for instance due to insufficient gene silencing.

4.6. ROS scavenging reverts aberrant gene expression in *Aldh1b1* null explants

Previous findings suggested that elevated ROS levels, caused by Aldh1b1 deletion, induce premature differentiation of embryonic pancreas progenitors. In order to investigate the effects of ROS on the process of progenitor cell differentiation, an *in vitro* explant culture was used so that ROS levels could be reduced by the addition of the ROS scavenger NAC. The pancreas explants were cultured in presence and absence of NAC in order to investigate if ROS scavenging could revert the *Aldh1b1* null phenotype. The explants were isolated at E14.5, approximately 2 days after the onset of secondary transition. At this age, the tip/trunk segregation is completed, and first markers of differentiated cells start to appear (Serafimidis et al., 2017). After two days in culture an increase in the expression of the key transcription factors of trunk identity, Nkx6.1 and Sox9, was detected in *Aldh1b1* null explants. Excitingly, this upregulation could be reverted to WT levels by NAC treatment, which strongly suggested that the reduction of oxidative stress, decreased progenitor cell differentiation in *Aldh1b1* null pancreas progenitors. Furthermore, quantification of double positive Nkx6.1[+] and TUNEL[+] progenitors revealed an increase in apoptotic Nkx6.1^{+} cells in explants lacking Aldh1b1 activity, indicating that differentiation pressure and oxidative stress induces cell death in *Aldh1b1* null trunk progenitors. Removal of oxidative stress by ROS scavenging resulted in a decrease in progenitor apoptosis back to WT levels. There was no difference in the appearance of Ptf1a^{+} cells detected, suggesting that the elevation of ROS levels did not affect tip progenitors. The analysis did also not reveal any differences in the appearance of the differentiation markers C-peptide, glucagon and Ck19. However, this assay considers just a single time point of

progenitor cell differentiation and should be extended to more time points since Ptf1a and the differentiation markers show a trend towards increase or reduction, respectively. Importantly, using the explant culture system as a model for pancreas progenitor differentiation, could reveal the effect of oxidative stress on progenitor differentiation and support the hypothesis that increased ROS levels induce premature differentiation.

In conclusion, the data presented in this thesis establish Aldh1b1 as a metabolic regulator of progenitor cell differentiation. Absence of the mitochondrial enzyme during pancreas development results in an increased production of ROS, attributed to reduced ACLy activity and increased utilization of the oxygen-dependent part of the TCA cycle. Elevated ROS levels were shown to cause the burst of progenitor differentiation at E14.5 (Anastasiou et al., 2016). In this thesis I show that this previously reported premature differentiation, resulted in a transcriptional as well as metabolic dysregulation and reduced chromatin accessibility of *Aldh1b1* null pancreas progenitors. These early defects in the process of embryonic progenitor cell differentiation had implications for the postnatal β-cell gene expression and conceivably the observed β-cell dysfunction in adult mice. Progenitor cells with continuous Aldh1b1 expression avoided the endocrine cell fate, suggesting that a downregulation of the Aldh1b1 activity in differentiated cells is necessary to accomplish β-cell identity.

The presented findings provide unique insights into certain processes of progenitor cell differentiation into fully functional β-cells and contribute to the understanding of the fundamental role of metabolic regulation. Investigation of the origins of ß cell dysfunction will help to design therapeutic interventions. for T2DM and MODY. Furthermore, elucidating the processes of progenitor cell differentiation into fully functional β-cells will contribute to potential cell therapeutic approaches.

Outlook

Aldh1b1 inactivity was shown to affect TCA cycle fluxes but in order to confirm and deepen the already gained knowledge, I am currently collecting samples to perform an extended metabolic flux experiment. To that end, 4-^{13}C$_6$-Glucose and 5-^{13}C$_6$-Glucose tracers have been used to improve the analysis of the glycolysis. In order to understand, which defects are a result of ROS signaling, I included a condition, in which NAC is present in the culture media, whereas previous analysis were performed only without NAC. Furthermore, I have increased the tracer concentration of 1,2-^{13}C$_2$-Glutamine and extended the incubation period for all tracers in order to increase label incorporation and improve the signal-to-noise ratio. Those measurements will increase the resolution of the analysis and provide a more in-depth insight into the Aldh1b1-regulated progenitor metabolism.

The examination of the chromatin accessibility by ATAC-seq at E14.5 revealed early changes in *Aldh1b1* null pancreas progenitors and suggested an early dysregulation in the establishment of the chromatin landscape. Furthermore, RNA-seq analysis detected an incipient dysregulation of gene expression at P10. To reach a better conclusion about how a defective chromatin accessibility affects postnatal gene expression I will perform the ATAC-seq experiments also for P10 mice in order to assess if altered chromatin accessibility contributes to β-cell dysfunction in older *Aldh1b1* null mice. To contribute to a better understanding of the β-cell defects, it would be beneficial to perform RNA-seq and ATAC-seq experiments also at a later timepoint subsequent to the onset of hyperglycaemia.

Furthermore, I showed that reduction of ROS affects the expression of key transcription factors in explants of *Aldh1b1* null mice. There were changes in the expression of the differentiation markers glucagon, insulin and CK19 that did not reach statistical significance. In order to investigate whether a dysregulation of these markers is detectable at a later timepoint, I am planning to repeat the experiments with explants that stayed in culture for 4 days. Moreover, since ACLy is considered the be the reason for the increase in reactive oxygen species, I am planning to culture WT E14.5 explants in presence of the ACLy inhibitor SB-204990 for 2 days to probe if this treatment, firstly, increases ROS levels and, secondly, results in a dysregulation of progenitor and differentiation marker similar to the phenotype seen in *Aldh1b1* null explants. Finally, I will investigate potential changes in ATP and NAD/NADH levels of expanded pancreas progenitors to further complete the understanding of the metabolic profile cause by Aldh1b1 inactivity.

Supplement

Results untargeted metabolomics

HMDB ID	Pval	FC
HMDB32889	8.02E-15	-10.699
HMDB38493	0.003817	-7.0977
HMDB59600	0.011976	-5.2644
HMDB01848	8.42E-06	-5.1352
HMDB29113	0.000177	-4.9437
HMDB13870	0.04897	-4.8496
HMDB29971	0.000769	-4.3688
HMDB37839	0.019073	-4.3336
HMDB39780	0.000675	-4.3318
HMDB32768	0.016887	-3.7767
HMDB30555	0.022014	-3.3174
HMDB29404	0.009073	-2.8124
HMDB37844	0.001219	-2.6076
HMDB15258	0.006242	-2.2322
HMDB41541	0.018309	-2.1526
HMDB00195	0.001804	-1.8501
HMDB00726	0.002653	-1.8304
HMDB41986	0.00715	-1.7842
HMDB35174	5.54E-05	-1.7603
HMDB60589	0.024611	-1.5904
HMDB60605	6.78E-06	-1.533
HMDB15352	0.027446	-1.4776
HMDB34937	0.007662	-1.3581
HMDB12107	0.001709	-1.2126
HMDB60617	0.008235	-1.0687
HMDB14383	0.001216	-1.0219
HMDB29747	0.025792	-1.0085
HMDB39061	8.07E-05	-0.81901
HMDB60974	0.029372	-0.81204
HMDB01256	0.005027	-0.77532

HMDB	Pval	FC
HMDB15152	0.000995	-0.75312
HMDB33659	0.003921	-0.71645
HMDB13067	0.05025	-0.67467
HMDB00301	0.027347	-0.66675
HMDB00755	0.005522	-0.61203
HMDB02172	0.011467	-0.58312
HMDB39897	0.002821	-0.57644
HMDB11745	0.015098	-0.51496
HMDB13286	0.003258	-0.49262
HMDB11152	0.024206	-0.48287
HMDB15430	0.040009	-0.45081
HMDB14443	0.02459	-0.44934
HMDB01325	0.005666	-0.42056
HMDB15090	0.00014	-0.36557
HMDB01406	0.014264	-0.27808
HMDB40940	0.040735	0.14491
HMDB61822	0.003024	0.16058
HMDB06809	0.000166	0.25445
HMDB11649	0.006602	0.27565
HMDB00641	0.002561	0.32826
HMDB00086	0.001693	0.38352
HMDB00148	0.000397	0.42561
HMDB00305	0.020951	0.49289
HMDB34694	0.038062	0.51319
HMDB32549	1.30E-05	0.61459
HMDB15109	0.000819	0.62496
HMDB00267	0.019948	1.8103
HMDB01138	0.038225	2.2886
HMDB12378	0.049046	2.9886
HMDB15338	5.28E-06	2.9961

Table S1: Regulated metabolites

E14.5 DESeq2 results

Cell migration

Gene	log2FoldChange	pvalue	padj	WT	Aldh1b1 null
Appl2	0.25	1.69E-09	1.29E-06	4605.5	5501.9
Ldb2	-0.61	2.26E-07	5.55E-05	172.6	76.2
Cav1	-0.59	3.95E-07	0.000105	534.2	264.2
Lmna	-0.27	1.03E-06	0.00017	2560.4	2099.7
Sinhcaf	0.27	2.54E-06	0.000293	1421.6	1742.3
Nedd9	0.31	4.75E-06	0.000481	973.3	1230.5
Scai	0.32	5.31E-06	0.000533	1017.2	1300.2
Sema6a	0.33	1E-05	0.000895	919.1	1188.3
Dpysl3	-0.51	1.01E-05	0.000934	578.5	318.8
Eng	-0.52	7.32E-06	0.000971	422.7	182.6
Ddx58	0.33	8.21E-06	0.001064	348.4	451.4
Pecam1	-0.51	1.24E-05	0.001426	400.3	178.5
Sema6c	-0.45	2.6E-05	0.001528	241	153.4
Srgap2	0.2	2.87E-05	0.001547	2619.3	3023.4
Rhoc	-0.28	9.36E-05	0.003778	687.5	554.6
Thbs1	-0.42	0.000141	0.005055	844	356.7
Rock2	0.16	0.000301	0.008583	4441.2	4998.5
Cpne3	0.23	0.000399	0.010149	2291.2	2717.1
Ptprk	0.16	0.000436	0.010601	3595.4	4037.6
Srgap3	0.22	0.000489	0.011675	2911.5	3425.5
F10	-0.37	0.000486	0.013877	352.7	247.8
Robo4	-0.34	0.000423	0.014383	142.8	50.4
Hspa5	-0.14	0.000734	0.014559	40267.7	36555.5
Arid2	0.19	0.000709	0.015558	3609.9	4168.8
Nf1	0.22	0.000863	0.016993	2194.5	2602.1
Plxna2	0.15	0.000806	0.017132	4027.4	4502.9
Col1a1	-0.33	0.001064	0.019888	12775.6	5192
Pak1	0.18	0.001165	0.019996	1343.7	1531.3
Zmynd8	0.14	0.001186	0.022365	4109.7	4538.4
Apc	0.17	0.001465	0.022982	6178.2	7004.9
Stk24	0.15	0.001423	0.023394	3063.9	3409.8
Sema3d	-0.36	0.001153	0.024418	187.4	88.5
Afdn	0.17	0.001681	0.024691	10314.8	11692.1
Ulk4	-0.33	0.001164	0.024884	414.6	307.6
Igf1r	0.24	0.001841	0.027165	2853.8	3455.9
Reck	-0.3	0.000964	0.0281	444.1	342.2
Ret	-0.17	0.00254	0.035008	3919.4	3469.3
Sema5b	-0.36	0.002036	0.03589	225	128.4
Spata13	0.18	0.003062	0.037423	2413.7	2754.9
Jag1	0.22	0.003116	0.040475	2864.7	3403.5

Gene					
Myo1c	-0.19	0.002862	0.041439	2004.5	1741.7
Grb7	0.14	0.003467	0.041569	3514.5	3895.2
Slit2	-0.31	0.003798	0.04664	1065.9	508.9
Snai2	-0.34	0.002851	0.049754	119.4	65.8
Dlc1	-0.26	0.004592	0.051859	750.7	597.1
Ptprj	0.19	0.005511	0.053723	2439.7	2814.5
Pdgfra	-0.28	0.002688	0.054105	503.4	195.3

Table S2: Differentially regulated genes involved in cell migration retrieved from E14.5 pancreas progenitors

ECM organization

Gene	log2FoldChange	pvalue	padj	wt	Aldh1b1 null
Vwf	-0.75	3.12E-11	6.45E-08	166.2	40.6
Loxl1	-0.52	1.25E-07	4.59E-05	333.4	210
P3h1	-0.4	3.7E-07	8.81E-05	713.7	519.7
Gsn	-0.55	5.68E-07	0.000128	807.8	464.2
Bgn	-0.56	1.72E-06	0.000272	513.8	235.1
P4ha2	-0.5	2.42E-06	0.000281	260.9	162.5
Loxl2	-0.51	8.18E-06	0.000683	296.3	170.4
Flrt2	0.28	1.06E-05	0.000856	9580.3	11806.6
Fbln5	-0.51	7.49E-06	0.000869	128.5	49.9
Adam19	-0.47	7.26E-06	0.000971	423.3	270.8
Col23a1	-0.51	1.38E-05	0.000971	334.5	148.6
Creb3	-0.3	1.1E-05	0.000985	1060.4	846.1
Pecam1	-0.51	1.24E-05	0.001426	400.3	178.5
Adamts2	-0.48	2.44E-05	0.001692	247.7	105.4
Col8a2	-0.46	2.32E-05	0.001692	204	73.4
Col26a1	-0.47	5.81E-05	0.003206	378.3	201.6
Mfap2	-0.38	9.7E-05	0.003822	609.1	437.3
Col7a1	-0.46	7.45E-05	0.005035	431.4	210
Thbs1	-0.42	0.000141	0.005055	844	356.7
Tgfbi	-0.4	0.000144	0.005827	974.5	658.6
Sh3pxd2a	-0.22	0.000199	0.006264	2820.5	2397.4
Ddr2	-0.44	0.000161	0.006567	413.7	207.8
Col3a1	-0.38	0.000288	0.007737	14257.4	5635.2
Nid2	-0.39	0.000314	0.007888	1660.9	1127
Col1a2	-0.36	0.000491	0.010753	9256	3640.1
Gnb4	-0.42	0.000414	0.013725	133.4	74.7
Col6a2	-0.34	0.000705	0.014267	2292.2	864.5
Nid1	-0.37	0.000665	0.016576	1231	535.6
Nf1	0.22	0.000863	0.016993	2194.5	2602.1
Col16a1	-0.37	0.000804	0.016993	933.3	426.1
Htra1	-0.33	0.000539	0.01704	139.6	49
Mmp2	-0.36	0.000524	0.019108	530.6	214
Lox	-0.35	0.000521	0.019434	639.5	239.1
Col1a1	-0.33	0.001064	0.019888	12775.6	5192
Postn	-0.36	0.000557	0.020269	698.2	284.7

Col5a2	-0.35	0.000862	0.020301	1700.4	709.8
Dcn	-0.34	0.001069	0.020785	850.7	358.7
Adam12	-0.38	0.000948	0.021825	283.5	142.4
Col6a1	-0.31	0.001251	0.022365	1912.2	724.5
Bad	-0.22	0.001107	0.023769	689.6	580.1
Timp2	-0.25	0.001501	0.024815	1612.9	1314.4
Reck	-0.3	0.000964	0.0281	444.1	342.2
Fbn2	-0.35	0.0016	0.029308	1553.3	785.1
Lama4	-0.36	0.001114	0.031332	666	313.1
Col5a1	-0.32	0.001821	0.032774	3042.7	1331.3
Lum	-0.29	0.001837	0.033249	377.4	138
Epas1	-0.36	0.001846	0.034774	186.5	101.9
Acan	0.22	0.002947	0.038287	4126.5	4920.9
Col8a1	-0.31	0.002126	0.041029	121.7	50.5
Adamts6	0.26	0.002592	0.042231	355.4	439.6
Col6a3	-0.29	0.002889	0.04454	1210.2	496.8
Flot1	-0.18	0.003358	0.048469	1137.9	993.8
Vcan	-0.32	0.004834	0.053542	901.2	486.6
Lamc1	0.2	0.004699	0.054102	17853.6	20809

Table S3: Differentially regulated genes involved in ECM organization retrieved from E14.5 pancreas progenitors

Markers of endo- and exocrine differentiation

Gene	log2FoldChange	pvalue	padj	wt	Aldh1b1 null
Sox9	0.38	4.3E-07	8.81E-05	3246.6	4353.1
Nr5a2	0.26	1.14E-06	0.000157	8035.7	9751
Wnt5a	-0.56	1.61E-06	0.000252	174.7	78.6
Prox1	0.29	3.62E-06	0.00035	8013.3	10003.8
Onecut1	0.33	4.53E-05	0.002579	1943.3	2521.2
Ins1	-0.42	0.000355	0.009321	3747.6	2001.7
Hnf1b	0.27	0.000334	0.009429	1321.8	1634.6
Mnx1	-0.32	0.000694	0.017671	628.8	476.3
Aldh1a2	-0.4	0.000673	0.01789	205.6	111.4
Adcyap1r1	-0.37	0.001399	0.023722	195.3	127.3
Ins2	-0.37	0.001598	0.024246	8720.5	5074.9
Clps	-0.31	0.002151	0.03056	14849.9	11141.5
Gata6	0.15	0.002404	0.032413	2598.9	2888.6
Amy2b	-0.32	0.003284	0.048253	1122.7	806
Glis3	0.25	0.004683	0.054682	1228.3	1507.2
Sox4	0.08	0.040731	0.197924	8720.7	9241.7

Table S4: **Differentially regulated genes involved in endo and exocrine differentiation retrieved from E14.5 pancreas progenitors**

Epithelial differentiation

Gene	log2FoldChange	pvalue	padj	wt	Aldh1b1 null
Sulf1	-0.53	1.07E-06	0.000191	1092.7	644.3
Sfrp2	-0.56	1.25E-06	0.000206	270.9	145.1
Med1	0.2	9.18E-05	0.003691	2555.1	2966.1

Gene	log2FoldChange	pvalue	padj	wt	Aldh1b1 null
Thbs1	-0.42	0.000141	0.005055	844	356.7
Ptprk	0.16	0.000436	0.010601	3595.4	4037.6
Apoe	-0.2	0.000691	0.013877	17540.4	15062.4
Brca2	0.21	0.00056	0.016451	1720.2	2009.9
Fgfr2	0.27	0.000799	0.016502	2705	3365.7
Nf1	0.22	0.000863	0.016993	2194.5	2602.1
Nr2f2	-0.4	0.000667	0.017146	601.6	343.7
Cdk6	0.23	0.00107	0.024691	2140.7	2556.7
Wdr77	0.16	0.002715	0.038936	2081.4	2331.9
Sparc	-0.3	0.003137	0.041439	6220.2	4682.2
Cdkn1c	-0.32	0.003962	0.048574	7416.2	5299
Snai2	-0.34	0.002851	0.049754	119.4	65.8
Cav1	-0.59	3.95E-07	0.000105	534.2	264.2

Table S5: Differentially regulated genes involved in epithelial differentiation retrieved from E14.5 pancreas progenitors

SLC transporters

Gene	log2FoldChange	pvalue	padj	wt	Aldh1b1 null
Slc38a4	0.29	5.07E-08	1.88E-05	6520.2	8055.1
Slc4a4	0.37	3.66E-07	8.81E-05	695	924.3
Slc38a2	0.25	6.46E-06	0.000533	7149.8	8579.9
Slc38a1	0.16	0.00022	0.006274	6324.1	7067.9
Slc25a37	0.19	0.000471	0.012458	1632.7	1874.5
Slc39a10	0.19	0.001133	0.021176	2814.1	3239.5
Slc25a36	0.22	0.001355	0.022	2582.5	3061.8
Slc17a4	0.35	0.002076	0.03056	81.8	121.2
Slc35f1	0.33	0.001577	0.030604	109	150.8
Slc45a3	-0.37	0.001642	0.031918	196.6	114.8
Slc9a5	-0.34	0.002475	0.045231	120.9	84.4
Slc15a4	-0.22	0.003019	0.045859	648.5	544.7
Slc28a3	0.26	0.003237	0.046327	967.8	1200.2
Slc12a2	0.15	0.004181	0.047714	2491.9	2787.8

Table S6: Differentially regulated genes encoding for SLC transporters retrieved from E14.5 pancreas progenitors

Transcriptional regulation

Gene	log2FoldChange	pvalue	padj	wt	Aldh1b1 null
Ogt	0.32	9.6E-11	1.13E-07	5973	7554.4
Hmga2	0.35	2E-10	1.91E-07	8488.7	11012.1
Etv5	0.36	2.81E-10	3.01E-07	1421.7	1860.8
Mllt3	0.29	7.05E-09	5.04E-06	1274.8	1569.5
Met	0.26	3.06E-08	1.39E-05	2837	3419.4
Klf4	-0.57	6.7E-08	4.21E-05	605	352.5
Dhx9	0.16	1.85E-07	5.11E-05	16957	19036.6
Smarcc1	0.2	3.44E-07	7.08E-05	8574.6	9855.2
Tcf7l2	0.34	4.6E-07	0.00011	1020.6	1321.7
Osr1	-0.58	8.46E-07	0.000144	239.5	110.4
Pogz	0.23	2.28E-06	0.000272	2464.1	2912.2

Gene	logFC	PValue	FDR	Val1	Val2
Ehf	0.31	4.86E-06	0.000531	1878.3	2376.8
Atad2	0.23	5.77E-06	0.000533	4175.1	4937.9
Usp22	0.18	7.39E-06	0.000621	5412.3	6166.9
Atf7ip	0.22	7.35E-06	0.000632	3605.5	4223.6
Naa15	0.19	1.03E-05	0.000816	5758.1	6587.2
Osr2	-0.5	7.65E-06	0.000861	141.6	54.2
Ebf3	-0.51	7.5E-06	0.000869	141.2	55.7
Creb3	-0.3	1.1E-05	0.000985	1060.4	846.1
Tead1	0.23	1.84E-05	0.001227	4402.8	5206.4
Rreb1	0.17	2.31E-05	0.001381	4380	4939.5
Nfat5	0.29	2.53E-05	0.001547	4826.1	6029.1
Junb	-0.39	3.25E-05	0.001685	3521.2	2502.9
Bclaf1	0.18	3.24E-05	0.001692	8824	10036.2
Asxl1	0.19	3E-05	0.001727	3750.4	4297.3
Blm	0.25	3.39E-05	0.002	1650.8	1996.8
Prdm10	0.25	3.88E-05	0.002254	745.8	901
Sin3a	0.16	5.05E-05	0.002383	4199.1	4704.4
Npat	0.26	4.09E-05	0.002579	1683	2055.3
Bcl11b	0.3	7.3E-05	0.003331	587.5	740.3
Atrx	0.18	8.04E-05	0.003481	9127.7	10428.8
Hipk2	0.22	0.000103	0.004151	4522.6	5317.8
Tnks	0.2	0.000111	0.00432	4779.9	5533.6
Rgmb	0.2	0.000127	0.004599	1652.9	1909.8
Caprin2	0.26	0.000144	0.005454	814	996.6
Paxbp1	0.21	0.000187	0.00575	2717.4	3162.2
Ppp1r12a	0.17	0.000222	0.006334	3738.6	4232.9
Elf4	0.2	0.000247	0.006809	3744.6	4325
Tcf12	0.15	0.000246	0.007099	4911.9	5451.3
Zbed4	0.22	0.000191	0.007157	1170	1381.7
Cep290	0.26	0.000206	0.007292	1172.4	1425.7
Jund	-0.27	0.000279	0.007302	9570.9	7728.2
Klf2	-0.4	0.000191	0.007305	498.1	338.4
Six4	0.34	0.000134	0.007412	308.8	409.7
Mrtfb	0.22	0.000277	0.007424	2591.7	3066.5
Hnf1b	0.27	0.000334	0.009429	1321.8	1634.6
Atad2b	0.18	0.000379	0.009604	2511.5	2871.9
Tlr3	0.37	0.000318	0.010405	244.4	342.7
Vezf1	0.21	0.000523	0.011569	3011.3	3509.8
Rest	0.26	0.000406	0.011865	1606.8	1972.3
Lpin2	0.21	0.000697	0.016188	1481.2	1730.6
Rps6ka3	0.16	0.000854	0.017116	3942.4	4427.6
Pfkm	-0.24	0.000694	0.017484	1092.1	906.6
Atf3	-0.35	0.0007	0.01757	553.8	396.4
Rbl1	0.19	0.001057	0.019507	2249.2	2580
Brd8	0.16	0.001249	0.02081	4016.8	4498.8
Hcfc1	0.14	0.001178	0.021277	10620.4	11751.2
Macc1	0.25	0.000971	0.022046	708.1	864.5

Nfatc3	0.21	0.001353	0.022365	3040	3553.8
Map2k1	-0.18	0.001135	0.02284	2217.9	1944.6
E2f7	0.2	0.001104	0.023103	1252.8	1453
Tet1	0.19	0.001416	0.024246	1205.6	1392.7
Rrp1b	0.18	0.001358	0.024596	1717.6	1956.1
Sp1	0.2	0.001531	0.024691	4191.6	4859.6
Cdk5rap2	0.17	0.00163	0.025179	2758.4	3128.2
Tcerg1	0.17	0.00179	0.025706	4807.6	5433.7
Trim44	0.14	0.001498	0.025706	8459	9342.6
Csrnp1	-0.35	0.001445	0.028535	297	207.2
Hoxa5	-0.35	0.001272	0.029308	132.9	63.1
Rnf4	0.12	0.001919	0.03016	4708.5	5116.9
Fiz1	0.15	0.001698	0.031242	1646.9	1831.8
Creb1	0.18	0.002245	0.031332	2719.6	3109.4
Arid1a	0.12	0.002352	0.032413	12084.4	13214.9
Wasl	0.16	0.002237	0.032678	2523.5	2846.8
Epas1	-0.36	0.001846	0.034774	186.5	101.9
Usf2	-0.18	0.002834	0.040098	1995.9	1744.7
Med14	0.16	0.00368	0.041594	2861.1	3225.8
Bclaf3	0.26	0.003321	0.042641	535.5	662.5
Sertad1	-0.3	0.002794	0.044954	248	189
Afap1l2	-0.34	0.003445	0.049615	140.6	84.6
Spin1	0.11	0.005428	0.052989	4088.7	4433.8
Med12	0.11	0.005037	0.053673	3678.8	3992.1
Bicral	0.19	0.004316	0.054754	972.4	1121.6

Table S7: Differentially regulated genes involved in transcriptional regulation retrieved from E14.5 pancreas progenitors

P10 DESeq2 results

G1/S transition

Gene	log2FoldChange	pvalue	padj	wt	Aldh1b1 null
Pola1	0.46	8.58E-07	0.000347	541.8	779.4
Tyms	0.48	1.73E-06	0.000548	379.9	562.5
Inhba	0.55	9.75E-06	0.00198	131.3	225.1
Cdk14	0.48	2.09E-05	0.003479	940.5	1439.7
Ccne2	0.39	6.44E-05	0.008194	518.8	716.6
Klf11	0.3	0.000138	0.013605	1018.2	1280.1
Cdkn2d	0.35	0.000229	0.018912	433.8	576.1
Cdc45	0.37	0.000616	0.034737	289.7	398.8
Pole	0.36	0.000848	0.045808	347.7	472.5

Table S8: Differentially regulated genes involved in G1/S transition retrieved from P10 β-cells

DNA metabolic processes

Gene	log2FoldChange	pvalue	padj	wt	Aldh1b1 null
Top2a	0.52	5.54E-09	9.24E-06	2304.9	3464.5
Brca1	0.54	1.5E-07	9.11E-05	325.4	513.9

Gene	log2FoldChange	pvalue	padj	wt	Aldh1b1 null
Rad51	0.54	1.47E-06	0.000492	294.3	472.6
Fanci	0.55	1.4E-05	0.001869	122.2	214
Polq	0.54	1.63E-05	0.002862	110	191.9
Fancd2	0.45	8.71E-05	0.008667	188.1	283.9
Cdk1	0.38	9.7E-05	0.012464	471.9	642.5
Fanca	0.45	0.000168	0.01567	202.6	308.3
Neil3	0.4	0.000177	0.016544	295.1	417.4
Rad51c	0.45	0.000248	0.018879	148.5	228.9
Ddx21	-0.28	0.000572	0.034125	2088.7	1681.9
Fancg	0.43	0.000873	0.039608	131.5	212.1
Sirt7	-0.28	0.000901	0.045808	968.8	776.5
Fam111a	0.36	0.001294	0.049135	360.6	492.7
Ube2t	0.4	0.001	0.049559	168.3	246.8

Table S9: Differentially regulated genes involved in DNA metabolic processes retrieved from P10 β-cells

Sister chromatid segregation

Gene	log2FoldChange	pvalue	padj	wt	Aldh1b1 null
Ncapg	0.61	9.74E-09	1.24E-05	310.2	522
Ncapg2	0.45	1.05E-06	0.000456	748.4	1067.8
Ndc80	0.53	7.34E-06	0.001474	198.1	322
Smc4	0.34	7.98E-06	0.001612	2056.4	2651.7
Nusap1	0.47	8.98E-06	0.001928	357.7	535.1
Smc2	0.37	3.05E-05	0.004705	798.9	1067.8
Cdk1	0.38	9.7E-05	0.012464	471.9	642.5
Ncapd2	0.3	0.000323	0.023364	1421.1	1791.7
Rec8	-0.36	0.000351	0.025477	728.1	543.8
Spag5	0.38	0.000742	0.03408	329.1	460.9
Dlgap5	0.36	0.000918	0.048034	286.3	393.1

Table S10: Differentially regulated genes involved in sister chromatid segregation retrieved from P10 β-cells

Mitotic spindle organization

Gene	log2FoldChange	pvalue	padj	wt	Aldh1b1 null
Ccnd1	-0.39	1.55E-07	9.07E-05	5680.9	4248.9
Pola1	0.46	8.58E-07	0.000347	541.8	779.4
Tyms	0.48	1.73E-06	0.000548	379.9	562.5
Nusap1	0.47	8.98E-06	0.001928	357.7	535.1
Inhba	0.55	9.75E-06	0.00198	131.3	225.1
Cdk14	0.48	2.09E-05	0.003479	940.5	1439.7
Ccne2	0.39	6.44E-05	0.008194	518.8	716.6
Klf11	0.3	0.000138	0.013605	1018.2	1280.1
Cdkn2d	0.35	0.000229	0.018912	433.8	576.1
Cdc45	0.37	0.000616	0.034737	289.7	398.8
Pole	0.36	0.000848	0.045808	347.7	472.5

Table S11: Differentially regulated genes involved in mitotic spindle organization retrieved from P10 β-cells

Dedifferentiation marker

Gene	log2FoldChange	pvalue	padj	wt	Aldh1b1 null
Amy2a1	0.77	5.73E-09	8.76E-06	200.3	497.8
Sst	0.58	1.09E-08	1.24E-05	9299.9	15172.7
Klf6	0.4	1.92E-06	0.000595	1491.5	2045.9
Klf11	0.3	0.000138	0.013605	1018.2	1280.1

Table S12: Differentially regulated genes associated with β-cell dedifferentiation retrieved from P10 β-cells

ROSA26[LSL Aldh1b1] **Locus**

98
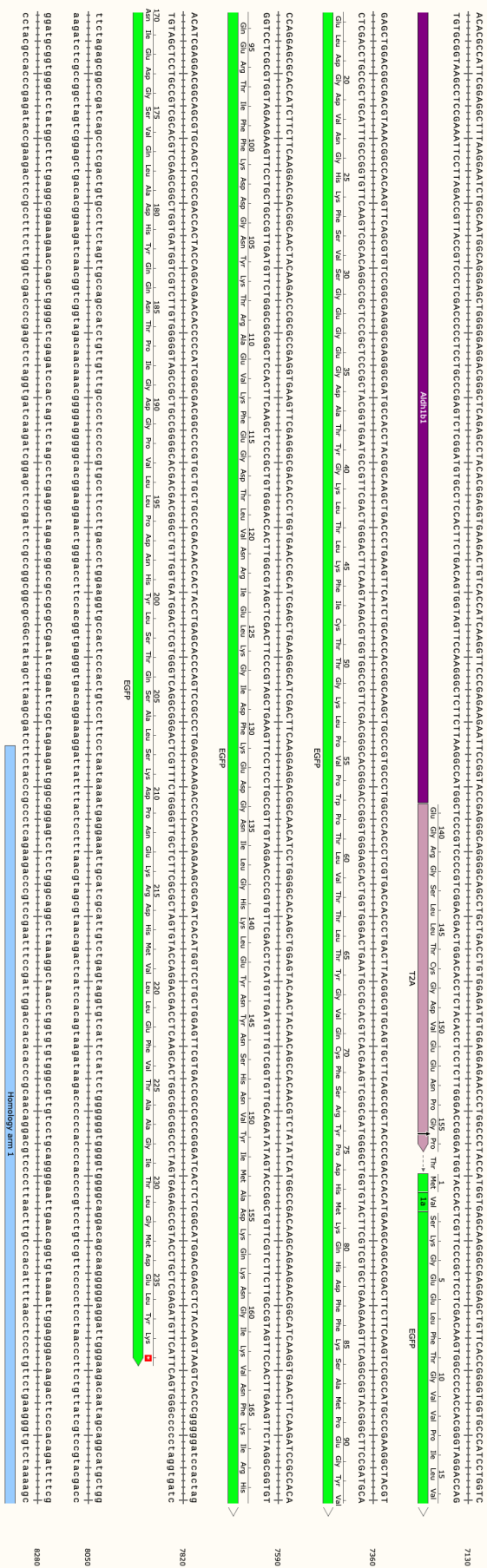
Bibliography

Abla H, Sollazzo M, Gasparre G, Iommarini L, Porcelli AM. 2020. The multifaceted contribution of α-ketoglutarate to tumor progression: An opportunity to exploit? Semin Cell Dev Biol 98:26–33.

Al-Khallaf H. 2017. Isocitrate dehydrogenases in physiology and cancer: biochemical and molecular insight. Cell Biosci 7:37.

Allahverdiyev A, Bagirova M, Nehir O, Yaman S, Sefik E, Cakir R, Canim S, Elcicek S, Yesilkir S. 2012. Aldehyde Dehydrogenase: Cancer and Stem Cells. Dehydrogenases, InTech.

Allis CD, Jenuwein T. 2016. The molecular hallmarks of epigenetic control. Nat Rev Genet 17:487–500.

Allmeroth K, Kim CS, Annibal A, Pouikli A, Koester J, Derisbourg MJ, Andrés Chacón-Martínez C, Latza C, Antebi A, Tessarz P, Wickström SA, Denzel MS. 2021. N 1-acetylspermidine is a determinant of hair follicle stem cell fate. J Cell Sci 134:9.

Alves TC, Pongratz RL, Zhao X, Yarborough O, Sereda S, Shirihai O, Cline GW, Mason G, Kibbey RG. 2015. Integrated, Step-Wise, Mass-Isotopomeric Flux Analysis of the TCA Cycle. Cell Metab 22:936–947.

Anastasiou V. 2017. Metabolic competence regulates the timing of differentiation in embryo pancreas development. Technische Universität, Medizinische Fakultät Dresden, Dissertation.

Anastasiou V, Ninou E, Alexopoulou D, Stertmann J, Müller A, Dahl A, Solimena M, Speier S, Serafimidis I, Gavalas A. 2016. Aldehyde dehydrogenase activity is necessary for beta cell development and functionality in mice. Diabetologia 59:139–150.

Anık A, Çatlı G, Abacı A, Böber E. 2015. Maturity-onset diabetes of the young (MODY): an update. Journal of Pediatric Endocrinology and Metabolism 28: 251-63.

Apelqvist Å, Li H, Sommer L, Beatus P, Anderson DJ, Honjo T, Angelis MH de, Lendahl U, Edlund H. 1999. Notch signalling controls pancreatic cell differentiation. Nature 400:877–881.

Aragón F, Karaca M, Novials A, Maldonado R, Maechler P, Rubí B. 2015. Pancreatic polypeptide regulates glucagon release through PPYR1 receptors expressed in mouse and human alpha-cells. Biochimica et Biophysica Acta (BBA) - General Subjects 1850:343–351.

Arnes L, Sussel L. 2015. Epigenetic modifications and long noncoding RNAs influence pancreas development and function. Trends in Genetics 31:290–299.

Bannister AJ, Kouzarides T. 2011. Regulation of chromatin by histone modifications. Cell Res 21:381–395.

Beres TM, Masui T, Swift GH, Shi L, Henke RM, MacDonald RJ. 2006. PTF1 Is an Organ-Specific and Notch-Independent Basic Helix-Loop-Helix Complex Containing the Mammalian Suppressor of Hairless (RBP-J) or Its Paralogue, RBP-L. Mol Cell Biol 26:117–130.

Bhandare R, Schug J, Lay J le, Fox A, Smirnova O, Liu C, Naji A, Kaestner KH. 2010. Genome-wide analysis of histone modifications in human pancreatic islets. Genome Res 20:428–433.

Bhushan A, Itoh N, Kato S, Thiery JP, Czernichow P, Bellusci S, Scharfmann R. 2001. Fgf10 is essential for maintaining the proliferative capacity of epithelial progenitor cells during early pancreatic organogenesis. Development 128:5109–5117.

Böni-Schnetzler M, Thorne J, Parnaud G, Marselli L, Ehses JA, Kerr-Conte J, Pattou F, Halban PA, Weir GC, Donath MY. 2008. Increased Interleukin (IL)-1β Messenger Ribonucleic Acid Expression in β-Cells of Individuals with Type 2 Diabetes and Regulation of IL-1β in Human Islets by Glucose and Autostimulation. J Clin Endocrinol Metab 93:4065–4074.

Bonner-Weir S, O'Brien TD. 2008. Islets in Type 2 Diabetes: In Honor of Dr. Robert C. Turner. Diabetes 57:2899–2904.

Bort R, Martinez-Barbera JP, Beddington RSP, Zaret KS. 2004. homeobox gene-dependent tissue positioning is required for organogenesis of the ventral pancreas. Development 131:797–806.

Bracha AL, Ramanathan A, Huang S, Ingber DE, Schreiber SL. 2010. Carbon metabolism–mediated myogenic differentiation. Nat Chem Biol 6:202–204.

Bramswig NC, Everett LJ, Schug J, Dorrell C, Liu C, Luo Y, Streeter PR, Naji A, Grompe M, Kaestner KH. 2013. Epigenomic plasticity enables human pancreatic α to β cell reprogramming. Journal of Clinical Investigation 123:1275–1284.

Brereton MF, Vergari E, Zhang Q, Clark A. 2015. Alpha-, Delta- and PP-cells. Journal of Histochemistry & Cytochemistry 63:575–591.

Brown M, Rivier J, Vale W. 1976. Biological Activity of Somatostatin and Somatostatin Analogs on Inhibition of Arginine-Induced Insulin and Glucagon Release in the Rat. Endocrinology 98:336–343.

Brunsdon H, Brombin A, Peterson S, Postlethwait JH, Patton EE. 2022. Aldh2 is a lineage-specific metabolic gatekeeper in melanocyte stem cells. Development 149:10.

Burganova G, Bridges C, Thorn P, Landsman L. 2021. The Role of Vascular Cells in Pancreatic Beta-Cell Function. Front Endocrinol (Lausanne) 12: 667170.

Cabrera O, Berman DM, Kenyon NS, Ricordi C, Berggren P-O, Caicedo A. 2006. The unique cytoarchitecture of human pancreatic islets has implications for islet cell function. PNAS 103: 2334-2339.

Campbell SA, Hoffman BG. 2016. Chromatin Regulators in Pancreas Development and Diabetes. Trends in Endocrinology & Metabolism 27:142–152.

Cao Y, Guo W, Tian S, He X, Wang X, Liu X, Gu K, Ma X, Huang D, Hu L, Cai Y, Zhang H, et al. 2015. miR-290/371-Mbd2-Myc circuit regulates glycolytic metabolism to promote pluripotency. EMBO J 34:609–623.

Chung S, Dzeja PP, Faustino RS, Perez-Terzic C, Behfar A, Terzic A. 2007. Mitochondrial oxidative metabolism is required for the cardiac differentiation of stem cells. Nat Clin Pract Cardiovasc Med 4:S60–S67.

Chypre M, Zaidi N, Smans K. 2012. ATP-citrate lyase: A mini-review. Biochem Biophys Res Commun 422:1–4.

Cinti S, Mitchell G, Barbatelli G, Murano I, Ceresi E, Faloia E, Wang S, Fortier M, Greenberg AS, Obin MS. 2005. Adipocyte death defines macrophage localization and function in adipose tissue of obese mice and humans. J Lipid Res 46:2347–2355.

Colas C, Ung PM-U, Schlessinger A. 2016. SLC transporters: structure, function, and drug discovery. Medchemcomm 7:1069–1081.

Collombat P, Hecksher-Sørensen J, Krull J, Berger J, Riedel D, Herrera PL, Serup P, Mansouri A. 2007. Embryonic endocrine pancreas and mature β cells acquire α and PP cell phenotypes upon Arx misexpression. Journal of Clinical Investigation 117:961–970.

Collombat P, Mansouri A, Hecksher-Sørensen J, Serup P, Krull J, Gradwohl G, Gruss P. 2003. Opposing actions of Arx and Pax4 in endocrine pancreas development. Genes Dev 17:2591–2603.

Collombat P, Xu X, Ravassard P, Sosa-Pineda B, Dussaud S, Billestrup N, Madsen OD, Serup P, Heimberg H, Mansouri A. 2009. The Ectopic Expression of Pax4 in the Mouse Pancreas Converts Progenitor Cells into α and Subsequently β Cells. Cell 138:449–462.

Crespo FL, Sobrado VR, Gomez L, Cervera AM, McCreath KJ. 2010. Mitochondrial Reactive Oxygen Species Mediate Cardiomyocyte Formation from Embryonic Stem Cells in High Glucose. Stem Cells 28:1132–1142.

Dean PM, Matthews EK. 1970. Glucose-induced electrical activity in pancreatic islet cells. J Physiol 210:255–264.

DeFronzo RA, Ferrannini E, Groop L, Henry RR, Herman WH, Holst JJ, Hu FB, Kahn CR, Raz I, Shulman GI, Simonson DC, Testa MA, et al. 2015. Type 2 diabetes mellitus. Nat Rev Dis Primers 1:15019.

Dezaki K, Hosoda H, Kakei M, Hashiguchi S, Watanabe M, Kangawa K, Yada T. 2004. Endogenous Ghrelin in Pancreatic Islets Restricts Insulin Release by Attenuating Ca2+ Signaling in β-Cells. Diabetes 53:3142–3151.

Dhawan S, Georgia S, Tschen S, Fan G, Bhushan A. 2011. Pancreatic β Cell Identity Is Maintained by DNA Methylation-Mediated Repression of Arx. Dev Cell 20:419–429.

DiGruccio MR, Mawla AM, Donaldson CJ, Noguchi GM, Vaughan J, Cowing-Zitron C, Meulen T van der, Huising MO. 2016. Comprehensive alpha, beta and delta cell transcriptomes reveal that ghrelin selectively activates delta cells and promotes somatostatin release from pancreatic islets. Mol Metab 5:449–458.

Dingler FA, Wang M, Mu A, Millington CL, Oberbeck N, Watcham S, Pontel LB, Kamimae-Lanning AN, Langevin F, Nadler C, Cordell RL, Monks PS, et al. 2020. Two Aldehyde Clearance Systems Are Essential to Prevent Lethal Formaldehyde Accumulation in Mice and Humans. Mol Cell 80: 996-1012.e9.

Dolenšek J, Rupnik MS, Stožer A. 2015. Structural similarities and differences between the human and the mouse pancreas. Islets 7:e1024405.

Donath MY. 2014. Targeting inflammation in the treatment of type 2 diabetes: time to start. Nat Rev Drug Discov 13:465–476.

Donath MY, Shoelson SE. 2011. Type 2 diabetes as an inflammatory disease. Nat Rev Immunol 11:98–107. Islets 11:98-107.

Drucker DJ, Nauck MA. 2006. The incretin system: glucagon-like peptide-1 receptor agonists and dipeptidyl peptidase-4 inhibitors in type 2 diabetes. The Lancet 368:1696–1705.

Dubois MP. 1975. Immunoreactive somatostatin is present in discrete cells of the endocrine pancreas. Proceedings of the National Academy of Sciences 72:1340–1343.

Dumayne C, Tarussio D, Sanchez-Archidona AR, Picard A, Basco D, Berney XP, Ibberson M, Thorens B. 2020. Klf6 protects β-cells against insulin resistance-induced dedifferentiation. Mol Metab 35:100958.

Dupuis J, Langenberg C, Prokopenko I, Saxena R, Soranzo N, Jackson AU, Wheeler E, Glazer NL, Bouatia-Naji N, Gloyn AL, Lindgren CM, Mägi R, et al. 2010. New genetic loci implicated in fasting glucose homeostasis and their impact on type 2 diabetes risk. Nat Genet 42:105–116.

Edlund H. 2002. Pancreatic organogenesis — developmental mechanisms and implications for therapy. Nat Rev Genet 3:524–532.

Estey T, Cantore M, Weston PA, Carpenter JF, Petrash JM, Vasiliou V. 2007. Mechanisms Involved in the Protection of UV-induced Protein Inactivation by the Corneal Crystallin ALDH3A1. Journal of Biological Chemistry 282:4382–4392.

Fajans SS, Bell GI, Polonsky KS. 2001. Molecular Mechanisms and Clinical Pathophysiology of Maturity-Onset Diabetes of the Young. New England Journal of Medicine 345:971–980.

Feingold KR. 2000. Oral and Injectable (Non-Insulin) Pharmacological Agents for the Treatment of Type 2 Diabetes. Endotext. South Dartmouth (MA): MDText.com, Inc.; 2000.

Filipp F v., Scott DA, Ronai ZA, Osterman AL, Smith JW. 2012. Reverse TCA cycle flux through isocitrate dehydrogenases 1 and 2 is required for lipogenesis in hypoxic melanoma cells. Pigment Cell Melanoma Res 25:375–383.

Folmes CDL, Martinez-Fernandez A, Faustino RS, Yamada S, Perez-Terzic C, Nelson TJ, Terzic A. 2013. Nuclear Reprogramming with c-Myc Potentiates Glycolytic Capacity of Derived Induced Pluripotent Stem Cells. J Cardiovasc Transl Res 6:10–21.

Folmes CDL, Nelson TJ, Martinez-Fernandez A, Arrell DK, Lindor JZ, Dzeja PP, Ikeda Y, Perez-Terzic C, Terzic A. 2011. Somatic Oxidative Bioenergetics Transitions into Pluripotency-Dependent Glycolysis to Facilitate Nuclear Reprogramming. Cell Metab 14:264–271.

Frank M, Duvezin-Caubet S, Koob S, Occhipinti A, Jagasia R, Petcherski A, Ruonala MO, Priault M, Salin B, Reichert AS. 2012. Mitophagy is triggered by mild oxidative stress in a mitochondrial fission dependent manner. Biochimica et Biophysica Acta (BBA) - Molecular Cell Research 1823:2297–2310.

Franklin I, Gromada J, Gjinovci A, Theander S, Wollheim CB. 2005. β-Cell Secretory Products Activate α-Cell ATP-Dependent Potassium Channels to Inhibit Glucagon Release. Diabetes 54:1808-1815.

Frantz C, Stewart KM, Weaver VM. 2010. The extracellular matrix at a glance. J Cell Sci 123:4195-4200.

Fu Z, Gilbert ER, Liu D. 2013. Regulation of insulin synthesis and secretion and pancreatic Beta-cell dysfunction in diabetes. Curr Diabetes Rev 9:25-53.

Gaisano HY, Leung YM. 2008. Pancreatic Islet α Cell Commands Itself: Secrete More Glucagon! Cell Metab 7:474-475.

Galdieri L, Vancura A. 2012. Acetyl-CoA Carboxylase Regulates Global Histone Acetylation. Journal of Biological Chemistry 287:23865-23876.

Gannon M, Tweedie Ables E, Crawford L, Lowe D, Offield MF, Magnuson MA, Wright CVE. 2008. pdx-1 function is specifically required in embryonic β cells to generate appropriate numbers of endocrine cell types and maintain glucose homeostasis. Dev Biol 314:406-417.

Georgia S, Kanji M, Bhushan A. 2013. DNMT1 represses *p53* to maintain progenitor cell survival during pancreatic organogenesis. Genes Dev 27:372-377.

Gialleonardo V di, Vries EFJ de, Girolamo M di, Quintero AM, Dierckx RAJO, Signore A. 2012. Imaging of β-Cell Mass and Insulitis in Insulin-Dependent (Type 1) Diabetes Mellitus. Endocr Rev 33:892-919.

Gilon P, Henquin J-C. 2001. Mechanisms and Physiological Significance of the Cholinergic Control of Pancreatic β-Cell Function. Endocr Rev 22:565-604.

Gradwohl G, Dierich A, LeMeur M, Guillemot F. 2000. *neurogenin3* is required for the development of the four endocrine cell lineages of the pancreas. Proceedings of the National Academy of Sciences 97:1607-1611.

Granata R, Settanni F, Biancone L, Trovato L, Nano R, Bertuzzi F, Destefanis S, Annunziata M, Martinetti M, Catapano F, Ghè C, Isgaard J, et al. 2007. Acylated and Unacylated Ghrelin Promote Proliferation and Inhibit Apoptosis of Pancreatic β-Cells and Human Islets: Involvement of 3′,5′-Cyclic Adenosine Monophosphate/Protein Kinase A, Extracellular Signal-Regulated Kinase 1/2, and Phosphatidyl Inositol 3-Kinase/Akt Signaling. Endocrinology 148:512–529.

Gudas LJ, Wagner JA. 2011. Retinoids regulate stem cell differentiation. J Cell Physiol 226:322–330.

Hale MA, Swift GH, Hoang CQ, Deering TG, Masui T, Lee Y-K, Xue J, MacDonald RJ. 2014. The nuclear hormone receptor family member NR5A2 controls aspects of multipotent progenitor cell formation and acinar differentiation during pancreatic organogenesis. Development 141:3123–3133.

Harding HP, Ron D. 2002. Endoplasmic Reticulum Stress and the Development of Diabetes. Diabetes 51:S455–S461.

He Q, Chen J, Xie Z, Chen Z. 2022. Wild-Type Isocitrate Dehydrogenase-Dependent Oxidative Decarboxylation and Reductive Carboxylation in Cancer and Their Clinical Significance. Cancers (Basel) 14:5779.

Hebrok M, Kim SK, Melton DA. 1998. Notochord repression of endodermal Sonic hedgehog permits pancreas development. Genes Dev 12:1705–1713.

Heby O. 1981. Role of Polyamines in the Control of Cell Proliferation and Differentiation. Differentiation 19:1–20.

Hellman B, Salehi A, Grapengiesser E, Gylfe E. 2012. Isolated mouse islets respond to glucose with an initial peak of glucagon release followed by pulses of insulin and somatostatin in antisynchrony with glucagon. Biochem Biophys Res Commun 417:1219–1223.

Henseleit KD, Nelson SB, Kuhlbrodt K, Hennings JC, Ericson J, Sander M. 2005. NKX6 transcription factor activity is required for α- andβ-cell development in the pancreas. Development 132:3139–3149.

Herrera PL. 2000a. Adult insulin- and glucagon-producing cells differentiate from two independent cell lineages. Development 127:2317–2322.

Holzer P, Reichmann F, Farzi A. 2012. Neuropeptide Y, peptide YY and pancreatic polypeptide in the gut–brain axis. Neuropeptides 46:261–274.

Hou Z, Gangjee A, Matherly LH. 2022. The evolving biology of the proton-coupled folate transporter: New insights into regulation, structure, and mechanism. The FASEB Journal 36:e22164.

Huijbregts L, Petersen MBK, Berthault C, Hansson M, Aiello V, Rachdi L, Grapin-Botton A, Honore C, Scharfmann R. 2019. Bromodomain and Extra Terminal Protein Inhibitors Promote Pancreatic Endocrine Cell Fate. Diabetes 68:761–773.

Huising MO, Meulen T van der, Huang JL, Pourhosseinzadeh MS, Noguchi GM. 2018. The Difference δ-Cells Make in Glucose Control. Physiology 33:403–411.

Hull RL, Westermark GT, Westermark P, Kahn SE. 2004. Islet Amyloid: A Critical Entity in the Pathogenesis of Type 2 Diabetes. J Clin Endocrinol Metab 89:3629–3643.

Husain S, Thrower E. 2009. Molecular and cellular regulation of pancreatic acinar cell function. Curr Opin Gastroenterol. 25: 466–471.

Hwang I-Y, Kwak S, Lee S, Kim H, Lee SE, Kim J-H, Kim YA, Jeon YK, Chung DH, Jin X, Park S, Jang H, et al. 2016. Psat1-Dependent Fluctuations in α-Ketoglutarate Affect the Timing of ESC Differentiation. Cell Metab 24:494–501.

In't Veld P, Marichal M. 2010. Microscopic Anatomy of the Human Islet of Langerhans. Springer, Dordrecht, p 1–19.

Jackson B, Brocker C, Thompson DC, Black W, Vasiliou K, Nebert DW, Vasiliou V. 2011. Update on the aldehyde dehydrogenase gene (ALDH) superfamily. Hum Genomics 5:283.

Jackson BC, Reigan P, Miller B, Thompson DC, Vasiliou V. 2015. Human ALDH1B1 Polymorphisms may Affect the Metabolism of Acetaldehyde and All-trans retinaldehyde - In Vitro Studies and Computational Modeling. Pharm Res 32:1648-1662.

Jeffery N, Chambers D, Invergo BM, Ames RM, Harries LW. 2021. Changes to the identity of EndoC-βH1 beta cells may be mediated by stress-induced depletion of HNRNPD. Cell Biosci 11:144.

Jia D, Sun Y, Konieczny SF. 2008. Mist1 Regulates Pancreatic Acinar Cell Proliferation Through p21CIP1/WAF1. Gastroenterology 135:1687–1697.

Jiang W, Wang J, Zhang Y. 2013. Histone H3K27me3 demethylases KDM6A and KDM6B modulate definitive endoderm differentiation from human ESCs by regulating WNT signaling pathway. Cell Res 23:122–130.

Johansson KA, Dursun U, Jordan N, Gu G, Beermann F, Gradwohl G, Grapin-Botton A. 2007. Temporal Control of Neurogenin3 Activity in Pancreas Progenitors Reveals Competence Windows for the Generation of Different Endocrine Cell Types. Dev Cell 12:457–465.

Jonsson J, Carlsson L, Edlund T, Edlund H. 1994. Insulin-promoter-factor 1 is required for pancreas development in mice. Nature 371:606–609.

Jorgensen P, Nishikawa JL, Breitkreutz B-J, Tyers M. 2002. Systematic Identification of Pathways That Couple Cell Growth and Division in Yeast. Science 297:395–400.

Kaimala S, Kumar CA, Allouh MZ, Ansari SA, Emerald BS. 2022. Epigenetic modifications in pancreas development, diabetes, and therapeutics. Med Res Rev 42:1343–1371.

Kalwat MA, Cobb MH. 2017. Mechanisms of the amplifying pathway of insulin secretion in the β cell. Pharmacol Ther 179:17–30.

Karpińska M, Czauderna M. 2022. Pancreas—Its Functions, Disorders, and Physiological Impact on the Mammals' Organism. Front Physiol 13: 807632.

Kartikasari AER, Zhou JX, Kanji MS, Chan DN, Sinha A, Grapin-Botton A, Magnuson MA, Lowry WE, Bhushan A. 2013. The histone demethylase Jmjd3 sequentially associates with the

transcription factors Tbx3 and Eomes to drive endoderm differentiation. EMBO J 32:1393–1408.

Katsarou A, Gudbjörnsdottir S, Rawshani A, Dabelea D, Bonifacio E, Anderson BJ, Jacobsen LM, Schatz DA, Lernmark Å. 2017. Type 1 diabetes mellitus. Nat Rev Dis Primers 3:17016.

Khacho M, Slack RS. 2018. Mitochondrial and Reactive Oxygen Species Signaling Coordinate Stem Cell Fate Decisions and Life Long Maintenance. Antioxid Redox Signal 28:1090–1101.

Kim YH, Larsen HL, Rué P, Lemaire LA, Ferrer J, Grapin-Botton A. 2015. Cell Cycle–Dependent Differentiation Dynamics Balances Growth and Endocrine Differentiation in the Pancreas. PLoS Biol 13:e1002111.

Kimmel JR, Hayden LJ, Pollock HG. 1975. Isolation and characterization of a new pancreatic polypeptide hormone. J Biol Chem 250:9369–76.

Kim-Muller JY, Fan J, Kim YJR, Lee S-A, Ishida E, Blaner WS, Accili D. 2016. Aldehyde dehydrogenase 1a3 defines a subset of failing pancreatic β cells in diabetic mice. Nat Commun 7:12631.

Kirova DG, Judasova K, Vorhauser J, Zerjatke T, Leung JK, Glauche I, Mansfeld J. 2022. A ROS-dependent mechanism promotes CDK2 phosphorylation to drive progression through S phase. Dev Cell 57:1712-1727.e9.

Kondoh H, Lleonart ME, Nakashima Y, Yokode M, Tanaka M, Bernard D, Gil J, Beach D. 2007. A High Glycolytic Flux Supports the Proliferative Potential of Murine Embryonic Stem Cells. Antioxid Redox Signal 9:293–299.

Krapp A, Knöfler M, Ledermann B, Bürki K, Berney C, Zoerkler N, Hagenbüchle O, Wellauer PK. 1998. The bHLH protein PTF1-p48 is essential for the formation of the exocrine and the correct spatial organization of the endocrine pancreas. Genes Dev 12:3752–3763.

Labib M, Kelley SO. 2020. Single-cell analysis targeting the proteome. Nat Rev Chem 4:143–158.

Lammert E, Cleaver O, Melton D. 2001. Induction of Pancreatic Differentiation by Signals from Blood Vessels. Science (1979) 294:564–567.

Lamouille S, Xu J, Derynck R. 2014. Molecular mechanisms of epithelial–mesenchymal transition. Nat Rev Mol Cell Biol 15:178–196.

Lenoir O, Flosseau K, Ma FX, Blondeau B, Mai A, Bassel-Duby R, Ravassard P, Olson EN, Haumaitre C, Scharfmann R. 2011. Specific Control of Pancreatic Endocrine β- and δ-Cell Mass by Class IIa Histone Deacetylases HDAC4, HDAC5, and HDAC9. Diabetes 60:2861–2871.

Levetan CS, Pierce SM. 2013. Distinctions between the islets of mice and men: Implications for new therapies for type 1 and 2 diabetes. Endocrine Practice 19:301–312.

Li C, Chen P, Vaughan J, Lee K-F, Vale W. 2007. Urocortin 3 regulates glucose-stimulated insulin secretion and energy homeostasis. Proceedings of the National Academy of Sciences 104:4206–4211.

Li J, Stouffs M, Serrander L, Banfi B, Bettiol E, Charnay Y, Steger K, Krause K-H, Jaconi ME. 2006. The NADPH Oxidase NOX4 Drives Cardiac Differentiation: Role in Regulating Cardiac Transcription Factors and MAP Kinase Activation. Mol Biol Cell 17:3978–3988.

Liang Y, Kesavan P, Wang LQ, Niswender K, Tanizawa Y, Permutt MA, Magnuson MA, Matschinsky FM. 1995. Variable effects of maturity-onset-diabetes-of-youth (MODY)-associated glucokinase mutations on substrate interactions and stability of the enzyme. Biochemical Journal 309:167–173.

Liggitt D, Dintzis S. 2018. 14 - Pancreas. Comparative Anatomy and Histology, p 241–250.

Ling C, Rönn T. 2019. Epigenetics in Human Obesity and Type 2 Diabetes. Cell Metab 29:1028–1044.

Longnecker DS. 2021. Anatomy and Histology of the Pancreas. The Pancreapedia: Exocrine Pancreas Knowledge Base 2:1-24.

Lyssenko V, Jonsson A, Almgren P, Pulizzi N, Isomaa B, Tuomi T, Berglund G, Altshuler D, Nilsson P, Groop L. 2008. Clinical Risk Factors, DNA Variants, and the Development of Type 2 Diabetes. New England Journal of Medicine 359:2220–2232.

MacDonald PE, Marinis YZ de, Ramracheya R, Salehi A, Ma X, Johnson PR v, Cox R, Eliasson L, Rorsman P. 2007. A KATP Channel-Dependent Pathway within α Cells Regulates Glucagon Release from Both Rodent and Human Islets of Langerhans. PLoS Biol 5:e143.

Marchetti P, Bugliani M, Tata V de, Suleiman M, Marselli L. 2017. Pancreatic Beta Cell Identity in Humans and the Role of Type 2 Diabetes. Front Cell Dev Biol 5:55.

Marchitti SA, Brocker C, Stagos D, Vasiliou V. 2008. Non-P450 aldehyde oxidizing enzymes: the aldehyde dehydrogenase superfamily. Expert Opin Drug Metab Toxicol 4:697–720.

Martano G, Borroni EM, Lopci E, Cattaneo MG, Mattioli M, Bachi A, Decimo I, Bifari F. 2019. Metabolism of Stem and Progenitor Cells: Proper Methods to Answer Specific Questions. Front Mol Neurosci 12:151.

Martínez-Reyes I, Chandel NS. 2020. Mitochondrial TCA cycle metabolites control physiology and disease. Nat Commun 11:102.

Mata NL, Moghrabi WN, Lee JS, Bui T v., Radu RA, Horwitz J, Travis GH. 2004. Rpe65 Is a Retinyl Ester Binding Protein That Presents Insoluble Substrate to the Isomerase in Retinal Pigment Epithelial Cells. Journal of Biological Chemistry 279:635–643.

McConnell BB, Ghaleb AM, Nandan MO, Yang VW. 2007. The diverse functions of Krüppel-like factors 4 and 5 in epithelial biology and pathobiology. BioEssays 29:549–557.

McDonald TJ, Ellard S. 2013. Maturity onset diabetes of the young: identification and diagnosis. Annals of Clinical Biochemistry: International Journal of Laboratory Medicine 50:403–415.

McGraw TE, Mittal V. 2010. Metabolism regulates differentiation. Nat Chem Biol 6:176–177.

Meng Y, Ren Z, Xu F, Zhou X, Song C, Wang VY-F, Liu W, Lu L, Thomson JA, Chen G. 2018. Nicotinamide Promotes Cell Survival and Differentiation as Kinase Inhibitor in Human Pluripotent Stem Cells. Stem Cell Reports 11:1347–1356.

Migita T, Okabe S, Ikeda K, Igarashi S, Sugawara S, Tomida A, Taguchi R, Soga T, Seimiya H. 2013. Inhibition of ATP Citrate Lyase Induces an Anticancer Effect via Reactive Oxygen Species. Am J Pathol 182:1800–1810.

Mikkelsen TS, Ku M, Jaffe DB, Issac B, Lieberman E, Giannoukos G, Alvarez P, Brockman W, Kim T-K, Koche RP, Lee W, Mendenhall E, et al. 2007. Genome-wide maps of chromatin state in pluripotent and lineage-committed cells. Nature 448:553–560.

Miller IJ, Bieker JJ. 1993. A novel, erythroid cell-specific murine transcription factor that binds to the CACCC element and is related to the Krüppel family of nuclear proteins. Mol Cell Biol 13:2776–2786.

Montanya E, Nacher V, Biarnés M, Soler J. 2000. Linear correlation between beta-cell mass and body weight throughout the lifespan in Lewis rats: role of beta-cell hyperplasia and hypertrophy. Diabetes 49:1341–1346.

Moore LD, Le T, Fan G. 2013. DNA Methylation and Its Basic Function. Neuropsychopharmacology 38:23–38.

Moussaieff A, Rouleau M, Kitsberg D, Cohen M, Levy G, Barasch D, Nemirovski A, Shen-Orr S, Laevsky I, Amit M, Bomze D, Elena-Herrmann B, et al. 2015. Glycolysis-Mediated Changes in Acetyl-CoA and Histone Acetylation Control the Early Differentiation of Embryonic Stem Cells. Cell Metab 21:392–402.

Nasr W, Fabian C, Arnold K, Köhl U, Sack U, Weiss R, Cross M, Hauschildt S. 2020. Nicotinamide Inhibits Self-renewal and Induces Granulocyte Differentiation of Multipotent Progenitor Cells. Stem Cell Rev Rep 16:1335–1342.

Nathan DM, Davidson MB, DeFronzo RA, Heine RJ, Henry RR, Pratley R, Zinman B. 2007. Impaired Fasting Glucose and Impaired Glucose Tolerance. Diabetes Care 30:753–759.

Newsholme P, Cruzat V, Arfuso F, Keane K. 2014. Nutrient regulation of insulin secretion and action. Journal of Endocrinology 221:R105–R120.

Nir T, Melton DA, Dor Y. 2007. Recovery from diabetes in mice by β cell regeneration. Journal of Clinical Investigation 117:2553–2561.

Nordmann TM, Dror E, Schulze F, Traub S, Berishvili E, Barbieux C, Böni-Schnetzler M, Donath MY. 2017. The Role of Inflammation in β-cell Dedifferentiation. Sci Rep 7:6285.

Oburoglu L, Tardito S, Fritz V, de Barros SC, Merida P, Craveiro M, Mamede J, Cretenet G, Mongellaz C, An X, Klysz D, Touhami J, et al. 2014. Glucose and Glutamine Metabolism Regulate Human Hematopoietic Stem Cell Lineage Specification. Cell Stem Cell 15:169–184.

Ohara-Imaizumi M, Cardozo AK, Kikuta T, Eizirik DL, Nagamatsu S. 2004. The Cytokine Interleukin-1β Reduces the Docking and Fusion of Insulin Granules in Pancreatic β-Cells, Preferentially Decreasing the First Phase of Exocytosis. Journal of Biological Chemistry 279:41271–41274.

Ohlsson H, Karlsson K, Edlund T. 1993. IPF1, a homeodomain-containing transactivator of the insulin gene. EMBO J 12:4251–4259.

Okamoto K, Kondo-Okamoto N, Ohsumi Y. 2009. Mitochondria-Anchored Receptor Atg32 Mediates Degradation of Mitochondria via Selective Autophagy. Dev Cell 17:87–97.

Öström M, Loffler KA, Edfalk S, Selander L, Dahl U, Ricordi C, Jeon J, Correa-Medina M, Diez J, Edlund H. 2008. Retinoic Acid Promotes the Generation of Pancreatic Endocrine Progenitor Cells and Their Further Differentiation into β-Cells. PLoS One 3:e2841.

Ott M, Gogvadze V, Orrenius S, Zhivotovsky B. 2007. Mitochondria, oxidative stress and cell death. Apoptosis 12:913-22.

Pan FC, Wright C. 2011. Pancreas organogenesis: From bud to plexus to gland. Developmental Dynamics 240:530–565.

Papizan JB, Singer RA, Tschen S-I, Dhawan S, Friel JM, Hipkens SB, Magnuson MA, Bhushan A, Sussel L. 2011. Nkx2.2 repressor complex regulates islet β-cell specification and prevents β-to-α-cell reprogramming. Genes Dev 25:2291–2305.

Pappa A, Chen C, Koutalos Y, Townsend AJ, Vasiliou V. 2003. Aldh3a1 protects human corneal epithelial cells from ultraviolet- and 4-hydroxy-2-nonenal-induced oxidative damage. Free Radic Biol Med 34:1178–1189.

Park S-Y, Kim J-S. 2020. A short guide to histone deacetylases including recent progress on class II enzymes. Exp Mol Med 52:204–212.

Parkhitko AA, Jouandin P, Mohr SE, Perrimon N. 2019. Methionine metabolism and methyltransferases in the regulation of aging and lifespan extension across species. Aging Cell 18:e13034.

Patel MS, Roche TE. 1990. Molecular biology and biochemistry of pyruvate dehydrogenase complexes. The FASEB Journal 4:3224–3233.

Pearson ER, Pruhova S, Tack CJ, Johansen A, Castleden HAJ, Lumb PJ, Wierzbicki AS, Clark PM, Lebl J, Pedersen O, Ellard S, Hansen T, et al. 2005. Molecular genetics and phenotypic characteristics of MODY caused by hepatocyte nuclear factor 4α mutations in a large European collection. Diabetologia 48:878–885.

Pearson ER, Starkey BJ, Powell RJ, Gribble FM, Clark PM, Hattersley AT. 2003. Genetic cause of hyperglycaemia and response to treatment in diabetes. The Lancet 362:1275–1281.

Presnell JS, Schnitzler CE, Browne WE. 2015. KLF/SP Transcription Factor Family Evolution: Expansion, Diversification, and Innovation in Eukaryotes. Genome Biol Evol 7:2289–2309.

Quesada I, Tudurí E, Ripoll C, Nadal Á. 2008. Physiology of the pancreatic α-cell and glucagon secretion: Role in glucose homeostasis and diabetes. J Endocrinol 199:5-19.

Quiros PM, Goyal A, Jha P, Auwerx J. 2017. Analysis of mtDNA/nDNA Ratio in Mice. Curr Protoc Mouse Biol 7:47–54.

Reza AMMT, Yuan Y-G. 2021. microRNAs Mediated Regulation of the Ribosomal Proteins and its Consequences on the Global Translation of Proteins. Cells 10:110.

Robertson RP, Harmon J, Tran POT, Poitout V. 2004. β-Cell Glucose Toxicity, Lipotoxicity, and Chronic Oxidative Stress in Type 2 Diabetes. Diabetes 53:S119–S124.

Romer AI, Sussel L. 2015. Pancreatic islet cell development and regeneration. Curr Opin Endocrinol Diabetes Obes 22:255–264.

Ruprecht JJ, Kunji ERS. 2020. The SLC25 Mitochondrial Carrier Family: Structure and Mechanism. Trends Biochem Sci 45:244–258.

Sakata N, Yoshimatsu G, Kodama S. 2019. Development and Characteristics of Pancreatic Epsilon Cells. Int J Mol Sci 20:1867.

Santana LS, Caetano LA, Costa-Riquetto AD, Franco PC, Dotto RP, Reis AF, Weinert LS, Silveiro SP, Vendramini MF, Prado FA, Abrahão GCP, Almeida AGFP, et al. 2019. Targeted sequencing identifies novel variants in common and rare MODY genes. Mol Genet Genomic Med 7:e962.

Schaffer AE, Freude KK, Nelson SB, Sander M. 2010. Nkx6 Transcription Factors and Ptf1a Function as Antagonistic Lineage Determinants in Multipotent Pancreatic Progenitors. Dev Cell 18:1022–1029.

Scialò F, Fernández-Ayala DJ, Sanz A. 2017. Role of Mitochondrial Reverse Electron Transport in ROS Signaling: Potential Roles in Health and Disease. Front Physiol 8:428.

Scott RA, Scott LJ, Mägi R, Marullo L, Gaulton KJ, Kaakinen M, Pervjakova N, Pers TH, Johnson AD, Eicher JD, Jackson AU, Ferreira T, et al. 2017. An Expanded Genome-Wide Association Study of Type 2 Diabetes in Europeans. Diabetes 66:2888–2902.

SenGupta S, Parent CA, Bear JE. 2021. The principles of directed cell migration. Nat Rev Mol Cell Biol 22:529–547.

Serafimidis I, Rodriguez-Aznar E, Lesche M, Yoshioka K, Takuwa Y, Dahl A, Pan D, Gavalas A. 2017. Pancreas lineage allocation and specification are regulated by sphingosine-1-phosphate signalling. PLoS Biol 15:e2000949.

Seymour PA, Freude KK, Tran MN, Mayes EE, Jensen J, Kist R, Scherer G, Sander M. 2007. SOX9 is required for maintenance of the pancreatic progenitor cell pool. Proceedings of the National Academy of Sciences 104:1865–1870.

Shih HP, Kopp JL, Sandhu M, Dubois CL, Seymour PA, Grapin-Botton A, Sander M. 2012. A Notch-dependent molecular circuitry initiates pancreatic endocrine and ductal cell differentiation. Development 139:2488–2499.

Shih HP, Panlasigui D, Cirulli V, Sander M. 2016. ECM Signaling Regulates Collective Cellular Dynamics to Control Pancreas Branching Morphogenesis. Cell Rep 14:169–179.

Shih HP, Wang A, Sander M. 2013. Pancreas Organogenesis: From Lineage Determination to Morphogenesis. Annu Rev Cell Dev Biol 29:81–105.

Shortall K, Djeghader A, Magner E, Soulimane T. 2021. Insights into Aldehyde Dehydrogenase Enzymes: A Structural Perspective. Front Mol Biosci 8:659550.

Shyh-Chang N, Locasale JW, Lyssiotis CA, Zheng Y, Teo RY, Ratanasirintrawoot S, Zhang J, Onder T, Unternaehrer JJ, Zhu H, Asara JM, Daley GQ, et al. 2013. Influence of Threonine Metabolism on *S*-Adenosylmethionine and Histone Methylation. Science (1979) 339:222–226.

Singh P, Tung S-P, Han EH, Lee I-K, Chi Y-I. 2019. Dimerization defective MODY mutations of hepatocyte nuclear factor 4α. Mutation Research/Fundamental and Molecular Mechanisms of Mutagenesis 814:1–6.

Smeitink JA, Zeviani M, Turnbull DM, Jacobs HT. 2006a. Mitochondrial medicine: A metabolic perspective on the pathology of oxidative phosphorylation disorders. Cell Metab 3:9–13.

Smeitink JA, Zeviani M, Turnbull DM, Jacobs HT. 2006b. Mitochondrial medicine: A metabolic perspective on the pathology of oxidative phosphorylation disorders. Cell Metab 3:9–13.

Son J, Du W, Esposito M, Shariati K, Ding H, Kang Y, Accili D. 2023. Genetic and pharmacologic inhibition of ALDH1A3 as a treatment of β-cell failure. Nat Commun 14:558.

Srere PA. 1969. Citrate synthase. Methods in Enzymology Volume 13 p 3–11.

Stagos D, Chen Y, Brocker C, Donald E, Jackson BC, Orlicky DJ, Thompson DC, Vasiliou V. 2010. Aldehyde Dehydrogenase 1B1: Molecular Cloning and Characterization of a Novel Mitochondrial Acetaldehyde-Metabolizing Enzyme. Drug Metabolism and Disposition 38:1679–1687.

Stanger BZ, Tanaka AJ, Melton DA. 2007. Organ size is limited by the number of embryonic progenitor cells in the pancreas but not the liver. Nature 445:886–891.

Steele AM, Shields BM, Shepherd M, Ellard S, Hattersley AT, Pearson ER. 2010. Increased all-cause and cardiovascular mortality in monogenic diabetes as a result of mutations in the HNF1A gene. Diabetic Medicine 27:157–161.

Steiner DJ, Kim A, Miller K, Hara M. 2010. Pancreatic islet plasticity: Interspecies comparison of islet architecture and composition. Islets 2:135-4.

Storms RW, Trujillo AP, Springer JB, Shah L, Colvin OM, Ludeman SM, Smith C. 1999. Isolation of primitive human hematopoietic progenitors on the basis of aldehyde dehydrogenase activity. Proceedings of the National Academy of Sciences 96:9118–9123.

Sumikawa MH, Iwata S, Zhang M, Miyata H, Ueno M, Todoroki Y, Nagayasu A, Kanda R, Sonomoto K, Torimoto K, Lee S, Nakayamada S, et al. 2022. An enhanced mitochondrial function through glutamine metabolism in plasmablast differentiation in systemic lupus erythematosus. Rheumatology 61:3049–3059.

Taborsky GJ, Mundinger TO. 2012. Minireview: The Role of the Autonomic Nervous System in Mediating the Glucagon Response to Hypoglycemia. Endocrinology 153:1055–1062.

Tanhauser SM, Laipis PJ. 1995. Multiple Deletions Are Detectable in Mitochondrial DNA of Aging Mice. Journal of Biological Chemistry 270:24769–24775.

Theis FJ, Lickert H. 2019. A map of β-cell differentiation pathways supports cell therapies for diabetes. Nature 569:342–343.

Thorens B, Tarussio D, Maestro MA, Rovira M, Heikkilä E, Ferrer J. 2015. Ins1 Cre knock-in mice for beta cell-specific gene recombination. Diabetologia 58:558–565.

Tormos KV, Anso E, Hamanaka RB, Eisenbart J, Joseph J, Kalyanaraman B, Chandel NS. 2011. Mitochondrial Complex III ROS Regulate Adipocyte Differentiation. Cell Metab 14:537–544.

Tsogtbaatar E, Landin C, Minter-Dykhouse K, Folmes CDL. 2020. Energy Metabolism Regulates Stem Cell Pluripotency. Front Cell Dev Biol 8:87.

Tsujita T, Peirce V, Baird L, Matsuyama Y, Takaku M, Walsh S v., Griffin JL, Uruno A, Yamamoto M, Hayes JD. 2014. Transcription Factor Nrf1 Negatively Regulates the Cystine/Glutamate Transporter and Lipid-Metabolizing Enzymes. Mol Cell Biol 34:3800–3816.

Uma L, Jayaram H, Sharam Y, Balasubramanian D. 1996. Letter to the Editors: Corneal Aldehyde Dehydrogenase Displays Antioxidant Properties. Exp Eye Res 63:117–119.

Utley RT, Ikeda K, Grant PA, Côté J, Steger DJ, Eberharter A, John S, Workman JL. 1998. Transcriptional activators direct histone acetyltransferase complexes to nucleosomes. Nature 394:498–502.

Valkovicova T, Skopkova M, Stanik J, Gasperikova D. 2019. Novel insights into genetics and clinics of the HNF1A-MODY. Endocr Regul 53:110–134.

Varum S, Momčilović O, Castro C, Ben-Yehudah A, Ramalho-Santos J, Navara CS. 2009. Enhancement of human embryonic stem cell pluripotency through inhibition of the mitochondrial respiratory chain. Stem Cell Res 3:142–156.

Vassalli G. 2019. Aldehyde Dehydrogenases: Not Just Markers, but Functional Regulators of Stem Cells. Stem Cells Int 2019:1–15.

Vaxillaire M, Boccio V, Philippi A, Vigouroux C, Terwilliger J, Passa P, Beckmann JS, Velho G, Lathrop GM, Froguel P. 1995. A gene for maturity onset diabetes of the young (MODY) maps to chromosome 12q. Nat Genet 9:418–423.

Viswanathan V, Cao H, Saiki J, Jiang D, Mattingly A, Nambiar D, Bloomstein J, Li Y, Jiang S, Chamoli M, Sirjani D, Kaplan M, et al. 2022. Aldehyde dehydrogenase 3A1 deficiency leads to mitochondrial dysfunction and impacts salivary gland stem cell phenotype. PNAS Nexus 1:1-14.

Vivas Y, Martínez-García C, Izquierdo A, Garcia-Garcia F, Callejas S, Velasco I, Campbell M, Ros M, Dopazo A, Dopazo J, Vidal-Puig A, Medina-Gomez G. 2011. Early peroxisome proliferator-activated receptor gamma regulated genes involved in expansion of pancreatic beta cell mass. BMC Med Genomics 4:86.

Wang Y, Zhao Y, Zhang J, Yang Y, Liu F. 2017. A case of a novel mutation in HNF1β -related maturity-onset diabetes of the young type 5 with diabetic kidney disease complication in a Chinese family. J Diabetes Complications 31:1243–1246.

Wentworth BM, Schaefer IM, Villa-Komaroff L, Chirgwin JM. 1986. Characterization of the two nonallelic genes encoding mouse preproinsulin. J Mol Evol 23:305–312.

Willcox A, Gillespie KM. 2015. Histology of Type 1 Diabetes Pancreas. p 105–117.

Williams JA, Williams L. 2006. Regulation of pancreatic acinar cell function Curr Opin Gastroenterol 26:478-83.

Wright JJ, Biner O, Chung I, Burger N, Bridges HR, Hirst J. 2022. Reverse Electron Transfer by Respiratory Complex I Catalyzed in a Modular Proteoliposome System. J Am Chem Soc 144:6791–6801.

Wu Y, Aegerter P, Nipper M, Ramjit L, Liu J, Wang P. 2021. Hippo Signaling Pathway in Pancreas Development. Front Cell Dev Biol 9:.

Xu C, Li L, Donahue G, Ying L, Zhang Y, Gadue P, Zaret KS. 2014. Dynamics of genomic H3K27me3 domains and role of EZH2 during pancreatic endocrine specification. EMBO J 33:2157–2170.

Xu C-R, Cole PA, Meyers DJ, Kormish J, Dent S, Zaret KS. 2011. Chromatin "Prepattern" and Histone Modifiers in a Fate Choice for Liver and Pancreas. Science (1979) 332:963–966.

Yahaya TO, Ufuoma SB. 2020. Genetics and Pathophysiology of Maturity-onset Diabetes of the Young (MODY): A Review of Current Trends. Oman Med J 35:e126–e126.

Yang Y-P, Thorel F, Boyer DF, Herrera PL, Wright CVE. 2011. Context-specific α-to-β-cell reprogramming by forced Pdx1 expression. Genes Dev 25:1680–1685.

Yaribeygi H, Farrokhi FR, Butler AE, Sahebkar A. 2019. Insulin resistance: Review of the underlying molecular mechanisms. J Cell Physiol 234:8152–8161.

Yoo HC, Yu YC, Sung Y, Han JM. 2020. Glutamine reliance in cell metabolism. Exp Mol Med 52:1496–1516.

Yu X-X, Qiu W-L, Yang L, Li L-C, Zhang Y-W, Xu C-R. 2018. Dynamics of chromatin marks and the role of JMJD3 during pancreatic endocrine cell fate commitment. Development 145: dev163162.

Zaret KS. 2008. Genetic programming of liver and pancreas progenitors: lessons for stem-cell differentiation. Nat Rev Genet 9:329–340.

Zhang J, Khvorostov I, Hong JS, Oktay Y, Vergnes L, Nuebel E, Wahjudi PN, Setoguchi K, Wang G, Do A, Jung H-J, McCaffery JM, et al. 2011. UCP2 regulates energy metabolism and differentiation potential of human pluripotent stem cells. EMBO J 30:4860–4873.

Zhang J, Zhao J, Dahan P, Lu V, Zhang C, Li H, Teitell MA. 2018. Metabolism in Pluripotent Stem Cells and Early Mammalian Development. Cell Metab 27:332–338.

Zhang Y, Xu J, Ren Z, Meng Y, Liu W, Lu L, Zhou Z, Chen G. 2021. Nicotinamide promotes pancreatic differentiation through the dual inhibition of CK1 and ROCK kinases in human embryonic stem cells. Stem Cell Res Ther 12:362.

Zhao S, Torres A, Henry RA, Trefely S, Wallace M, Lee JV, Carrer A, Sengupta A, Campbell SL, Kuo Y-M, Frey AJ, Meurs N, et al. 2016. ATP-Citrate Lyase Controls a Glucose-to-Acetate Metabolic Switch. Cell Rep 17:1037–1052.

Zhao Z, Shilatifard A. 2019. Epigenetic modifications of histones in cancer. Genome Biol 20:245.

Zheng H, Fu J, Xue P, Zhao R, Dong J, Liu D, Yamamoto M, Tong Q, Teng W, Qu W, Zhang Q, Andersen ME, et al. 2015. CNC-bZIP Protein Nrf1-Dependent Regulation of Glucose-Stimulated Insulin Secretion. Antioxid Redox Signal 22:819–831.

Zorova LD, Popkov VA, Plotnikov EY, Silachev DN, Pevzner IB, Jankauskas SS, Babenko VA, Zorov SD, Balakireva A v., Juhaszova M, Sollott SJ, Zorov DB. 2018a. Mitochondrial membrane potential. Anal Biochem 552: 50-59.

Acknowledgement

First and foremost, I want to express my great gratitude towards Anthony for allowing me to work on this exciting and challenging project. I thank you for all the guidance and support throughout those 4 years of my PhD, and also for your persisting confidence in my skills.

I also would like to express my gratitude to my thesis committee, Dr. Tiago Alves and Prof. Michele Solimena, for all the helpful advice and training you provided me with. Tiago, thank you that you took your time to teach me and to answer all of my questions. And thanks Michele for reading and reviewing my thesis.

A special thanks to Zeina! You were always there if I needed support, mentally and professionally. You kept everything together and I really appreciate all the effort you made to motivate and support us as well as your enduring patience with all of us.

A big thank you to the whole Gavalas group for all the fun times outside and inside the lab! You are all great people and I really appreciated working with you!

I am very grateful to all my friends for their immense support and would like to express my deepest appreciation to Sarah, Anne and Hao. Thank you for all the great memories, support and happy times. You made Dresden more like a home for me. Thanks also to Andy, Giovanni, Francesca and Laura and the rest of the idiots for all of the pub quizzes, dinners as well as bar nights and for all the times we were traveling together. My time in Dresden wouldn't have been the same without you!

My dearest friends from Jena: Theresa, Nora, Lina, Jonas and Flo. I am very grateful for the friendship we have and although we are spread all over Germany now, we still feel connected and you always had a word of advice or support when I needed it.

Major thanks to Frank for your never-ending patience and support! You believed in me even when I didn't and I am extremely grateful for this!

Furthermore, I want to thank my parents and grandparents, who always tried to support me mentally in the best possible way, especially in the time after my surgery. I wouldn't have made it so far without you!

Anlage 1

Technische Universität Dresden
Medizinische Fakultät Carl Gustav Carus
Promotionsordnung vom 24. Juli 2011

Erklärungen zur Eröffnung des Promotionsverfahrens

1. Hiermit versichere ich, dass ich die vorliegende Arbeit ohne unzulässige Hilfe Dritter und ohne Benutzung anderer als der angegebenen Hilfsmittel angefertigt habe; die aus fremden Quellen direkt oder indirekt übernommenen Gedanken sind als solche kenntlich gemacht.

2. Bei der Auswahl und Auswertung des Materials sowie bei der Herstellung des Manuskripts habe ich Unterstützungsleistungen von folgenden Personen erhalten: **entfällt**

3. Weitere Personen waren an der geistigen Herstellung der vorliegenden Arbeit nicht beteiligt. Insbesondere habe ich nicht die Hilfe eines kommerziellen Promotionsberaters in Anspruch genommen. Dritte haben von mir weder unmittelbar noch mittelbar geldwerte Leistungen für Arbeiten erhalten, die im Zusammenhang mit dem Inhalt der vorgelegten Dissertation stehen.

4. Die Arbeit wurde bisher weder im Inland noch im Ausland in gleicher oder ähnlicher Form einer anderen Prüfungsbehörde vorgelegt.

5. Die Inhalte dieser Dissertation wurden in folgender Form veröffentlicht: **entfällt**

6. Ich bestätige, dass es keine zurückliegenden erfolglosen Promotionsverfahren gab.

7. Ich bestätige, dass ich die Promotionsordnung der Medizinischen Fakultät der Technischen Universität Dresden anerkenne.

8. Ich habe die Zitierrichtlinien für Dissertationen an der Medizinischen Fakultät der Technischen Universität Dresden zur Kenntnis genommen und befolgt.

Ort, Datum   Mandy Rödiger

Anlage 2

Hiermit bestätige ich die Einhaltung der folgenden aktuellen gesetzlichen Vorgaben im Rahmen meiner Dissertation

- das zustimmende Votum der Ethikkommission bei Klinischen Studien, epidemiologischen Untersuchungen mit Personenbezug oder Sachverhalten, die das Medizinproduktegesetz betreffen

  Aktenzeichen der zuständigen Ethikkommission:
  - **entfällt**

- die Einhaltung der Bestimmungen des Tierschutzgesetzes

  Aktenzeichen der Genehmigungsbehörde zum Vorhaben/zur Mitwirkung:
  - TVV 45/2019 (DD24-5131/346/2)
  - TVA 9/2016 (DD24-5131/367/10)
  - TVA 18/2021 (25-5131/474/48)

- die Einhaltung des Gentechnikgesetzes *Projektnummer:*
  - Az.: 54-8451/227

- die Einhaltung von Datenschutzbestimmungen der Medizinischen Fakultät und des Universitätsklinikums Carl Gustav Carus.

Dresden, den   Mandy Rödiger